

6. LATE-STAGE MELT EVOLUTION AND TRANSPORT IN THE SHALLOW MANTLE BENEATH THE EAST PACIFIC RISE¹

Henry J.B. Dick² and James H. Natland³

ABSTRACT

This paper reports the igneous petrology and geochemistry of harzburgite-tectonites, crosscutting dunites, and local gabbroic segregations drilled from a tectonically exposed outcrop of shallow East Pacific Rise mantle at Ocean Drilling Program Site 895 near Hess Deep. Melting of the Hess Deep mantle section, as for most abyssal peridotites, occurred in the four-phase field olivine-enstatite-diopside-spinel limited by the diopside-out phase boundary. The Site 895 peridotites are clinopyroxene-poor harzburgites at the most depleted end of the range for abyssal peridotites. Unlike similar highly depleted peridotites from the Atlantic and Indian Oceans, however, these are not spatially associated with a mantle hot spot. Abyssal basalts from the walls of Hess Deep near Site 895, believed to have erupted at the East Pacific Rise, are N-type mid-ocean-ridge basalt (MORB). These indicate that the Site 895 peridotites are residues of melting of an N-type MORB source. Like ridge basalts near hot spots, however, the Hess Deep basalts, and Hole 894G gabbros nearby, require crystallization from very low sodium primary liquids consistent with the very depleted Hess Deep residual mantle peridotites.

Given seismic data that indicate a somewhat thin East Pacific Rise crust in the region, and an absence of any chemical or physical evidence for a mantle hot spot, we suggest that the high degree of depletion of the Hess Deep peridotites and the inferred primary basalt compositions, reflect moderate degrees of melting of a refractory mantle section poor in basaltic components under a normal geothermal gradient. This region of the East Pacific Rise, then, does not fit the proposed global correlation of Klein and Langmuir (1987) between ridge basalt and crustal thickness. Rather, it implies that crustal thickness at ocean ridges may be as much a function of variations of initial mantle composition as initial mantle temperature (e.g., Dick et al., 1984).

Primary melts transported through the Site 895 mantle section, as inferred from the geochemistry of gabbroic segregations in dunites crosscutting the harzburgite tectonites, were fully aggregated MORB. They were not, therefore, in equilibrium with the shallow mantle since clinopyroxenes in the Hess Deep harzburgites have trace element compositions in equilibrium with highly refractory melts previously only reported as inclusions in phenocrysts in Atlantic MORBs. This supports, and may require, highly focused flow and aggregation of melt through the underlying mantle-melting-column. The crystallization sequence of MORB in the Hess Deep shallow mantle section is the same as for normal abyssal tholeiites. However, high-magnesium diopside and high-calcium plagioclase (up to An₆₉), present in some of the gabbroic segregations, are believed to be the product of late-stage reaction between melt and the harzburgite tectonite to produce high calcium and alumina melts. Similar sporadic xenocrysts widely distributed in MORBs might then be explained by mixing of MORB with stagnated highly reacted melts in shallow mantle conduits.

The dike-like form and compound nature of some gabbroic segregations in the dunites crosscutting the residual mantle harzburgite tectonites at Site 895 demonstrate that late-stage melt transport was, at least in part, fracture controlled. The segregations themselves, and small amounts of late-magmatic-textured intergranular clinopyroxene impregnating the harzburgite tectonites, also demonstrate that magma mass was decreasing as melt was transported through the transition zone in the mantle immediately beneath the crust. This requires that the mantle temperature there is depressed below the mantle adiabat due to conductive heat loss. The presence of this conductive lid is a significant factor in the evolution of MORB and impacts estimates of the composition of the oceanic crust. Such a lid limits the extent of melting of the upwelling mantle, traps late melt fractions generated at the top of the mantle melting column, and creates a zone where melt-rock reaction produces small, but apparently significant, quantities of high alumina and calcic MORB magmas.

INTRODUCTION

The composition and structure of the ocean crust and mantle are as yet poorly known. This is largely a consequence of the availability of little direct stratigraphic information for anything other than the shallowest levels of the modern ocean crust. Models for the formation of the ocean crust, accordingly have relied heavily on inference from marine geophysical data and analogy to ophiolites of ambiguous oceanic provenance. As a consequence, the nature of the lower crust and the mechanisms of melt transport through the mantle and

the crust and how these vary with spreading rate and magma supply are widely debated (Cannat, 1993; Sinton and Detrick, 1992; Swift and Stephen, 1992). This is a study of the igneous petrology and geochemistry of residual harzburgites and related crosscutting dunites and gabbroic segregations from six holes drilled at Ocean Drilling Program Site 895 in an outcrop of the shallow East Pacific Rise (EPR) mantle exposed on a tectonic block on the floor of Hess Deep in the equatorial eastern Pacific (Table 1). These rocks, and 154 m of gabbros drilled at Hole 894G nearby, represent the first sections of plutonic rocks from Pacific lower crust and mantle with enough key stratigraphic relationships preserved to allow a reasonable direct reconstruction of portions of the original stratigraphy. The results of shipboard studies (Gillis, Mével, Allan, et al., 1993), prior work on dredge and dive samples from Hess Deep (Hekinian et al., 1993), and this paper find a similarity between the Site 895 mantle sections and zones of melt transport exposed in the shallow mantle sections of ophiolites such as Oman (Ceuleneer and Rabinowicz, 1992). There, as at Hess Deep, evidence of late-stage melt migration is seen where

¹Mével, C., Gillis, K.M., Allan, J.F., and Meyer, P.S. (Eds.), 1996. *Proc. ODP, Sci. Results, 147*: College Station, TX (Ocean Drilling Program).

²Woods Hole Oceanographic Institution, Woods Hole, MA 02543, U.S.A.
hdick@whoi.edu

³Rosenstiel School of Marine and Atmospheric Science, University of Miami, 4600 Rickenbacker Causeway, Miami, FL 33149, U.S.A. jnatland@umigw.miami.edu

depleted harzburgite tectonite is crosscut by irregular to tabular dunite bodies. These mark zones where melts passed through the shallow mantle, reacted out pyroxene, and precipitated olivine in porous melt flow channels (Boudier and Nicolas, 1972; Cassard et al., 1981; Dick, 1977a, 1977b; Quick, 1981a, 1981b). Locally, these dunites contain gabbroic segregations, ranging from troctolite, where plagioclase impregnates disaggregated dunite, to olivine gabbro and gabbro. These segregations then allow the composition and evolution of the primary magmas migrating through the shallow mantle beneath the East Pacific Rise to be directly inferred.

The tabular character and compound nature of some gabbroic segregations suggest that the last stages of shallow melt transport were fracture dominated. The initial composition of the migrating melt was N-type mid-ocean-ridge basalt (MORB), based on the trace element composition of diopside in the gabbroic segregations within the dunites. In some cases the original melt appears to have reacted with the wall-rock harzburgite to make extreme melt compositions in equilibrium with high-calcium plagioclase and high-magnesium diopside. The latter minerals also occur as occasional, but widely distributed, xenocrysts in MORB and have previously been used to suggest high-pressure fractional crystallization (Elthon, 1989; Elthon and Scarfe, 1984), or the formation of ultra-depleted melts high in the melting column (Duncan and Green, 1980; Sobolev and Shimizu, 1993).

The Hess Deep residual harzburgites exhibit one of the greatest major- and trace-element depletions yet found for abyssal peridotites, and would be in equilibrium with only extremely depleted melts, not MORB. Such extreme depletion is consistent with fractional melting in the mantle beneath ocean ridges (Johnson and Dick, 1992; Johnson et al., 1990). The harzburgites have REE patterns unlike any found previously associated with N-MORB far from mantle hot spots. The shape of the REE pattern is characterized by a strong depletion of the middle rare earths relative to the heavy rare earths, a feature that is similar to patterns found for abyssal peridotites dredged near the Marion and Bouvet hot spots on the Southwest Indian Ridge (Johnson et al., 1990). Because seismic data for the EPR in the Hess Deep region suggest a normal or somewhat thin ocean crust (Zonen-shain et al., 1980), we speculate that this unusual pattern is best explained if the mantle beneath this region of the EPR was initially more depleted in major- and trace-element composition than typical for mantle regions beneath the Atlantic and Indian Oceans away from hot spots. This would be consistent with the composition of N-MORB and gabbros from Hess Deep that require crystallization from very soda-poor primary melts generally believed to reflect very high degrees of mantle melting (Dick et al., 1984; Klein and Langmuir, 1987), but is inconsistent with the correlation between crustal thickness and basalt chemistry postulated by Klein and Langmuir (1987).

ANALYTICAL TECHNIQUES

Modal Analysis

Modal analysis was done by point counting primary relict phases and their pseudomorphs. Talc, talc-amphibole, and serpentine pseudomorphs of each primary phase were counted separately from the primary mineral relicts, and the primary mode was calculated without a correction for volume expansion. Typically between 1800 and 2500 points were counted at a 1-mm interval. This yields estimates of precision (1 sigma) for analyzing a peridotite with 77.5 vol% olivine 20% enstatite, 2% clinopyroxene, and 0.5% spinel of: +0.85, +0.82, +0.29, and +0.14%, respectively (Chayes, 1956; Chayes, pers. comm., 1990). Orientation problems could arise if samples were cut parallel to layering, which can radically bias a mode. Here, however, spinel lineations, contacts, and layering in the peridotites, where observed, dip approximately 70°, and as our chips were all cut in the 1 l vertical plane orthogonal to observable foliation, bias is unlikely.

Table 1. Samples used in this study.

Hole, core, section, interval (cm)	Piece	Depth (mbsf)	Rock type	Source
147-895A-2R-1, 7-10	3	9.68	Harzburgite	Allan, IR
147-895B-1R-1, 71-76	9b	5.11	Harzburgite	
147-895C-1R-1, 28-32	5	2.80	Harzburgite	
3R-1, 35-39	7	20.06	Harzburgite	
4R-1, 10-12	?	28.21	Harzburgite	Allan, IR
4R-1, 75-78	?	30.19	Troctolitic dunite	Allan
4R-1, 126-128	?	31.75	Troctolitic dunite	Allan
4R-2, 62-65	2	33.06	Troctolite	
4R-2, 63-68	2	33.09	Troctolitic dunite	Allan
4R-2, 108-112	6b	34.46	Troctolite	
4R-2, 108-112	6b	34.46	Olivine gabbro	
4R-2, 108-112	6b	34.46	Troctolite	
4R-3, 32-35	3	36.68	Plag. dunite	
4R-2a, 102-105a	14	34.28	Troctolite	
4R-2b, 102-105b	14	34.28	Gabbro	
4R-2c, 102-105c	14	34.28	Troctolite	
147-895D-2R-2, 43-46	3a	23.72	Harzburgite	IR
3R-1, 38-43	6d	28.41	Harzburgite	
3R-1, 116-120	14	33.37	Harzburgite	
4R-1, 34-37	6a	35.25	Harzburgite	Allan
4R-3, 55-60	6b	39.23	Harzburgite	IR
4R-3, 97-101	11	39.91	Harzburgite	
5R-1, 7-11	2	43.60	Harzburgite	IR
5R-2, 90-95	13	53.48	Harzburgite	
5R-2, 103-105	14	54.04	Harzburgite	IR
7R-1, 5-9	2	64.75	Troctolite	
7R-1, 99-101a	16	67.59	Troctolite c. gr.	
7R-1, 99-101b	16	67.59	Troctolite m. gr.	
7R-2, 58-61	8	70.79	Troctolite c. gr.	
7R-2, 61-63	8	70.89	Troctolitic gabbro	
7R-2, 63-65	8	70.95	Troctolite m. gr.	
7R-2, 129-133	16	72.94	Harzburgite	
7R-2, 123-126	15	72.76	Harzburgite	Allan
7R-2, 71-75	9	71.19	Olivine gabbro	Allan
8R-2, 6-9	1	79.15	Olivine gabbro	
8R-2, 139-144	18	83.63	Dunite	
9R-2a, 60-65	10	93.34	Gabbro	
9R-2b, 60-65	10	93.34	Olivine gabbro	
9R-2c, 60-65	10	93.34	Olivine gabbro	
147-895E-1R-3, 14-17	1	12.39	Harzburgite	IR
1R-3, 32-36	2b	13.14	Dunite	
2R-1, 51-54	9	21.67	Olivine gabbro	
2R-1, 36-39	8	21.06	Olivine gabbro	Allan
3R-1, 21-23	4	30.17	Dunite	
3R-1, 21-23	4	30.17	Troctolite	
4R-3, 16-22	3	47.58	Olivine gabbro	
4R-3, 55-58	7	48.61	Gabbro	
5R-1, 23-26	5	49.50	Olivine gabbro	
7R-4, 86-89	8	77.70	Harzburgite	
8R-4, 4-7	2	84.90	Dunite	
147-895F-1R-1, 11-16	2	11.78	Harzburgite	
2R-2, 73-80	9	26.02	Harzburgite	

Notes: Depth = meters below seafloor based on expanding the curated recovery to fill the drilled interval. Source = data for samples from sources other than this paper: IR = Initial Reports Vol. 147 (Gillis, Mével, Allan, et al., 1993); Allan = Allan et al., this volume. c. gr. = coarse grained; m. gr. = medium grained.

Another source of potential error is differential expansion during serpentinization. In theory, up to 32% volume expansion can occur during isochemical hydration of peridotite (Komor et al., 1985b; O'Hanley, 1992). If olivine or pyroxene is preferentially serpentinized, this may introduce errors in estimating the primary mode by counting pseudomorphs. The data in Table 2 show that olivine is generally but not always preferentially altered relative to pyroxene, and the degree of serpentinization generally increases with increasing modal olivine. The amount of serpentine goes up by as much as 30% with only a 10% increase in overall olivine content, suggesting that the presence of pyroxene may have a mechanical or chemical effect which stabilizes olivine. As a consequence of preferential alteration, the volume percentage of primary olivine in our samples tends to be overestimated. Since enstatite is also heavily altered, however, gen-

Table 2. Modal analyses of Site 895 harzburgites.

Sample	Counts	Relict	Serp	TcAm	Relict	Serp	TcAm	Relict	Serp	TcAm	Pg	Total Serp	Primary mode					Corrected for volume expansion					
		Ol	Ol	Ol	En	En	En	Di	Di	Di			Ol	En	Di	Sp	Pg	Ol	En	Di	Sp	Pg	
147-895A- 2R-1, 7-10													85.5	13.1	0.50	0.90	0.00						
147-895B- 1R-1, 71-76	1970	14.3	74.6	0.00	3.96	4.72	1.62	0.25	0.00	0.00	0.10	79.3	88.8	10.3	0.25	0.51	0.1	87.7	11.3	0.31	0.62	0.12	
147-895C- 1R-1, 28-32	1925	22.8	60.7	0.00	6.13	8.05	0.21	0.99	0.05	0.00	0.00	68.8	83.5	14.4	1.04	1.04	0.0	82.6	14.9	1.22	1.24	0.00	
3R-1, 35-39	2105	30.2	51.7	0.38	4.56	6.46	4.47	1.24	0.00	0.00	0.00	58.2	82.3	15.5	1.24	0.90	0.0	81.3	16.2	1.43	1.04	0.00	
4R-1, 10-12													92.2	7.4	0.00	0.40	0.0						
147-895D- 2R-2, 43-46													86.8	12.5	0.00	0.50	0.0						
3R-1, 38-43	2386	23.2	55.8	0.29	11.27	7.08	1.42	0.34	0.00	0.00	0.00	62.9	79.3	19.8	0.34	0.63	0.0	77.6	21.2	0.39	0.74	0.00	
3R-1, 116-120	2521	23.8	59.6	0.20	4.01	4.88	5.71	0.95	0.04	0.00	0.00	64.5	83.6	14.6	0.99	0.67	0.0	82.2	15.9	1.16	0.79	0.00	
4R-3, 56-60	2167	26.0	57.6	0.00	0.00	13.84	0.00	1.11	0.42	0.00	0.00	71.9	83.6	13.8	1.52	1.02	0.0	84.3	12.8	1.71	1.22	0.00	
4R-3, 97-101	2356	28.9	50.9	0.21	9.08	2.04	5.77	1.78	0.42	0.00	0.00	53.4	80.1	16.9	2.21	0.76	0.0	78.0	18.7	2.41	0.87	0.00	
5R-1, 7-11													81.4	17.0	0.50	1.60	0.0						
5R-2, 90-95	2242	23.5	58.8	0.09	4.64	5.13	5.62	1.74	0.09	0.00	0.00	64.0	82.4	15.4	1.83	0.36	0.0	80.8	16.7	2.12	0.42	0.00	
5R-2, 103-105													83.8	13.6	1.70	0.90	0.0						
7R-2, 129-135	2298	5.5	79.2	0.04	4.83	3.48	5.13	1.35	0.04	0.00	0.00	82.7	84.8	13.4	1.39	0.39	0.0	82.2	15.6	1.71	0.48	0.00	
147-895E- 1R-3, 14-17													82.7	16.5	0.00	0.80	0.0						
7R-4, 86-89	2115	13.8	70.7	0.99	0.85	3.92	8.65	0.24	0.05	0.00	0.00	74.7	85.5	13.4	0.28	0.76	0.0	83.6	15.1	0.33	0.91	0.00	
147-895F- 1R-1, 11-16	2190	32.1	46.3	0.14	8.45	2.74	9.09	0.78	0.00	0.00	0.00	49.0	78.5	20.3	0.78	0.41	0.0	76.5	22.1	0.88	0.46	0.00	
2R-2, 73-80	2055	12.4	67.2	0.63	2.63	4.53	8.47	0.68	3.02	0.00	0.00	74.7	80.1	15.6	3.70	0.54	0.0	78.1	17.6	3.63	0.65	0.00	
Average	2194	21.4	61.1	0.25	5.03	5.57	4.68	0.95	0.34	0.00	0.01	67.0	83.6	14.6	1.0	0.7	0.0	81.1	16.6	1.44	0.86	0.01	
St. deviation		8.1	10.0	0.3	3.3	3.1	3.2	0.5	0.9	0.0	0.01	0.3	3.4	3.0	1.0	0.3	0.0	82.7	15.3	1.30	0.67	0.01	

Notes: Counts = total points counted (1 mm spacing). Relict = primary unaltered mineral: Ol = olivine, En = enstatite, Di = diopside, Pg = plagioclase (includes alteration after plagioclase), Sp = spinel. Serp and TcAm = serpentine, talc and/or amphibole pseudomorphs replacing the phase listed immediately below. Analyses where the number of counts and pseudomorph proportions are not shown are from the *Initial Reports* volume for Leg 147 (Gillis, Mével, Allan, et al., 1993). Primary mode = sum of relict primary phase and all its pseudomorphs. Numbers in italics are the average mode, uncorrected for the effects of serpentinization.

erally around 50%, the overall effect is typically small. Shown for comparison in Table 2 are primary modes recalculated assuming a 30% volume expansion during serpentinization. As can be seen by comparison to the uncorrected average mode given in italics, on average, using uncorrected modes results in a fairly small errors in estimating mineral abundance, and would have little effect on the conclusions drawn in this paper.

As we wish to use the additional data collected on board ship, and to compare our results to those for other abyssal peridotite localities, for which alteration phases were not counted separately, we use uncorrected modes in our plots and in the discussion. Any violation of the isochemical serpentinization assumption also means that actual errors in point counting primary mineral modes are likely to be less than the theoretical maximum. Overall, modal mineral trends, where the mineral data are not corrected for changes in volume due to serpentinization, will have increased scatter and will be somewhat compressed toward the olivine apex of the modal pyroxene-olivine ternary.

Electron Microprobe

Major element analyses of silicates and oxides was done with the MIT 4-spectrometer JEOL 733 Superprobe, using an accelerating voltage of 15 KeV and a beam current of 10 nA for all phases. Data

were reduced using Bence-Albee matrix corrections (Albee and Ray, 1970; Bence and Albee, 1968) (Tables 3–7). A beam spot size of 10 μm was used for analysis of pyroxenes, with 10 spots each analyzed along approximately a 100- μm traverse in order to obtain bulk analyses of grains incorporating any solid-solution lamellae. The analytical standard deviations observed when a 200- μm traverse using 20 spots was made were essentially identical to those for the 100- μm traverses (Table 4; Sample 147-895D-3R-1, 116–120 cm), suggesting that the technique accurately determined pyroxene bulk composition in our samples for the plane we traversed. A 1- μm -beam spot size was used for analysis of all other phases. Three- to seven-point analyses were made on chromian spinel, representing core to rim traverses. Little zoning was observed, and these analyses were then averaged to give a bulk composition for each grain.

Ion Microprobe

Rare earth and other trace element analyses (Table 8) were made using the Woods Hole Oceanographic Institution Cameca IMS-3f ion microprobe facility under the direction of Dr. Nobu Shimizu. Analytical techniques are the same as those used by Johnson et al. (1990). Overall accuracy and precision of the data are generally believed to be: $\pm 5\%$ – 10% for Ti, Cr, and V, $\pm 10\%$ – 15% for Sr and Zr, and $\pm 10\%$ – 20% for light rare earth elements (LREE) and $\pm 10\%$ –

Table 3. Site 895 olivine analyses.

Hole	Core, section, interval (cm)	Rock type	Pts.	Gr.	MgO	Al ₂ O ₃	SiO ₂	CaO	TiO ₂	Cr ₂ O ₃	MnO	FeO	NiO	Total	Mg#
895E	5R-1, 23–26	Olivine gabbro	5	1	45.9	0.00	39.7	0.08	0.08	0.07	0.17	13.38	0.18	99.6	85.9
			sd	1	0.2	0.00	0.1	0.01	0.05	0.04	0.08	0.06	0.06	0.2	0.1
895C	4R-2, 108–112	Olivine gabbro	3	1	49.1	0.00	40.2	0.06	0.02	0.01	0.18	11.01	0.24	100.9	88.8
			sd	1	0.3	0.01	0.1	0.01	0.01	0.01	0.02	0.12	0.01	0.3	0.2
895C	4R-2, 108–112	Olivine gabbro	10	1	47.5	0.00	40.2	0.05	0.05	0.06	0.13	11.05	0.26	99.2	88.4
			sd	1	0.2	0.00	0.3	0.02	0.03	0.04	0.06	0.12	0.05	0.5	0.1
895D	7R-2, 61–63	Troctolitic gabbro	6	1	47.0	0.01	39.7	0.05	0.05	0.06	0.15	12.81	0.24	100.1	86.7
			sd	1	0.3	0.02	0.2	0.02	0.03	0.02	0.03	0.17	0.04	0.4	0.2
895C	4R-2, 102–105	Troctolite	6	1f	48.3	0.00	40.0	0.02	0.01	0.00	0.22	10.59	0.26	99.5	89.0
			sd	1f	0.2	0.01	0.2	0.01	0.02	0.00	0.04	0.17	0.01	0.3	0.1
895C	4R-2, 102–105	Troctolite	7	2g	48.5	0.02	40.2	0.05	0.00	0.01	0.21	10.50	0.25	99.8	89.2
			sd	2g	0.4	0.01	0.2	0.02	0.01	0.01	0.03	0.11	0.01	0.6	0.1
895D	7R-1, 99–101	Troctolite, m. gr.	5	1	49.3	0.02	40.3	0.04	0.00	0.02	0.21	10.22	0.26	100.4	89.6
			sd	1	0.2	0.02	0.3	0.01	0.00	0.02	0.03	0.09	0.02	0.5	0.1
895D	7R-1, 99–101	Troctolite, c. gr.	6	2f	49.1	0.02	40.2	0.04	0.02	0.00	0.20	10.35	0.27	100.2	89.4
			sd	2f	0.2	0.02	0.1	0.01	0.01	0.01	0.03	0.14	0.02	0.4	0.1
895D	7R-2, 58–61	Troctolite c. gr.	3	1	47.5	0.02	40.1	0.06	0.01	0.03	0.22	12.57	0.15	100.7	87.1
			sd	1	0.1	0.02	0.2	0.02	0.01	0.00	0.02	0.02	0.13	0.4	0.0
895C	4R-3, 32–35	Plagioclase dunite	3	1	49.0	0.00	40.2	0.09	0.01	0.00	0.19	10.50	0.25	100.3	89.3
			sd	1	0.0	0.00	0.0	0.01	0.01	0.00	0.01	0.15	0.01	0.2	0.1
895D	8R-2, 139–144	Dunite	7	1	48.8	0.04	40.0	0.15	0.04	0.04	0.11	9.39	0.29	98.8	90.3
			sd	1	0.5	0.03	0.2	0.14	0.03	0.03	0.07	0.11	0.06	0.5	0.1
895E	1R-3, 32–36	Dunite	4	1	40.4	0.05	32.7	0.00	0.03	0.02	0.08	5.46	0.23	79.0	93.0
			sd	1	2.4	0.02	5.1	0.01	0.02	0.02	0.06	1.19	0.09	2.1	1.2
895E	3R-1, 21–23	Dunite	5	1	48.7	0.01	34.1	0.10	0.02	0.00	0.20	10.28	0.28	93.7	89.4
			sd	1	0.2	0.01	13.4	0.05	0.02	0.01	0.03	0.16	0.01	13.4	0.1
895E	8R-4, 4–7	Dunite	5	1	48.2	0.08	40.4	0.20	0.04	0.09	0.16	10.08	0.26	99.6	89.5
			sd	1	0.3	0.02	0.1	0.09	0.05	0.05	0.06	0.20	0.07	0.4	0.2
895B	1R-1, 71–76	Harzburgite	5	1	50.2	0.02	40.8	0.11	0.00	0.01	0.16	9.00	0.29	100.6	90.9
			sd	1	0.5	0.01	0.3	0.00	0.01	0.02	0.01	0.20	0.02	0.5	0.1
895C	1R-1, 28–32	Harzburgite	7		49.9	0.00	40.5	0.09	0.05	0.04	0.10	8.80	0.33	99.8	91.0
			sd		0.2	0.01	0.1	0.02	0.03	0.03	0.07	0.17	0.06	0.4	0.2
895C	3R-1, 35–39	Harzburgite	3	1	49.9	0.02	40.8	0.09	0.02	0.01	0.15	9.31	0.31	100.6	90.5
			sd	1	0.5	0.02	0.4	0.02	0.02	0.01	0.01	0.14	0.00	0.3	0.1
895D	3R-1, 38–43	Harzburgite	6	1	50.8	0.01	40.4	0.08	0.06	0.06	0.09	8.77	0.32	100.5	91.2
			sd	1	0.1	0.01	0.2	0.02	0.03	0.02	0.03	0.10	0.01	0.3	0.1
895D	3R-1, 116–121	Harzburgite	3	2	50.5	0.03	40.5	0.09	0.01	0.02	0.16	8.97	0.29	100.6	90.9
			sd	2	0.5	0.00	0.1	0.01	0.01	0.02	0.04	0.11	0.01	0.5	0.1
895D	4R-3, 97–101	Harzburgite	6	1	50.0	0.00	40.7	0.08	0.04	0.05	0.11	9.07	0.38	100.4	90.8
			sd	1	0.2	0.01	0.1	0.02	0.04	0.04	0.06	0.12	0.02	0.4	0.1
895D	5R-2, 90–95	Harzburgite	7	1	50.4	0.00	40.4	0.08	0.05	0.08	0.08	8.74	0.31	100.1	91.1
			sd	1	0.2	0.01	0.2	0.02	0.01	0.03	0.03	0.12	0.02	0.4	0.1
895D	7R-2, 129–133	Harzburgite	3	1	50.3	0.02	40.7	0.08	0.00	0.13	0.14	8.84	0.31	100.5	91.0
			sd	1	0.6	0.02	0.3	0.01	0.00	0.20	0.03	0.12	0.01	0.5	0.1
895E	7R-4, 86–89	Harzburgite	8	1	49.7	0.01	40.1	0.05	0.05	0.04	0.12	9.06	0.37	99.5	90.7
			sd	1	0.3	0.02	0.2	0.03	0.04	0.03	0.10	0.13	0.02	0.4	0.1
895F	1R-1, 11–16	Harzburgite	7	1	50.2	0.04	40.4	0.09	0.06	0.08	0.10	8.96	0.33	100.3	90.9
			sd	1	0.2	0.03	0.1	0.06	0.02	0.01	0.03	0.11	0.02	0.3	0.1
895F	2R-2, 73–80	Harzburgite	7	1	49.8	0.02	40.3	0.05	0.04	0.06	0.11	9.35	0.30	100.0	90.5
			sd	1	0.6	0.02	0.2	0.03	0.02	0.01	0.03	0.64	0.01	0.1	0.7

Notes: Pts. = number of points analyzed; sd = one standard deviation. Gr. = number of grain analyzed. Mg# = molecular ratio: (Mg-100)/(Mg+Fe). m. gr. = medium grained; c. gr. = coarse grained.

15% for the heavy rare earth elements (HREE) (Johnson et al., 1990). In our more depleted harzburgites, however, relatively large errors are associated with analysis of the LREE, Sr and Zr, which occur close to, or below, the analytical detection limit. In a few cases La and Ce are deleted from Table 8 for the most questionable analyses, and as we are not certain of the reliability of La concentrations for all the harzburgite diopside analyses, and thus it is not used in the figures. Analytical uncertainties at the very low levels of analysis of the harzburgites varied with the electronic stability of the instrument, which, in turn, varied over the course of the year-long analytical program. For this reason, almost all the analyses quoted in Table 8 for the harzburgites represent multiple analyses which have been averaged, rejecting obviously bad data. The average counting errors for these analyses are also given in Table 8 as a guide to interpreting the data. Any data with an average counting error of more than 40% must be regarded as unreliable.

TECTONIC SETTING

Hess Deep (Fig. 1) is a local basin near the largely amagmatic tip of a V-shaped rift valley breaking into 0.3–1.0 Ma crust on the eastern flank of the EPR ahead of the westward propagating Cocos-Nazca Ridge (Lonsdale, 1988). From its tip, about 20 km from the EPR, the "Cocos-Nazca" rift valley deepens eastward to >5400 m at Hess Deep, while its walls rise to about 2200 m. The EPR west of Hess Deep is spreading at a half-rate of 6.5 cm/yr (65 km/m.y.; Lonsdale, 1988). Approximately 50 km east of the EPR, the Cocos-Nazca Ridge begins to build a volcanic ridge on the rift valley floor, which matures to the east to a 2.5 cm/yr half-rate spreading center (Lonsdale, 1988). Multichannel seismic reflection data across Hess Deep and onto normally north-south lineated smooth Pacific crust formed at the EPR collected by Zonenshain et al. (1980) show highly disturbed crust beneath the valley floor. More typical, but variable thickness, crust occurs north and south of the edge of the V-shaped rift, with crustal thickness decreasing somewhat towards the flanks of the rift. The EPR crust is generally somewhat thinner than that normally calculated using simple layered crustal models (~6 km) averaging about 5 km, and ranging from 4 to 7 km.

French and U.S. submersibles (P. Lonsdale, unpubl. data, 1993; Francheteau et al., 1990; Hekinian et al., 1993; Karson et al., 1992) found a dismembered but apparently nearly complete composite section of EPR crust and shallow mantle exposed on the north wall of the rift valley and on an intrarift ridge between the northern rift valley wall and Hess Deep. A 1200-m-thick subvertical north-south striking sheeted dike complex, with 50–500 m of mixed extrusives and intrusives capped by 100–300 m of pillow lava is exposed on the north wall. Gabbros are also locally exposed beneath the sheeted dikes along this wall. The intrarift ridge, on the other hand, represents a foundered tectonic block of largely plutonic rock including dikes gabbros and massive serpentinized peridotites, exposed and locally uplifted during the opening of the rift.

The intrarift ridge is an elongated east-west oriented tectonic block-lying parallel to the axis of the Cocos-Nazca Ridge with eastern and western highs and an intervening saddle (Fig. 2). The *Nautila* made a series of south to north transects up and over the western and eastern highs. On the western transect, the rift valley sloped 15°–20° gently up from Hess Deep for 5–6 km. Gabbro and rare dunite crop out from 5400 to 4500 m, and diabase ledges occur between 4500 and 4000 m. From 4000 to 2900 m the slope steepens to form the south wall of the intrarift ridge. Gabbros crop out on both the north and south walls of the ridge, with an isolated basalt outcrop at the crest. Along the eastern transect mostly dunite and harzburgite are exposed in subhorizontal northward-dipping ledges with scattered outcrops of gabbroic rock along a gently dipping slope from 3500 to 4500 m. Pillow lavas and dikes are exposed over the crest of the ridge, and low-temperature hydrothermal activity was observed. In situ north-south dikes crop out on the north slope of the summit. Gabbros were dredged between the east and west *Nautila* transects. Large land-slip scars on the south wall of the intrarift ridge demonstrate significant local mass wasting. A disrupted magnetic stratigraphy, low recovery, and poor drilling conditions at at least one hole drilled during ODP Leg 147 (Hole 895D) likely reflect minor local slip and disruption of the section.

The distribution of rocks over the intrarift ridge indicates a complex internal structure (Hekinian et al., 1993); the result of unroofing and block emplacement during the opening of Hess Deep. Alternative models explaining the opening of Hess Deep and the exposure of

Table 4. Site 895 orthopyroxene compositions.

Hole	Core, section, interval (cm)	Gr.	Loc.	Pts.	Na ₂ O	MgO	Al ₂ O ₃	SiO ₂	CaO	TiO ₂	Cr ₂ O ₃	MnO	FeO	Total	Mg#	Wo	En	Fs
Harzburgites																		
895B	1R-1, 71–76	1		9	0.00	33.0	2.00	56.1	2.44	0.06	0.71	0.12	5.7	100.1	91.1	4.6	86.9	8.5
				sd	0.00	0.9	0.05	0.3	1.27	0.01	0.03	0.02	0.2	0.2	0.14	0.14	0.14	0.14
895B	1R-1, 71–76	2		10	0.00	32.7	2.04	56.1	2.49	0.05	0.71	0.13	5.7	100.0	91.1	4.7	86.8	8.5
				sd	0.00	0.8	0.03	0.2	1.10	0.01	0.02	0.02	0.2	0.2	0.10	0.10	0.10	0.10
895C	1R-1, 28–32	1		10	0.00	32.8	2.23	55.8	2.53	0.07	0.87	0.13	5.6	100.0	91.3	4.8	86.9	8.3
				sd	0.00	0.3	0.04	0.2	0.40	0.01	0.02	0.02	0.1	0.3	0.10	0.10	0.10	0.10
895C	3R-1, 35–39	1		10	0.00	33.2	2.16	56.1	1.91	0.07	0.73	0.14	6.0	100.3	90.8	3.6	87.5	8.9
				sd	0.00	0.2	0.02	0.1	0.17	0.01	0.02	0.02	0.1	0.2	0.08	0.08	0.08	0.08
895D	3R-1, 38–43	1	C	10	0.03	32.9	2.57	55.8	1.87	0.04	0.81	0.13	5.6	99.8	91.3	3.6	88.0	8.4
				sd	0.01	0.1	0.08	0.2	0.10	0.01	0.03	0.01	0.1	0.3	0.09	0.09	0.09	0.09
895D	3R-1, 38–43	1	R	10	0.03	33.3	2.36	56.3	1.40	0.03	0.71	0.14	5.9	100.2	91.0	2.7	88.5	8.8
				sd	0.01	0.1	0.04	0.2	0.03	0.01	0.02	0.01	0.0	0.2	0.07	0.07	0.07	0.07
895D	3R-1, 116–120	1		20	0.00	33.0	2.18	56.0	1.95	0.02	0.78	0.14	5.8	99.9	91.0	3.7	87.7	8.6
				sd	0.00	0.3	0.04	0.5	0.30	0.01	0.02	0.02	0.1	0.6	0.11	0.11	0.11	0.11
895D	4R-3, 97–101	1		10	0.00	32.4	2.19	55.9	2.45	0.02	0.78	0.15	5.6	99.6	91.1	4.7	86.8	8.4
				sd	0.00	0.1	0.06	0.2	0.22	0.01	0.01	0.02	0.1	0.2	0.09	0.09	0.09	0.09
895D	5R-2, 90–95	1		10	0.00	32.3	2.18	55.9	2.09	0.02	0.75	0.14	5.7	99.1	91.0	4.1	87.3	8.6
				sd	0.01	0.2	0.03	0.2	0.15	0.01	0.03	0.02	0.1	0.3	0.08	0.08	0.08	0.08
895D	7R-2, 129–133	1		10	0.00	32.7	2.10	56.1	2.24	0.02	0.75	0.15	5.7	99.8	91.1	4.3	87.2	8.6
				sd	0.00	0.2	0.03	0.2	0.36	0.01	0.03	0.02	0.1	0.2	0.11	0.11	0.11	0.11
895E	7R-4, 86–89	1		10	0.00	32.7	2.18	56.2	2.30	0.02	0.76	0.14	5.8	100.0	91.0	4.4	87.0	8.6
				sd	0.00	0.3	0.09	0.3	0.33	0.01	0.01	0.03	0.1	0.3	0.08	0.08	0.08	0.08
895F	1R-1, 11–16	1		10	0.00	32.8	2.08	56.2	2.13	0.02	0.70	0.14	5.8	99.9	91.0	4.1	87.3	8.7
				sd	0.00	0.1	0.03	0.1	0.16	0.01	0.01	0.01	0.1	0.2	0.06	0.06	0.06	0.06
Olivine gabbronorite																		
895C	4R-2, 108–112	1		10	0.03	32.1	2.08	56.5	2.12	0.21	0.66	0.16	6.8	100.6	89.4	4.1	85.8	10.2
				sd	0.01	0.3	0.05	0.3	0.44	0.03	0.02	0.05	0.1	0.4	0.11	0.9	0.77	0.14

Notes: Gr. = grain number. Loc. = location in grain (C = core or R = rim). Pts. = number of points analyzed; sd = one standard deviation. Mg# = molecular ratio: (Mg-100)/(Mg+Fe). Wollastonite, enstatite, and ferrosilite proportions computed with all iron as FeO.

Table 5. Site 895 clinopyroxene analyses.

Hole	Core, section, interval (cm)	Gr.	Loc.	Size	Pts.	Na ₂ O	MgO	Al ₂ O ₃	SiO ₂	CaO	TiO ₂	Cr ₂ O ₃	MnO	FeO	Total	Mg#	Wo	En	Fs	
Gabbro																				
895E	4R-3, 55-58	1	C		10	0.28	16.2	3.48	52.2	23.3	0.32	1.10	0.09	3.00	99.9	90.6	48.3	46.8	4.9	
						0.02	0.3	0.24	0.6	0.5	0.01	0.03	0.03	0.10	0.5	0.2	1.0	0.9	0.2	
895E	4R-3, 55-58	1	I		10	0.27	16.2	3.34	52.5	23.2	0.33	1.00	0.08	2.94	99.8	90.7	48.3	46.9	4.8	
						0.02	0.3	0.25	0.5	0.3	0.02	0.06	0.03	0.06	0.2	0.3	0.3	0.3	0.1	
895E	4R-3, 55-58	1	R		10	0.30	16.1	3.68	51.9	23.1	0.34	1.08	0.07	3.28	99.9	89.8	48.0	46.6	5.3	
						0.03	0.2	0.16	0.4	0.2	0.01	0.04	0.03	0.09	0.2	0.2	0.4	0.3	0.1	
Olivine gabbro																				
895D	8R-2, 6-9	1	C		10	0.31	16.4	4.21	51.4	22.3	0.30	1.23	0.10	3.37	99.7	89.7	46.7	47.8	5.5	
						0.05	0.5	0.56	0.8	1.0	0.02	0.06	0.03	0.29	0.6	0.5	2.0	1.5	0.5	
895D	8R-2, 6-9	1	R		10	0.27	15.9	3.28	52.0	23.2	0.52	1.05	0.14	3.69	100.0	88.5	48.1	45.9	6.0	
						0.03	0.2	0.39	0.5	0.4	0.06	0.08	0.03	0.10	0.3	0.4	0.6	0.7	0.2	
895D	9R-2, 60-65B	1	C		10	0.27	16.2	3.78	51.5	22.6	0.30	1.18	0.11	2.96	98.9	90.7	47.6	47.5	4.9	
						0.02	0.3	0.27	0.5	0.4	0.01	0.08	0.03	0.20	0.9	0.7	0.7	0.8	0.3	
895D	9R-2, 60-65B	1	R		10	0.30	16.3	2.89	52.7	23.2	0.32	1.10	0.14	3.56	100.5	89.1	47.8	46.5	5.7	
						0.03	0.2	0.29	0.3	0.3	0.03	0.08	0.02	0.12	0.3	0.3	0.6	0.5	0.2	
895E	5R-1, 23-26	1	C		7	0.27	17.5	3.33	51.9	21.4	0.29	0.92	0.11	3.52	99.3	89.9	44.0	50.3	5.7	
						0.04	0.8	0.63	1.1	1.1	0.04	0.15	0.02	0.16	0.8	0.7	2.2	2.3	0.3	
895E	5R-1, 23-26	1	R		10	0.24	16.9	2.96	51.7	22.7	0.40	0.95	0.11	3.66	99.6	89.2	46.3	47.9	5.8	
						0.03	0.3	0.25	0.2	0.4	0.06	0.06	0.04	0.07	0.3	0.3	0.8	0.8	0.1	
Olivine gabbro																				
895C	4R-2, 108-112	1	C		10	0.27	18.4	3.57	52.6	20.2	0.29	1.40	0.11	3.71	100.6	89.9	41.5	52.6	5.9	
						0.03	1.0	0.03	0.2	1.4	0.00	0.02	0.03	0.35	0.3	0.4	3.1	2.6	0.5	
895C	4R-2, 108-112	1	R		10	0.40	16.4	3.39	52.2	22.9	0.35	1.33	0.14	3.31	100.3	89.8	47.5	47.2	5.4	
						0.05	0.2	0.19	0.3	0.3	0.02	0.06	0.02	0.18	0.3	0.5	0.6	0.5	0.3	
Troctolitic gabbro																				
895D	7R-2, 61-63	1	C		10	0.40	16.1	4.06	50.4	22.3	1.36	1.08	0.13	3.59	99.4	88.9	46.9	47.2	5.9	
						0.02	0.2	0.12	0.2	0.2	0.05	0.05	0.02	0.20	0.2	0.6	0.5	0.5	0.3	
895D	7R-2, 61-63	1	R		10	0.39	16.8	4.26	50.1	21.3	1.24	1.08	0.14	3.87	99.2	88.6	44.5	49.1	6.3	
						0.05	1.1	1.35	2.1	2.3	0.22	0.14	0.03	0.56	1.7	0.9	4.5	3.6	1.0	
895D	7R-2, 61-63	2			10	0.41	16.4	3.45	51.6	22.6	1.19	1.08	0.13	3.52	100.4	89.3	46.9	47.4	5.7	
						0.03	0.3	0.17	0.3	0.3	0.06	0.03	0.03	0.15	0.2	0.5	0.8	0.8	0.2	
Troctolite																				
895C	4R-2, 62-65	1	C	1.13	0.57	10	0.34	17.6	3.16	52.6	21.5	0.55	1.19	0.11	3.41	100.4	90.2	44.2	50.4	5.5
						0.02	0.3	0.04	0.2	0.5	0.05	0.04	0.04	0.18	0.3	0.3	1.0	0.8	0.3	
895C	4R-2, 62-65	1	R	1.13	0.57	10	0.25	17.0	2.16	53.3	24.0	0.61	0.53	0.10	2.66	100.6	92.0	48.2	47.6	4.2
						0.10	0.2	0.57	0.6	0.6	0.16	0.18	0.02	0.29	0.2	0.9	0.8	0.4	0.5	
895C	4R-2, 62-65	2		3.10	0.06	10	0.38	16.5	3.31	51.9	23.4	0.95	1.06	0.12	2.96	100.6	90.9	48.0	47.3	4.7
						0.06	0.4	0.44	0.4	0.4	0.14	0.16	0.02	0.13	0.3	0.4	0.8	0.8	0.2	
Plagioclase-bearing dunite																				
895C	4R-3, 32-35	4		0.80	0.14	10	0.53	16.6	2.86	53.0	23.0	0.56	1.14	0.10	2.74	100.6	91.5	47.7	47.8	4.4
						0.05	0.1	0.15	0.3	0.2	0.02	0.07	0.02	0.09	0.3	0.2	0.4	0.3	0.1	
895C	4R-3, 32-35	5	R	0.51	0.26	10	0.45	16.6	3.11	52.2	23.4	0.62	1.24	0.09	2.77	100.5	91.4	48.1	47.5	4.4
						0.03	0.1	0.05	0.3	0.5	0.04	0.03	0.02	0.14	0.2	0.4	0.7	0.5	0.2	
Harzburgite																				
895B	1R-1, 71-76	1		0.33	0.06	10	0.00	18.0	2.58	53.2	22.6	0.01	1.05	0.10	2.73	100.3	92.1	45.5	50.2	4.3
						0.01	0.3	0.05	0.6	0.4	0.01	0.03	0.02	0.10	0.4	0.2	0.8	0.7	0.1	
895B	1R-1, 71-76	2			10	0.00	18.5	2.76	52.9	21.9	0.02	1.09	0.09	2.86	100.1	92.0	44.0	51.5	4.5	
						0.01	0.4	0.10	0.2	0.7	0.01	0.04	0.02	0.13	0.3	0.2	1.4	1.2	0.2	
895C	1R-1, 28-32	1	C	0.93	0.87	10	0.00	17.8	3.23	52.2	22.6	0.02	1.44	0.09	2.77	100.0	91.9	45.6	50.0	4.4
						0.00	0.3	0.09	0.2	0.5	0.01	0.02	0.02	0.09	0.2	0.1	1.0	0.9	0.1	
895C	1R-1, 28-32	1	R	0.93	0.87	10	0.00	17.9	2.95	52.1	22.8	0.01	1.19	0.10	2.65	99.7	92.3	45.9	49.9	4.2
						0.00	0.2	0.05	0.2	0.3	0.01	0.04	0.02	0.03	0.4	0.1	0.5	0.6	0.1	
895C	1R-1, 28-32	2		0.35	0.18	10	0.00	18.0	2.70	52.5	22.7	0.02	1.09	0.10	2.65	99.8	92.4	45.6	50.3	4.1
						0.00	0.2	0.10	0.2	0.3	0.01	0.08	0.01	0.07	0.2	0.2	0.6	0.5	0.1	
895C	3R-1, 35-39	1		0.50	0.15	10	0.01	17.9	2.57	52.7	22.9	0.02	0.95	0.11	2.81	100.0	91.9	45.7	49.9	4.4
						0.01	0.2	0.10	0.4	0.4	0.01	0.04	0.02	0.20	0.3	0.5	0.8	0.5	0.3	
895C	3R-1, 35-39	2	R		10	0.00	18.3	2.73	52.9	22.0	0.02	1.07	0.10	2.95	100.0	91.7	44.1	51.2	4.6	
						0.00	0.1	0.10	0.2	0.1	0.01	0.06	0.02	0.05	0.3	0.1	0.2	0.2	0.1	
895C	3R-1, 35-39	2	C		9	0.00	18.3	2.96	52.3	22.0	0.02	1.24	0.10	2.97	99.9	91.6	44.2	51.1	4.7	
						0.01	0.1	0.06	0.2	0.1	0.01	0.03	0.02	0.05	0.2	0.1	0.2	0.2	0.1	
895D	3R-1, 38-43	1		0.22	0.20	10	0.35	17.7	3.16	52.3	21.9	0.04	1.20	0.10	2.73	99.5	92.0	44.9	50.7	4.4
						0.05	0.3	0.08	0.2	0.4	0.01	0.03	0.03	0.12	0.2	0.3	0.8	0.7	0.2	
895D	3R-1, 116-120	1	C	0.36	0.32	10	0.00	18.5	2.96	51.8	21.8	0.01	1.20	0.11	2.78	99.2	92.2	43.8	51.8	4.4
						0.01	0.3	0.12	0.3	0.3	0.01	0.04	0.01	0.13	0.3	0.3	0.8	0.6	0.2	
895D	3R-1, 116-120	1	R	0.36	0.32	10	0.00	18.6	2.82	51.6	21.6	0.02	1.10	0.10	2.82	98.6	92.2	43.5	52.1	4.4
						0.01	0.4	0.14	0.7	0.5	0.01	0.04	0.02	0.13	1.3	0.3	0.7	0.5	0.2	
895D																				

Table 5 (continued).

Hole	Core, section, interval (cm)	Gr.	Loc.	Size	Pts.	Na ₂ O	MgO	Al ₂ O ₃	SiO ₂	CaO	TiO ₂	Cr ₂ O ₃	MnO	FeO	Total	Mg#	Wo	En	Fs
895E	7R-4, 86-89	1	R	0.70 0.72	10	0.01 0.02	18.4 0.3	2.94 0.06	53.1 0.2	22.3 0.5	0.03 0.02	1.17 0.04	0.08 0.03	2.55 0.08	100.6 0.3	92.8 0.2	44.7 0.9	51.3 0.8	4.0 0.1
895F	1R-1, 11-16	1	C	1.05 0.80	9	0.01 0.02	18.4 0.2	3.22 0.07	52.9 0.4	22.1 0.3	0.04 0.02	1.30 0.03	0.09 0.03	2.65 0.09	100.7 0.4	92.5 0.2	44.4 0.5	51.4 0.4	4.2 0.2
895F	1R-1, 11-16	1	R	1.05 0.80	10	0.01 0.01	18.3 0.2	2.55 0.07	54.2 0.3	22.9 0.4	0.04 0.03	1.00 0.04	0.08 0.03	2.49 0.14	101.6 0.3	92.9 0.3	45.4 0.8	50.7 0.6	3.9 0.2
895F	2R-2, 73-80	1		1.00 0.30	10	0.11 0.02	19.4 0.5	2.93 0.16	52.9 0.6	20.9 0.9	0.03 0.02	1.26 0.05	0.07 0.02	2.95 0.17	100.6 0.6	92.1 0.3	41.7 1.6	53.7 1.4	4.6 0.3

Notes: Gr. = grain number. Loc. = location in grain (C = core, R = rim, I = interior). Size = maximum length and width of grain analyzed given in millimeters; Pts. = number of points analyzed. Mg# = molecular ratio: (Mg/100)/(Mg+Fe). Wollastonite, enstatite, and ferrosilite proportions computed with all iron as FeO.

plutonic rocks along the intrarift ridge emphasize vertical movement of mantle horsts or serpentine diapirs, and low-angle faulting, respectively (Francheteau et al., 1990). On-bottom gravity and seismic data from the intrarift ridge, however, indicate that it is a high-density high-velocity block (L. Dorman and J. Hildebrand, pers. comm., 1993), which seems to preclude emplacement by serpentine diapirism.

Site 895 is located on the intrarift ridge 9 km to the east of Hole 894G between 3821 and 3693 m, near the eastern *Nautile* transect (Fig. 2). Harzburgite tectonites were recovered with dunite and related gabbroic rocks from six holes on the south flank of the high there (Fig. 3). In all, 272.9 m was drilled, with an average recovery of 23.5%, ranging from 7.7% in Hole 895F to 37.6% in Hole 895E. Holes 895A to 895D are within 50 m of one another. Significant penetrations occurred only in Holes 895C and 895D (37.6 and 93.7 m). Holes 895E and 895F were drilled 270 and 570 m, respectively, to the north, directly up slope, penetrating 87.6 and 26.2 m. These rocks are similar to the mantle transition zone in many ophiolite complexes, and were interpreted by the Leg 147 scientific party as lying close to the crust-mantle boundary (Gillis, Mével, Allan, et al., 1993).

The *JOIDES Resolution* (SEDCO/BP 471) also drilled at Site 894 on the crest of the intrarift ridge near the western *Nautile* transect during Leg 147 (Fig. 2). Although many test holes were drilled at Site 894, only Hole 894G attempted and made significant penetration into the block (154 m) recovering 45.8 m of fine- to medium-grained gabbroic rock, mostly gabbro. These rocks, though geochemically cumulates (not representing melt compositions), are not layered. Coarse-grained intervals were generally found as small irregular patches, subvertical lenses and pipes, often containing abundant ilmenite, apatite, and zircon. The section closely resembles gabbroic rocks seen in the upper parts of many plutonic sequences in ophiolites (Gillis, Mével, Allan, et al., 1993). Several dikes were drilled at Site 894 in chilled contact with gabbro, a feature also frequently seen in high-level gabbro suites in ophiolites. The Hole 894G gabbros, however, entirely lack evidence for high-temperature ductile deformation and dynamic alteration which is prominent in gabbros formed at slow-spreading ridges (Dick et al., 1991a; Dick et al., 1992; Stakes et al., 1991). Rather, the Site 894 gabbros exhibit an initial phase of pervasive static amphibolitization beginning at temperatures around 750°C, and a later phase of lower temperature greenschist facies alteration attributed to hydrothermal circulation accompanying the propagation of the Cocos-Nazca Rift and the opening of Hess Deep (Gillis, Mével, Allan, et al., 1993; Manning and MacLeod, this volume). Natland and Dick (this volume) interpret the Site 894 gabbroic sequence as representing a series of small intrusions emplaced immediately beneath the shallow "melt lens" believed to exist beneath the sheeted dikes at the EPR (e.g., Sinton and Detrick, 1992).

It is important to note that the EPR crust that extends to the edge of the Cocos-Nazca rift some 9 km north of Site 895 is normally north-south lineated parallel to the present-day EPR, as is much of the present-day seafloor immediately west of the tip of the amagmatic Cocos Nazca rift valley. As there has been considerable north-south extension of the original EPR crustal section due to opening of Hess

Deep, the present-day wall of the rift valley north of the intrarift ridge likely represents a point on the paleo-EPR close to that at which the Site 895 peridotites were originally emplaced. This suggests that the initial formation of the EPR crust broken open at Hess Deep reflects only the stress field of the paleo EPR, and was not directly and immediately influenced by the Cocos-Nazca propagator.

SITE 895 STRATIGRAPHY

Hole stratigraphies are reported here on the basis of "expanded recovery." When there is only partial recovery from a drill hole, there are two approaches to reporting the relative abundances of lithologies. One is to assume that the partial recovery from each cored interval is representative of the interval as a whole, and that by treating each core as a separate sampling interval, the overall distribution and abundance of lithologies can be best interpolated. For this approach, the actual recovery is expanded statistically to fill the entire cored interval, and each interval is then weighted based on its length in reconstructing the stratigraphy of the entire hole. The other approach makes the assumption that the recovery from the entire hole is representative of all the lithologies drilled and disregards the sampling information provided by stopping drilling and retrieving core at regularly spaced intervals. Many factors control recovery. These include external mechanical factors such as fluid pressure, bit type, and bit life at the time a section of the hole is drilled; geologic conditions including the nature and grain size of the lithology and the extent of alteration and formation cementation; and drilling conditions such as overall hole stability and sea-state. It is unrealistic, therefore to assume constant conditions over the course of drilling an entire hole, or even that recovery from the same lithology will be constant with time.

Accordingly we believe that utilizing the sampling information provided by individual drilling intervals, and weighing the recovery by the length of the cored interval provides the best approximation to the actual stratigraphy. In particular, we draw attention to the similarity of the expanded recoveries in Holes 895A to 895D, all of which were drilled within 50 m of each other at the same location. Despite depths ranging from less than 10 m to 94 m, the relative proportions of the rock types as calculated from expanded recoveries varies little between these holes. This would appear to justify to some degree our use of expanded recoveries in reconstructing the stratigraphy. There is, however, no substitute for 100% recovery, and it is realistic to consider the data provided in Figure 3 as only a starting point for interpreting the geologic relationships at Site 895.

In all, 50 dunites, 16 troctolites, 10 olivine gabbros, and 12 gabbros, intercalated with harzburgite tectonite, were drilled at Site 895. The thickness of individual dunites averages 0.6 m in Hole 895D and 1.9 m in Hole 895E, occurring in units up to 12 m, or if gabbroic segregations are ignored, up to 18 m in Hole 895E. Gabbros and troctolites range from 0.5 to 2 m thick, with a few intervals up to 7 m thick. Actual unit thicknesses, given the steep orientation of the few intact contacts, are likely half that measured vertically. The harzburgite in-

Table 6. Site 895 spinel compositions.

Hole	Core, section, interval (cm)	Rock type	Gr.	Size	Pts.	MgO	Al ₂ O ₃	SiO ₂	CaO	TiO ₂	Cr ₂ O ₃	MnO	FeO*	NiO	FeO	Fe ₂ O ₃	Total*	Total	Fe ³⁺ #	Mg#	Cr#	
895E	3R-1, 21-23	Gabbro?	1	0.30	0.20	5	13.5	21.8	0.00	0.09	1.08	44.1	0.28	18.7	0.20	15.2	3.90	99.8	100.2	4.6	61.2	57.6
						sd	0.6	0.5	0.00	0.02	0.03	0.4	0.02	0.6	0.02	0.9	0.71	0.2	0.2	0.8	2.4	0.8
895E	3R-1, 21-23	Gabbro?	2	0.70	0.30	5	13.6	23.7	0.00	0.08	0.93	42.5	0.28	19.1	0.20	15.4	4.13	100.5	100.9	4.8	60.8	54.6
						sd	3.4	1.6	0.00	0.00	0.04	0.9	0.06	3.8	0.02	4.7	1.00	0.4	0.5	1.1	13.7	2.2
895C	4R-2, 108-112	Olivine gabbro	1	1.70	1.50	9	12.7	21.3	0.00	0.10	1.14	40.9	0.37	22.9	0.37	16.2	7.41	99.8	100.5	8.8	58.2	56.3
						sd	0.3	0.4	0.00	0.02	0.04	0.4	0.04	0.5	0.05	0.4	0.38	0.5	0.5	0.4	1.1	0.7
895E	5R-1, 23-26	Olivine gabbro	1	0.30	0.20	3	12.0	19.5	0.00	0.08	1.49	41.3	0.39	24.7	0.34	17.3	8.19	99.8	100.6	10.0	55.3	58.7
						sd	0.4	0.6	0.00	0.01	0.01	0.9	0.03	0.3	0.02	0.6	0.47	0.1	0.0	0.5	1.7	1.3
895E	5R-1, 23-26	Olivine gabbro	2	0.10	0.10	3	13.0	23.2	0.00	0.07	1.29	37.9	0.35	24.7	0.33	16.6	9.03	100.8	101.7	10.6	58.4	52.2
						sd	0.2	1.4	0.00	0.01	0.02	2.0	0.01	0.2	0.06	0.2	0.43	0.3	0.2	0.4	0.7	2.8
895D	7R-2, 61-63	Troctolitic gabbro	1	0.10	0.10	3	8.6	16.8	0.00	0.09	2.42	40.8	0.45	29.7	0.41	22.6	7.84	99.2	100.0	10.2	40.4	62.0
						sd	0.1	0.1	0.00	0.01	0.07	0.2	0.01	0.2	0.03	0.2	0.06	0.3	0.3	0.1	0.4	0.4
895D	7R-2, 61-63	Troctolitic gabbro	2	0.07	0.07	3	9.6	18.7	0.00	0.15	2.82	39.1	0.37	28.3	0.45	21.8	7.22	99.4	100.1	9.3	43.8	58.4
						sd	0.2	0.4	0.00	0.03	0.14	0.1	0.02	0.5	0.02	0.4	0.36	0.2	0.3	0.5	0.8	0.6
895D	7R-1, 99-101a	Troctolite, m. gr.	3			3	1.0	0.0	1.18	0.67	0.88	11.0	0.47	74.8	0.57	28.9	51.03	90.6	95.7	81.3	5.6	100.0
						sd	0.8	0.0	1.46	0.34	0.08	6.9	0.10	7.2	0.05	1.0	9.03	2.7	1.9	12.2	3.9	0.0
895D	7R-1, 99-101a	Troctolite, m. gr.	2	0.12	0.12	3	9.7	17.1	0.00	0.09	1.58	45.6	0.38	24.8	0.22	20.6	4.65	99.4	99.9	5.9	45.6	64.2
						sd	0.1	0.0	0.00	0.01	0.02	0.2	0.01	0.2	0.01	0.1	0.14	0.2	0.2	0.2	0.3	0.1
895D	7R-1, 99-101b	Troctolite, c. gr.	1	0.10	0.10	3	9.9	14.2	0.00	0.09	1.73	48.5	0.36	24.2	0.23	19.9	4.81	99.1	99.6	6.2	47.0	69.6
						sd	0.2	0.1	0.00	0.00	0.24	0.5	0.02	0.1	0.02	0.3	0.28	0.9	0.8	0.4	0.4	0.4
895D	7R-2, 58-61	Troctolite, c. gr.	1	0.17	0.16	5	11.6	19.2	0.00	0.01	3.21	38.7	0.30	25.8	0.20	19.5	7.00	99.0	99.7	9.0	51.5	57.4
						sd	0.1	0.4	0.01	0.01	0.15	0.2	0.02	0.4	0.02	0.3	0.26	0.4	0.4	0.3	0.6	0.6
895C	4R-2, 102-105a	Troctolite, c. gr.	1	0.15	0.20	3	10.4	18.3	0.13	0.00	1.71	40.5	0.27	28.4	0.22	20.4	8.87	99.9	100.7	11.1	47.5	59.7
						sd	0.2	0.4	0.04	0.00	0.03	0.0	0.01	0.3	0.03	0.2	0.35	0.5	0.6	0.4	0.7	0.5
895C	4R-2, 102-105c	Troctolite, c. gr.	2	0.80	0.50	5	11.0	18.1	0.13	0.00	2.46	39.7	0.24	28.6	0.25	20.2	9.28	100.4	101.3	11.7	49.2	59.6
						sd	0.6	0.4	0.00	0.00	0.21	0.2	0.01	0.5	0.02	0.8	0.33	0.2	0.2	0.4	2.4	0.6
895C	4R-3, 32-35	Plagioclase dunite	1	0.65	0.45	5	12.0	21.0	0.00	0.01	1.10	41.2	0.30	23.2	0.15	17.3	6.51	99.0	99.6	7.9	55.2	56.8
						sd	0.1	0.5	0.00	0.01	0.04	0.4	0.02	0.1	0.01	0.2	0.14	0.3	0.3	0.2	0.5	0.8
895D	7R-1, 5-9	Dunite	2	0.30	0.30	8	11.4	18.6	0.00	0.08	2.06	42.6	0.33	24.5	0.25	18.8	6.35	99.7	100.4	7.9	51.9	60.6
						sd	0.8	0.7	0.00	0.01	0.04	0.6	0.01	1.5	0.02	1.1	0.60	0.2	0.2	0.8	3.2	1.0
895D	8R-2, 139-144	Dunite	1	2.90	1.00	5	14.3	23.9	0.00	0.07	0.63	40.5	0.31	19.5	0.32	13.7	6.42	99.5	100.1	7.4	65.0	53.2
						sd	0.4	0.8	0.00	0.00	0.01	0.3	0.02	1.1	0.06	0.4	0.74	0.4	0.4	0.9	1.4	0.7
895E	1R-3, 32-36	Dunite	1	0.40	0.40	4	13.8	23.4	0.00	0.07	0.43	40.5	0.33	20.9	0.36	14.3	7.32	99.8	100.5	8.5	63.3	53.7
						sd	0.2	0.7	0.00	0.00	0.01	0.6	0.01	0.1	0.05	0.3	0.26	0.4	0.4	0.3	0.8	1.1
895E	1R-3, 32-36	Dunite	2	1.20	0.60	4	3.1	0.6	1.26	0.11	0.54	38.4	0.66	51.5	0.44	27.7	26.47	96.6	99.3	39.1	16.6	97.7
						sd	0.3	0.2	0.27	0.01	0.01	0.6	0.03	0.6	0.03	0.4	0.34	0.2	0.2	0.7	1.7	0.7
895E	3R-1, 21-23	Dunite	1	0.70	0.30	5	12.7	21.7	0.00	0.08	0.89	41.5	0.30	22.0	0.23	16.1	6.56	99.4	100.1	7.8	58.5	56.2
						sd	0.5	0.3	0.00	0.01	0.02	0.4	0.01	0.3	0.01	0.5	0.62	0.8	0.8	0.7	1.6	0.5
895E	8R-4, 4-7	Dunite	1	1.70	0.70	5	12.8	24.4	0.00	0.08	0.71	39.3	0.34	21.9	0.32	16.3	6.31	99.9	100.5	7.3	58.2	52.0
						sd	2.4	1.6	0.00	0.01	0.02	1.3	0.03	3.0	0.06	3.5	0.77	0.2	0.2	0.8	10.0	2.4
895B	1R-1, 71-76	Harzburgite	1	0.54	0.95	5	14.3	24.9	0.01	0.00	0.06	43.1	0.22	16.2	0.11	13.6	2.90	98.8	99.1	3.3	65.2	53.7
						sd	0.4	0.4	0.01	0.00	0.00	0.1	0.01	0.2	0.01	0.7	0.54	0.2	0.2	0.6	1.9	0.4
895C	1R-1, 28-32	Harzburgite	1	0.70	0.70	5	15.0	24.0	0.06	0.01	0.05	42.6	0.24	17.7	0.25	12.6	5.67	99.9	100.5	6.4	67.8	54.4
						sd	0.1	0.1	0.02	0.01	0.02	0.2	0.02	0.1	0.06	0.1	0.17	0.3	0.3	0.2	0.3	0.2
895C	3R-1, 35-39	Harzburgite	1	1.18	0.58	5	14.1	24.9	0.01	0.00	0.08	42.5	0.21	17.5	0.11	14.0	3.81	99.3	99.7	4.4	64.1	53.4
						sd	0.3	0.0	0.01	0.00	0.01	0.2	0.02	0.1	0.02	0.3	0.42	0.4	0.5	0.5	0.9	0.1
895D	3R-1, 38-43	Harzburgite	1	0.44	0.33	7	15.9	28.7	0.00	0.07	0.22	39.0	0.24	15.5	0.18	11.9	3.93	99.9	100.3	4.4	70.4	47.7
						sd	0.3	0.1	0.00	0.01	0.01	0.4	0.02	0.2	0.02	0.3	0.38	0.5	0.5	0.4	1.0	0.2
895D	3R-1, 116-120	Harzburgite	1	1.35	0.65	5	15.0	24.9	0.00	0.00	0.06	43.5	0.21	15.5	0.11	12.6	3.27	99.3	99.7	3.7	68.0	54.0
						sd	0.1	0.1	0.00	0.00	0.01	0.2	0.01	0.1	0.00	0.1	0.20	0.4	0.4	0.2	0.4	0.2
895D	4R-3, 97-101	Harzburgite	1	0.25	0.02	3	14.0	24.0	0.04	0.17	0.21	42.7	0.31	17.3	0.30	13.7	4.06	99.1	99.5	4.7	64.6	54.4
						sd	0.2	0.7	0.06	0.10	0.01	0.2	0.03	0.4	0.03	0.4	0.69	0.3	0.2	0.8	0.9	0.6
895D	4R-3, 97-101	Harzburgite	2	0.30	0.30	5	14.6	23.3	0.00	0.07	0.21	44.3	0.31	16.5	0.30	12.9	4.08	99.6	100.0	4.7	66.9	56.0
						sd	0.4	0.4	0.00	0.01	0.01	0.2	0.02	0.2	0.07	0.7	0.65	0.3	0.3	0.7	1.8	0.5
895D	5R-2, 90-95	Harzburgite	1	0.65	0.55	7	15.2	24.6	0.02	0.09	0.21	42.7	0.27	16.6	0.17	12.4	4.73	99.8	100.3	5.4	68.6	53.8
						sd	0.2	0.3	0.06	0.04	0.01	0.2	0.02	0.2	0.03	0.3	0.24	0				

Table 7. Site 895 plagioclase analyses.

Hole	Core, section, interval (cm)	Rock type	Gr.	Size	Pts.	Na ₂ O	MgO	Al ₂ O ₃	SiO ₂	CaO	FeO	K ₂ O	Total	An	Ab	Or	
895D	9R-2a, 60-65	Gabbro	1e	3.4	1.5	5	1.65	0.10	33.6	47.1	16.9	0.05	99.4	84.6	14.9	0.5	
						sd	0.05	0.03	0.2	0.1	0.2	0.05	0.2	0.4	0.4	0.1	
895E	4R-3, 55-58	Gabbro	1e	10.0	5.0	5	0.53	0.02	35.8	44.2	19.0	0.00	99.5	95.0	4.8	0.2	
						sd	0.11	0.02	0.3	0.2	0.00	0.03	0.4	1.1	1.0	0.2	
895C	4R-2, 102-105	Gabbro	1i	7.5	6.0	9	1.59	0.07	34.0	46.7	17.1	0.02	99.6	85.3	14.3	0.4	
						sd	0.20	0.02	0.3	0.4	0.03	0.05	0.3	2.0	1.8	0.3	
895D	8R-2, 6-9	Olivine gabbro	2c	0.5	0.5	3	0.24	0.01	36.5	43.8	19.7	0.11	100.4	97.8	2.1	0.1	
						sd	0.11	0.02	0.2	0.3	0.2	0.10	0.3	1.0	0.9	0.1	
895D	8R-2, 6-9	Olivine gabbro	1e	3.0	2.0	5	0.34	0.02	36.3	44.2	19.6	0.07	100.6	96.9	3.0	0.1	
						sd	0.12	0.01	0.2	0.5	0.2	0.12	0.4	1.1	1.1	0.1	
895D	9R-2b, 60-65	Olivine gabbro	2e	3.0	5.0	5	0.38	0.01	36.3	44.0	19.6	0.04	100.4	96.5	3.4	0.1	
						sd	0.18	0.01	0.6	0.2	0.3	0.04	0.7	1.5	1.6	0.1	
895D	9R-2C, 60-65	Olivine gabbro	1e	4.4	3.5	5	0.26	0.05	36.1	43.7	19.5	0.00	99.7	97.4	2.4	0.2	
						sd	0.04	0.05	0.4	0.3	0.2	0.01	0.7	0.3	0.4	0.1	
895E	2R-1, 51-54	Olivine gabbro	1e	2.4	2.1	5	0.16	0.02	36.2	43.6	19.6	0.00	99.7	98.2	1.4	0.4	
						sd	0.04	0.02	0.4	0.3	0.2	0.00	0.6	0.4	0.3	0.1	
895E	5R-1, 23-26	Olivine gabbro	1e	4.8	3.5	5	1.58	0.10	34.1	47.1	17.3	0.23	100.4	85.6	14.2	0.2	
						sd	0.23	0.04	0.5	0.6	0.2	0.04	0.3	1.9	1.9	0.1	
895D	9R-2b, 60-65	Olivine gabbro?	1c	0.7	0.6	3	2.14	0.02	33.4	48.2	16.4	0.20	100.4	80.9	19.1	0.0	
						sd	0.24	0.03	0.3	0.6	0.4	0.01	0.3	2.1	2.1	0.0	
895E	4R-3, 16-22	Olivine? gabbro	1e	5.0	4.0	5	0.37	0.22	35.4	43.8	19.1	0.00	99.3	94.2	3.3	2.5	
						sd	0.16	0.48	0.2	0.6	0.4	0.00	0.79	0.5	3.6	1.5	4.4
895C	4R-2, 108-112	Olivine gabbro	1f			6	1.75	0.05	33.9	47.1	17.1	0.21	100.2	84.2	15.6	0.2	
						sd	0.12	0.01	0.3	0.4	0.3	0.03	0.1	0.3	1.1	1.1	0.0
895D	7R-2, 61-63	Troctolite gabbro	1e	1.4	1.2	5	2.45	0.06	32.9	48.9	15.9	0.20	100.4	78.0	21.8	0.2	
						sd	0.34	0.02	0.5	0.9	0.6	0.03	0.1	0.3	2.9	3.0	0.1
895C	4R-2, 62-65	Troctolite	1e			6	1.73	0.06	34.0	47.2	17.0	0.23	100.3	84.4	15.5	0.1	
						sd	0.21	0.02	0.3	0.4	0.2	0.03	0.1	0.2	1.7	1.7	0.1
895D	7R-1, 99-101	Troctolite c. gr.	2e	1.8	1.2	5	1.51	0.13	34.0	47.1	17.3	0.01	100.2	86.0	13.5	0.5	
						sd	0.05	0.02	0.4	0.5	0.1	0.02	0.6	0.6	0.5	0.1	
895E	3R-1, 21-23	Troctolite c. gr.	1e	9.0	7.0	5	1.50	0.15	33.6	46.7	17.4	0.00	99.6	86.1	13.4	0.5	
						sd	0.09	0.03	0.4	0.3	0.2	0.00	0.6	0.8	0.7	0.3	
895D	7R-1, 5-9	Troctolite m. gr.	1e	3.8	1.7	5	1.42	0.09	34.2	46.9	17.3	0.00	100.0	86.7	12.9	0.5	
						sd	0.13	0.03	0.5	0.1	0.2	0.01	0.5	1.0	1.1	0.1	
895D	7R-1, 99-101	Troctolite m. gr.	1e	2.4	1.5	5	1.89	0.12	33.8	48.1	16.4	0.00	100.4	82.4	17.1	0.5	
						sd	0.14	0.02	0.6	0.8	0.2	0.00	0.4	1.2	1.2	0.2	
895C	4R-3, 32-35	Plagioclase dunite	1e			5	1.49	0.03	34.0	46.6	17.4	0.15	99.6	86.5	13.4	0.1	
						sd	0.04	0.01	0.2	0.4	0.2	0.04	0.2	0.5	0.5	0.1	
895C	4R-3, 32-35	Plagioclase dunite	2f			6	1.57	0.04	34.2	46.7	17.4	0.22	100.2	85.9	14.0	0.1	
						sd	0.11	0.01	0.2	0.2	0.04	0.01	0.3	0.9	0.9	0.1	

Notes: Gr. = grain number. Size = maximum length and width of grain analyzed, given in millimeters. Pts. = number of points analyzed; sd = one standard deviation. c. gr. = coarse grained; m. gr. = medium grained. An = molecular ratio of Ca/(Ca+Na+K). Ab = molecular ratio Na/(Ca+Na+K). Or = molecular ratio K/(Ca+Na+K).

tervals vary considerably in thickness, forming screens of depleted mantle peridotite between crosscutting subvertical dunite and gabbroic "dikes."

Contacts between harzburgite and dunite, between dunite and the gabbroic rocks, and between different gabbros are either gradational over 10 cm or less, or sharp with a sutured igneous contact. Where orientation was preserved, they are generally steep, averaging close to 70°. Contacts that could be reoriented paleomagnetically were subvertical with a strike similar to the subvertical magmatic foliations of Hole 894G gabbroites (Gillis, Mével, Allan, et al., 1993). These orientations differ from those associated with the Hess Deep opening, which is east-west, nearly orthogonal to the EPR, and can be related directly to the north-south EPR stress field (MacLeod, Célérier, et al., this volume). Thus, the Site 895 peridotite gabbro sequence, and the Site 894 gabbroites, despite very different stratigraphic positions and a 9-km offset along the intrarift ridge, reflect deep and shallow melt transport, respectively, controlled by the same stress field beneath the EPR.

The reconstructed stratigraphy at each location drilled at Site 895 is strikingly different (Fig. 3). Holes 895A to 895D have expanded recoveries of 76.9% harzburgite-tectonite, 7.7% dunite, 11.7% gabbroic rocks, and 3.7% rodingitized basaltic dikes of probable Cocos Nazca origin. Hole 895E, on the other hand, recovered only 13.5% harzburgite, 65.2% dunite, and 21.4% gabbros, and Hole 895F recovered only harzburgite.

The recovery is high enough to reconstruct the likely original relationships between lithologies. Where preserved, both modal and lithologic contacts appear planar and are often quite steep. Gabbroic segregations were almost always recovered in association with dunite, which often is found as core fragments both above and below the

gabbroic rocks. Where contacts are preserved, gabbro is generally in contact with dunite, not harzburgite. Only one 2-cm gabbro seam was found directly in contact with harzburgite; otherwise, harzburgite occurs next to gabbroic rocks only where there is a missing interval in the recovery. A consistent sequence was observed during description of the core on board ship, which may be present in all or part at any one location. This sequence consists of harzburgite tectonite enclosing dunite, followed by dunite enclosing troctolite, followed by olivine-gabbro, then gabbro and in some cases gabbroite (Fig. 4). Many dunites crosscutting the harzburgite, however, do not contain gabbroic segregations (Fig. 3).

Dunite formation in harzburgites is commonly associated with late focused flow of melt through the mantle. As will be discussed later, the similarity of these dunites to those in many ophiolites, the structure and chemistry of the gabbroic segregations, and the large lateral variation in lithology over the half-kilometer mantle section drilled at Site 895, suggest that Leg 147 drilled across a major conduit for melt-migration in the shallow mantle.

HARZBURGITES

Petrography

The Hess Deep harzburgites are petrographically typical of residual mantle peridotites sampled previously at Hess Deep (Girardeau and Francheteau, 1993; Hekinian et al., 1993), at the Garret Fracture Zone on the EPR to the south (Hebert et al., 1983), and at slow-spreading ridges (e.g., Dick, 1989). The harzburgite tectonites contain abundant relict olivine enclosing porphyroclastic enstatite and diopside with accessory chromian spinel. Spinel is generally highly

Table 8. Site 895 clinopyroxene rare earth and other trace element abundances.

Hole	Core, section, interval (cm)	Gr.	Pts.	La	Ce	Nd	Sm	Eu	Dy	Er	Yb	Gr.*	Pts.	Ti	V	Cr	Sr	Y	Zr	Ti/Zr
Concentration in ppm																				
Gabbro																				
895E	4R-3, 55-58	1	1	0.187	0.724	1.355	0.948	0.333	1.737	1.201	1.233		3	1718	293	6578	4.7	5.9	4.2	409.1
895E	4R-3, 55-58	1 amp	1	0.084	0.341	0.815	0.555	0.240	1.215	0.689	0.762		1	1270	226	5450	2.6	6.0	3.8	334.1
Olivine gabbro																				
895C	4R-2, 108-111	ave	6	0.120	0.490	0.939	0.669	0.342	1.488	0.921	0.911		3	1631	260	7642	6.1	8.5	5.0	206.7
Olivine gabbro																				
895D	8R-2, 6-9	1R	2											2271	227	5644	4.6	7.8	22.1	102.7
895D	8R-2, 6-9	1C	1											1336	196	5705	5.9	6.7	3.4	392.9
895D	9R-2, 60-65	1	1	0.136	0.549	1.318	0.952	0.364	1.639	1.115	1.066	ave	3	1573	245	6534	6.1	8.5	5.8	275.4
895E	5R-1, 23-26	1	2	3.340	2.048	3.190	2.836	2.440	3.139	3.212	1.971		3	1763	284	6165	8.3	9.5	6.6	276.3
Troctolitic gabbro																				
895D	7R-2, 61-63	ave	5	0.523	2.471	4.445	2.611	0.660	5.261	3.105	2.968	2C	2	6758	499	7055	9.9	30.9	81.2	83.7
895D	7R-2, 61-63	1	1											7263	484	6458	10.3	34.6	95.4	76.1
895D	7R-2, 61-63	1R	1											2646	232	3072	6.3	15.5	36.8	71.9
Troctolite																				
895C	4R-2, 62-65	1	2	0.338	1.787	2.874	2.072	0.478	4.908	2.827	2.691			3012	338	8291	5.5	25.5	26.5	113.9
895C	4R-2, 62-65	2	2	0.468	2.701	4.822	3.230	0.614	7.537	4.126	3.935		3	4382	363	7931	12.8	32.4	57.5	78.7
Plagioclase dunite																				
895C	4R-3, 32-35	ave	5	0.532	2.670	4.048	2.362	0.554	4.939	2.899	2.452									
Harzburgite																				
895B	1R-1, 71-76	1	5	0.022	0.013	0.111	0.167	0.036	0.135	0.161	0.212			147	215	6387	0.5	0.8	0.4	483.6
895C	1R-1, 28-32	1	2	0.005	0.010	0.023	0.021	0.006	0.126	0.165	0.229	ave	3	150	194	7511	0.4	1.0	0.2	751.8
895C	1R-1, 28-32	ave	2	0.000	0.004	0.015	0.010	0.002	0.018	0.033	0.071		2	173	227	7165	0.7	0.9	0.5	387.8
895C	3R-1, 35-39	2	4	0.003	0.010	0.018	0.014	0.007	0.132	0.168	0.204	ave	5	184	201	6740	0.8	1.0	0.3	983.6
895D	3R-1, 116-120	ave	4	0.002	0.002	0.016	0.033	0.007	0.117	0.163	0.218		4	156	201	6535	0.6	0.9	0.4	270.0
895D	4R-3, 97-101	1	4	0.005	0.015	0.033	0.046	0.009	0.142	0.186	0.231	ave	6	208	202	7599	0.4	0.8	0.3	912.0
895D	7R-2, 129-133	1	3	0.021	0.019	0.044	0.063	0.020	0.137	0.193	0.215	ave	4	163	219	7137	0.9	0.9	0.6	548.0
895E	7R-4, 37-40	ave	4	0.013	0.020	0.038	0.032	0.017	0.144	0.169	0.231	1	2	157	207	6858	2.4	0.6	1.1	163.5
Percent mean deviation																				
Gabbro																				
895E	4R-3, 55-58	1	1	17.9	12.8	3.3	6.3	11.0	7.5	7.5			3	4	5	7	13	7	18	
895E	4R-3, 55-58	1 amp	1	6.2	5.8	16.4	22.7	10.1	2.7	3.9			1	3	1	2	11	4	11	
Olivine gabbro																				
895C	4R-2, 108-111	ave	6	21.6	12.4	12.0	15.7	7.3	10.0	6.1			3	1	2	2	6	4	11	
Olivine gabbro																				
895D	8R-2, 6-9	1R	2											1	4	6	8	4	4	
895D	8R-2, 6-9	1C	1											2	0	2	12	2	7	
895D	9R-2, 60-65	1	1	37.4	14.8	6.1	11.3	10.4	8.3	6.6		ave	3	1	2	1	9	7	9	
895E	5R-1, 23-26	1	2	7.8	5.4	6.2	4.7	4.0	4.3	4.8			3	1	2	3	11	4	10	
Troctolitic gabbro																				
895D	7R-2, 61-63	ave	5	11.4	8.6	6.4	5.8	10.1	6.8	5.7		2 core	2	1	4	3	6	3	3	
895D	7R-2, 61-63	1	1											3	1	2	2	7	2	
895D	7R-2, 61-63	1R	1											3	4	5	5	4	5	
Troctolite																				
895C	4R-2, 62-65	1	2	12.6	11.6	6.3	1.2	7.1	3.0	4.2				2	2	3	11	3	3	
895C	4R-2, 62-65	2	2	12.7	11.1	6.6	7.1	5.0	5.9	5.1			3	9	12	17	6	8	10	
Plagioclase dunite																				
895C	4R-3, 32-35	ave	5	14.2	7.3	6.3	9.4	9.6	8.5	7.2										
Harzburgite																				
895B	1R-1, 71-76	1	5	136.1	48.4	47.2	41.0	65.9	27.5	32.3				4	4	2	21	17	71	
895C	1R-1, 28-32	1	2	58.3	15.0	10.1	28.0	33.8	6.6	7.5		ave	3	28	2	3	62	23	102	
895C	1R-1, 28-32	ave	2	302.2	17.1	25.4	63.9	53.4	11.3	14.2			2	6	7	10	11	12	61	
895C	3R-1, 35-39	2	4	81.2	37.1	26.3	69.6	29.8	26.4	15.4		ave	5	2	2	3	27	12	81	
895D	3R-1, 116-120	ave	4			41.6	28.2	81.8	11.9	24.0			4	28	2	3	21	17	34	
895D	4R-3, 97-101	1	4	49.5	25.8	35.0	26.9	33.1	12.9	8.1		ave	6	3	3	2	72	20	84	
895D	7R-2, 129-133	1	3	95.4	52.7	67.7	21.1	35.6	34.3	30.7		ave	4	4	4	4	17	21	44	
895E	7R-4, 37-40	ave	4	29.0	14.4	29.2	27.6	31.9	10.0	12.7		1	2	5	2	2	18	49	25	

Notes: Gr. = grain number and position on grain (R = rim, C = core); amp = amphibole patch in clinopyroxene; ave = average of several spots on grain. Pts. = number of points analyzed. Percent mean deviation given is the average percent mean deviation for the points analyzed determined from the counting statistics. Gr.* = grain number and location if different than for REE analysis.

irregular, ranging from vermiform to holly leaf textured, though in some cases it is equant subhedral. Orthopyroxene ranges from coarse granular textured to porphyroclastic. In the former, relatively coarse 2- to 6-mm grains are characterized by smooth, curved boundaries, deep embayments, and projecting lobes where the pyroxene interlocks with the enclosing olivine to form a protogranular texture. The protogranular texture is generally modified by later solid-state deformation, and individual pyroxenes have been variously stretched, rounded, deformed, and recrystallized at grain boundaries. Clinopyroxene consistently has three morphologies: (1) subequant anhedral granular, with smooth, curved, often deeply embayed or projecting

lobes, similar to the earliest formed orthopyroxene textures, (2) intergranular, ranging from thin films and selvages between olivine grains and adjacent to orthopyroxene, and (3) small equant neoblasts occurring in a matrix of recrystallized orthopyroxene. The clinopyroxene neoblasts are generally interpreted as the result of exsolution of diopside from the enstatite during mechanical recrystallization accompanying late-stage solid-state deformation and flow (Medaris, 1972; Medaris and Dott, 1970).

Intergranular clinopyroxene and spinel are similar in their occurrence, are often intergrown, and may form small stringers in the olivine. We interpret these trains of aligned mineral grains as the result

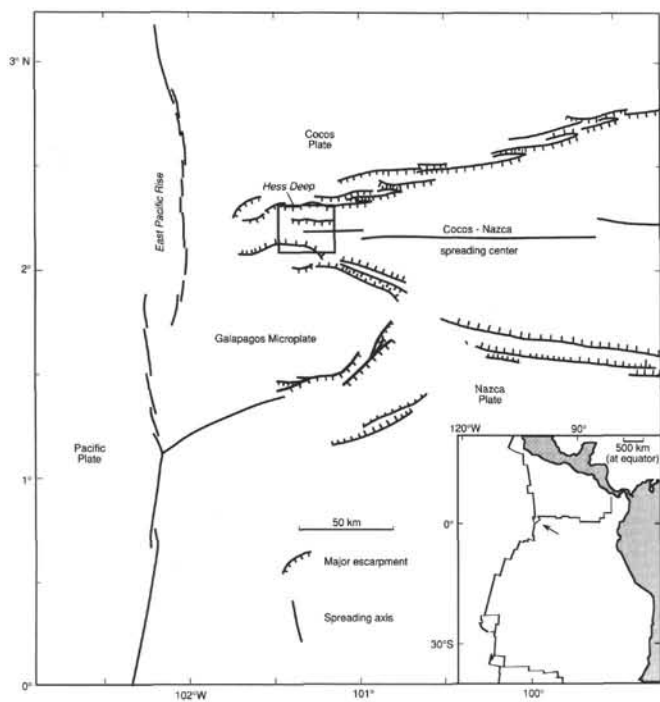


Figure 1. Map of the eastern Pacific seafloor showing the relevant portions of the EPR, the Cocos-Nazca Ridge, and Hess Deep, modified from Lonsdale, 1988.

of crystallization of clinopyroxene and spinel from late-melts migrating through the peridotite. In many cases, the stringers consist only of spinel enclosed in olivine, and therefore cannot represent solid-state breakdown of recrystallized aluminous-pyroxene to a spinel-bearing assemblage due to the lack of appropriate reaction products. At the same time, the clinopyroxene trains preserve complex intergranular textures unlikely to survive plastic deformation. We also observe a gradation from the intergranular clinopyroxene to the relatively coarse granular clinopyroxene. While the granular clinopyroxene may be residual, given its depleted composition and morphological similarity to residual orthopyroxene, the textural gradation to intergranular clinopyroxene also suggests late overgrowth from melt migrating through the harzburgite. Girardeau and Francheau (1993) and Hekinian et al. (1993) also reached similar conclusions for the origin of "wehrlitic" clinopyroxene patches in Hess Deep harzburgites sampled by dredging and submersible.

Melts migrating upward through the mantle are generally believed to dissolve pyroxene and precipitate olivine and spinel in order to maintain equilibrium with peridotite due to the expansion of the field of olivine on the basalt liquidus with decreasing pressure (Dick, 1977a; Dick, 1977b; Dickey et al., 1971; Kelemen et al., 1990; O'Hara, 1968; Quick, 1981a). This is generally the case where the mantle is melting and melt mass is increasing. The situation can be quite different where the mantle is no longer melting, melt mass is decreasing, and mantle mass is increasing due to crystallization of minerals from melts percolating through it (Kelemen et al., 1992). The coprecipitation of spinel and clinopyroxene in the Hess Deep harzburgites indicates such a situation. While late-state melts may have been dissolving enstatite as they percolated through the Hess Deep peridotites, their compositions must have reached saturation with respect to clinopyroxene. Based on the known liquidus phase relations for mantle peridotites, this indicates a significant decrease in melt mass due to crystallization of the migrating magma reacting with the host peridotite. This in turn requires that the geotherm immediately beneath the East Pacific Rise was cooler than the mantle adiabat, and provides the

first direct evidence for a significant conductive lid on the upwelling mantle there.

The spinel trains and tectonically elongated pyroxenes define a foliation recognizable in most of the harzburgites. This foliation, when paleomagnetically reoriented has a highly variable dip, but a strong preferred north-northeast strike roughly parallel to the EPR (Gillis, Mével, Allan, et al., 1993). This foliation is more weakly defined by spinel trains in the dunite, but is absent to rare in the troctolites, which show little evidence of the late high-temperature deformation seen in the peridotites.

Taken together, the petrography and microstructures in the harzburgite indicate high temperature-low deviatoric stress conditions expected for solid-state flow in the asthenosphere (Nicolas et al., 1973). Estimates of the temperature of emplacement of the Hess Deep harzburgites based on their fabrics are close to the mantle solidus near 1200°C (Gillis, Mével, Allan, et al., 1993; Boudier et al., this volume; Kennedy et al., this volume).

The harzburgites are heavily altered, containing on average 67% serpentine (Table 2). The percentages of serpentine pseudomorphs of olivine and enstatite are given in Table 2. These data show that in most cases, olivine is preferentially serpentinized, although in one instance enstatite is more altered, while in other cases enstatite and olivine are equally altered. This suggests variable fluid chemistries and conditions of alteration. Unlike dredged samples, the Site 895 harzburgites are relatively little weathered, containing little or no clay replacing olivine, except for those from the shallowest levels. There is also an additional 5.6% pseudomorphs of talc and/or amphibole after enstatite and 0.25% talc and/or amphibole pseudomorphs after olivine on average. The talc-amphibole pseudomorphs include three different assemblages: talc, talc-amphibole, and amphibole. These assemblages indicate hydration over a broad range of conditions, likely up to lower amphibolite facies conditions. The amphiboles in thin section appear to be mostly tremolite, though cumingtonite is also locally present. In addition, the assemblage talc-secondary olivine occurs in some veins cross-cutting enstatite, with very-fine-grained olivine occurring enclosed in the talc at the center of the vein. The presence of these higher temperature assemblages is not, in itself, unusual, and they are ubiquitous in small quantities in the several hundred different suites of abyssal peridotites previously examined by the senior author. The volume of this alteration in the Hess Deep peridotites, however, is atypically high in our experience, and suggests extensive late hydrothermal circulation during emplacement at the time of Hess Deep opening.

The average of 18 primary modes is very refractory, containing 83.6 vol.% olivine, 14.6% enstatite, 1.0% diopside and 0.7% spinel. For comparison, the average plagioclase-free abyssal peridotite contains 75% olivine, 21% enstatite, 3.5% diopside and 0.5% spinel (Dick, 1989). The most depleted Southwest Indian Ridge peridotites from the Bouvet Fracture Zone, which cuts the Bouvet hot spot, contain an average of 81.6% olivine, 16.1% enstatite, 1.6% diopside, and 0.5% spinel (ave. of 15 modes). While errors due to variable degrees of serpentinization and differential volume expansion may be significant in comparing individual samples, they are not large enough to account for the 60% greater average diopside content of the Bouvet harzburgites, particularly as the overall degree of serpentinization of the Bouvet and Hess Deep harzburgites is similar. The difference in modal diopside content, however, might reflect outcrop scale heterogeneities, and fortuitous sampling near a dunite complex at Hess Deep and far from a dunite complex at the Bouvet Fracture Zone, rather than reflecting a regional difference in the degree of mantle melting.

Despite the presence of the gabbroic segregations, we observe virtually no relict or pseudomorphed plagioclase in the thin sections counted, though it could always be present in samples we have not examined. Individual modes are plotted in Figure 5. Similar to many abyssal peridotite suites, these modes show a strong tendency for di-

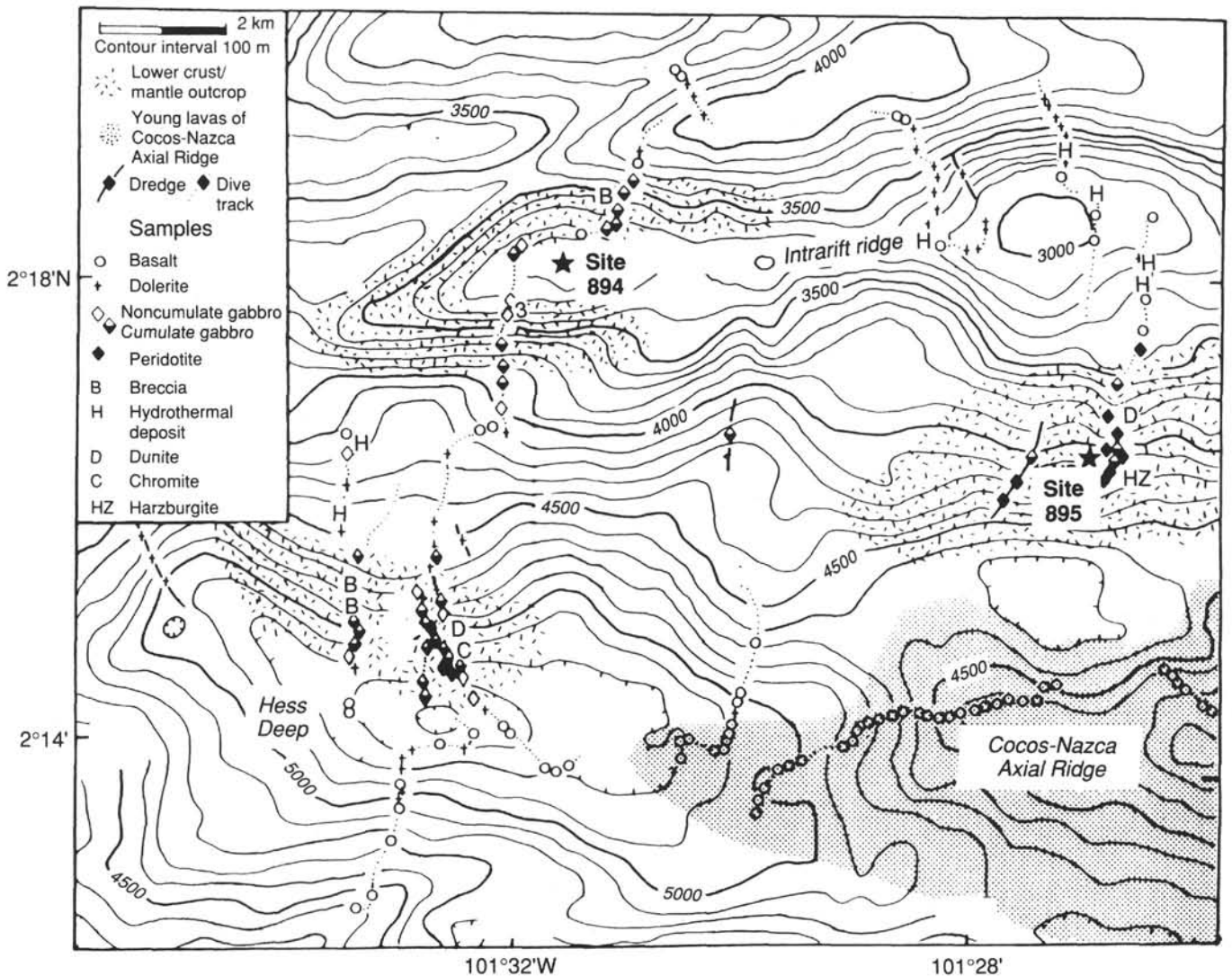


Figure 2. Bathymetric map of the western end of the Cocos-Nazca Ridge showing the V-shaped amagmatic rift valley and the locations of Hess Deep and the intrarift ridge where Sites 894 and 895 are situated.

opside and enstatite to decrease together as olivine increases in abundance (e.g., Dick, 1989; Dick et al., 1984; Johnson and Dick, 1992; Michael and Bonatti, 1985b).

Mineralogy

Major element analyses of the primary phases are given in Tables 3 through 6. Olivine is forsteritic relative to most abyssal peridotites, averaging $Fo_{90.6}$ with a standard deviation of only 0.22% forsterite. Peridotites from near the Bouvet hot spot, for comparison, have on average $Fo_{90.8}$, while the average abyssal peridotite has $Fo_{90.4}$, and peridotites dredged far from mantle hot spots average about $Fo_{90.1}$ (Dick, 1989; Dick et al., 1984). Diopside and enstatite compositions are given in Tables 4 and 5 and are plotted in the pyroxene quadrilateral in Figure 6. The principal variation exhibited by pyroxenes from the Site 895 harzburgites and gabbros in the quadrilateral is a simple variation in wollastonite content lying directly on a join between diopside and enstatite. This likely reflects varying degrees of exsolution of diopside from enstatite, and of enstatite from diopside, during subsolidus reequilibration and recrystallization that accompanied cooling and emplacement to the base of the crust prior to unroofing of the mantle section at Hess Deep. Any significant chemical frac-

tionation related to either varying degrees of melting or fractional crystallization during formation of the peridotites and gabbros, respectively, would cause a small but significant spread in the data parallel to the enstatite-ferrosilite join.

The average composition of enstatite and diopside is refractory compared to pyroxenes in other abyssal peridotites suites, including those associated with hot-spots in the Atlantic and Indian oceans. This is clearest for the concentrations of the more incompatible elements such as soda, titanium, and alumina. Sodium and titanium are virtually below the detection limit for the electron microprobe in all the pyroxenes we analyzed in the harzburgites. Alumina content of enstatite has been shown experimentally and theoretically to be a good monitor of mantle melting, decreasing systematically with increasing depletion of peridotite (e.g., Dick, 1977b; Dick et al., 1984; Jaques and Green, 1980; Johnson and Dick, 1992; Michael and Bonatti, 1985a; Mysen and Boettcher, 1975). The average alumina content of enstatite in Hess Deep harzburgites is only $2.19 \pm 0.15\%$. By comparison, undepleted harzburgites far from mantle hot spots contain 5% alumina or more, while the peridotites from near the Southwest Indian Ridge near the Bouvet hot spot contain 3.2% alumina, and those from $43^\circ N$ on the Mid-Atlantic Ridge near the Azores hot spot contain 2.27 wt%.

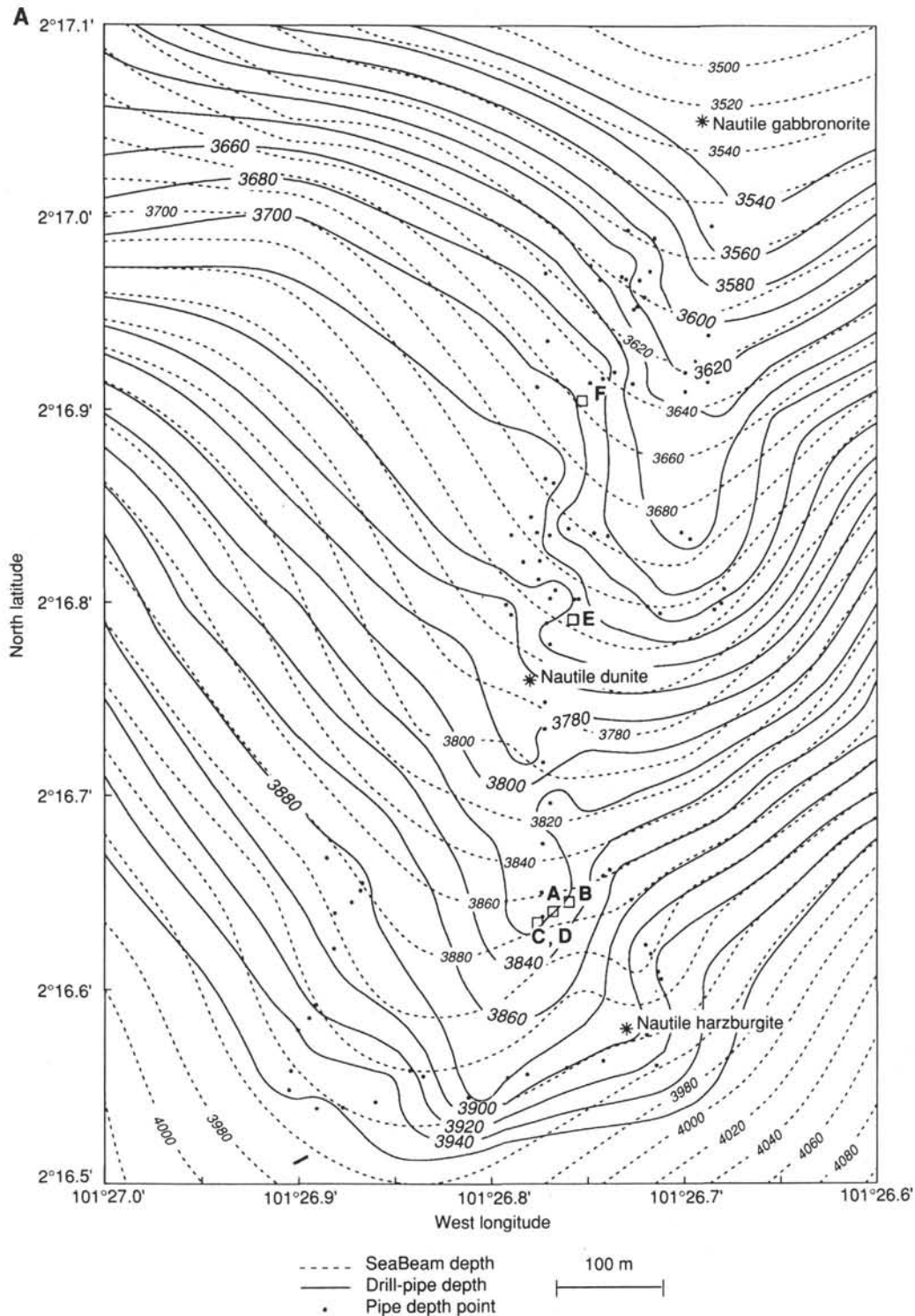


Figure 3. **A.** Bathymetric map contoured for depth from gridded SeaBeam data (dashed lines) and for soundings with the drill pipe (solid lines) showing locations of Holes 895A–895F. From Gillis, Mével, Allan, et al. (1993). **B.** Expanded stratigraphies of Holes 895D and 895E. The expanded recovery is based on the assumption that the partial recovery from each drilled interval is representative of the lithologic interval drilled for each core. For example, the percentages of different rock types recovered for an entire hole may differ somewhat from the percentages calculated based on expanded recovery, as the recovery from each interval drilled (core) is often quite different. The first column shows the position of each cored interval, the second column shows the amount of rock or sediment recovered (solid black bar), and the third column shows the stratigraphy after expanding the recovered rock proportionately to fill the cored interval. The orientation of the contacts between units is generally steep, though variable, and horizontal bars represent only the vertical dimension of individual rock units. **C.** Expanded recovery stacked by rock type for Holes 895A–895F. Holes 895A–895D were drilled within several tens of meters of one another, whereas Hole 895E was drilled 270 m upslope and Hole 895F an additional 200 m upslope. The plot does not reflect the stratigraphic order of these rock types, which are complexly intercalated with one another as shown graphically in (B). The plot does show that the section drilled is laterally very heterogeneous, and that the gabbroic rocks are strongly associated with the dunites.

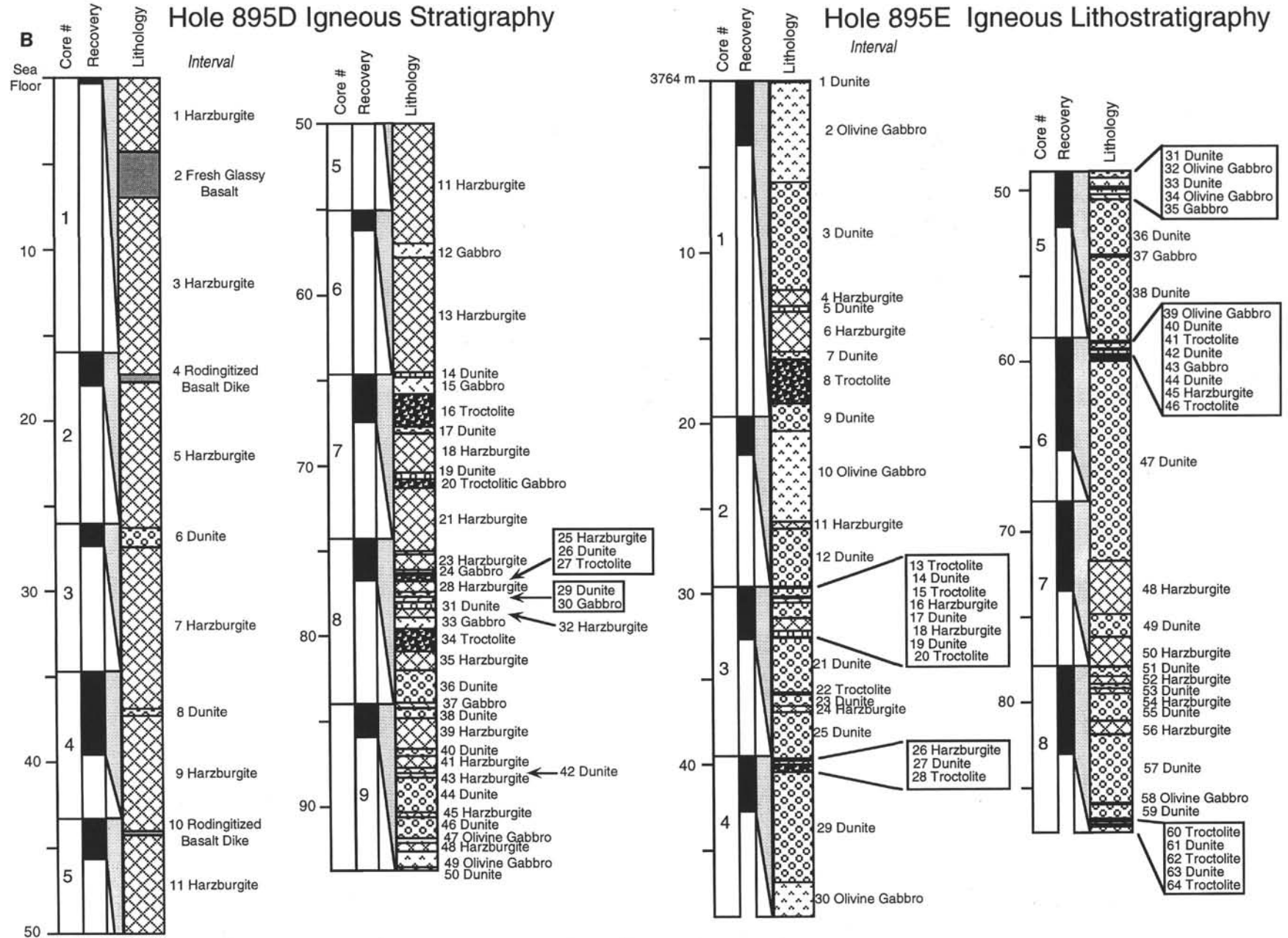


Figure 3 (continued).

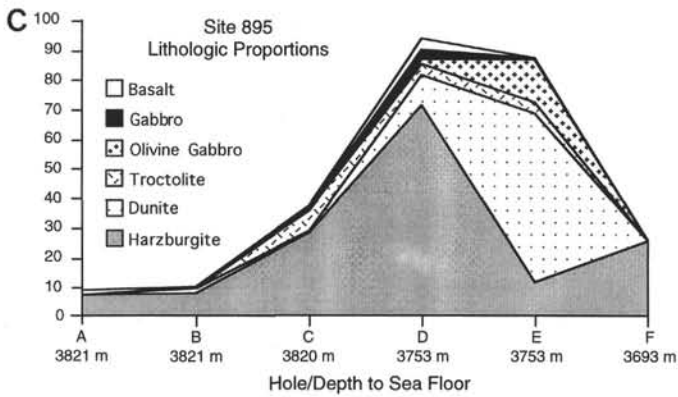


Figure 3 (continued).

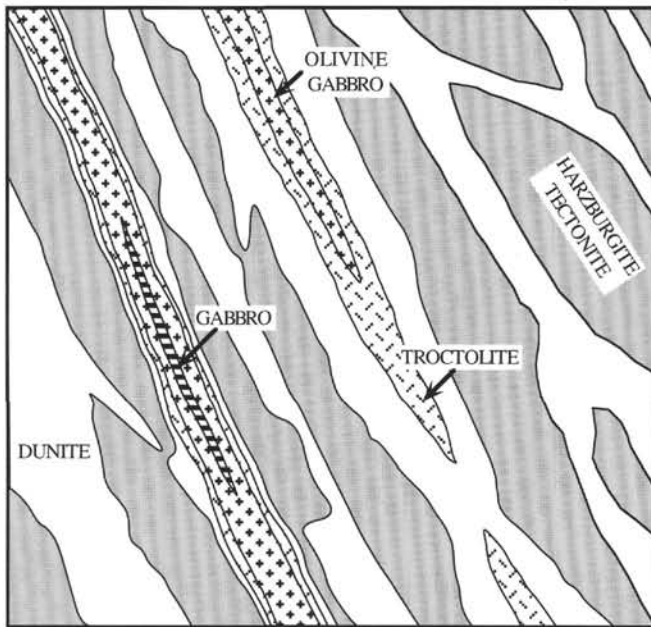


Figure 4. Possible lithostratigraphic relationships between harzburgite-tectonite screens and crosscutting dunitites at Site 895 based on features of the recovered core and the outcrop-scale relationships of similar features found in ophiolite mantle sections. Dark shaded area is harzburgite-tectonite; light shaded region is crosscutting dunite. Dunite is inferred to enclose sequentially: troctolite (hashed), olivine gabbro (crosses), and gabbro (horizontal lines).

There are no evident correlations between mineral mode and pyroxene or olivine composition. Alumina and calcium in enstatite plotted against modal olivine is shown, for example, in Figure 7. These analyses are believed to approximate their bulk composition prior to cooling and subsolidus exsolution. Given the relatively uniform degree of serpentinization of the olivine ($67 \pm 10\%$; Table 2), the large range in olivine mode (78.5–92.2%) is undoubtedly quite real. There is, however, no significant variation in the calcium or alumina contents of enstatite that relates to modal proportions (Fig. 7B). In contrast, the global data set for the Mid-Atlantic, Southwest Indian, and American-Antarctic Ridges has a strong negative correlation between alumina in enstatite and modal olivine (Fig. 7A) (Bonatti, 1992; Dick, 1989; Dick et al., 1984; Michael and Bonatti, 1985a). This systematic global variation in mineral mode and chemistry exists also for the trace element composition of diopside and spinel $\text{Cr}/(\text{Cr}+\text{Al})$, and correlates directly with the composition of spatially as-

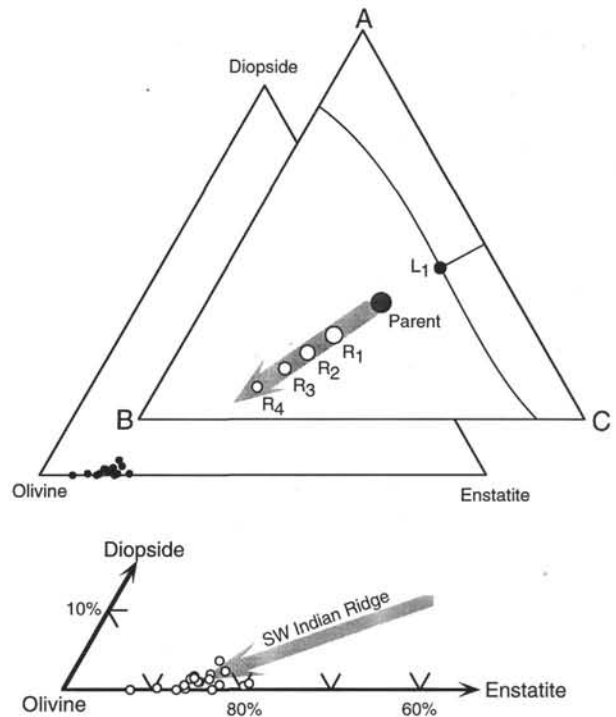


Figure 5. Mineral modes plotted in the olivine-diopside-ternary. A blow-up of the olivine corner of the ternary is shown at the bottom of the figure, with the modal trend for Southwest Indian Ridge peridotites from Dick et al. (1984) shown for reference. At the upper right is a cartoon illustrating pseudo-eutectic melting of mantle peridotite to illustrate how varying degrees of mantle melting produce linear modal trends. A full discussion of this can be found in Dick et al. (1984). R_{1-4} = sequential residues of melting; L_1 = liquid produced at the reaction point. Curved lines show the inferred cotectic boundaries for the system A-B-C; the arrow shows the trend for progressive melting and melt removal from the parent composition.

sociated abyssal tholeiites, demonstrating a systematic increase in the degree of mantle melting beneath ocean ridges near mantle hot spots (Dick et al., 1984). The lack of a systematic variation in pyroxene composition with mineral mode, which is also the case for spinel composition, demonstrates that the Site 895 harzburgites have last equilibrated with a relatively homogeneous pervasively percolating melt. Modal variations in the Site 895 harzburgites, then, do not arise from variations in the degree of batch-equilibrium or fractional melting, but rather, reflect other physical-chemical processes such as melt-rock reaction, or the formation of modal layering by mechanical processes (Dick and Sinton, 1979).

Spinel in the Hess Deep harzburgites lies at the extreme Cr-rich end of the range for abyssal peridotites (Fig. 8). The abyssal spinel peridotites plotted in Figure 8 define the field for the Atlantic and Indian Oceans, and have been shown to define a mantle-melting array (Dick and Bullen, 1984), with a sharp cutoff at $\text{Cr}/(\text{Cr}+\text{Al})$ (Cr#) of around 0.6, which is believed to correspond to the activity of Cr and Al in the mantle at the point at which diopside disappears from the mantle residue during melting (Dick and Fisher, 1984). Cr# sharply increases during partial melting of peridotite reflecting the contrasting behaviors of Cr and Al. In contrast, even though bulk rock $\text{Mg}/(\text{Mg}+\text{Fe})$ also increases with melting, $\text{Mg}/(\text{Mg}+\text{Fe})$ in spinel shows a slight iron-enrichment due to the changing partition coefficients for Mg and Fe between spinel and olivine with increasing spinel Cr# (Dick and Bullen, 1984; Irvine, 1965).

Dick et al. (1984) have shown that the upper limit for abyssal peridotite spinel Cr# is exceeded in many alpine-type peridotites, which

Hess Deep, Site 895 & Hole 894G Pyroxenes

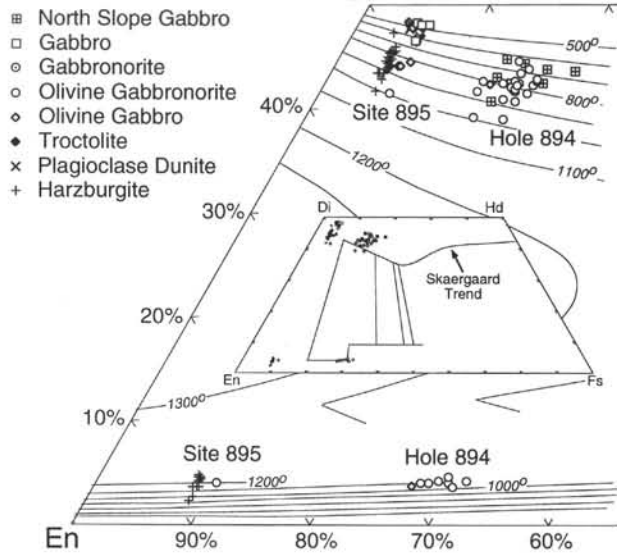


Figure 6. Pyroxene quadrilateral showing the composition of all pyroxenes from Sites 895 and 894. Compositions with ferrosilite (Fs) greater than 10% are all Hole 894G gabbronorites and olivine gabbronorites; those with less than 10% ferrosilite are from Site 894 harzburgites and gabbros. Hole 894G analyses are from Natland and Dick (this volume). Shown for comparison are pyroxene composition isotherms for coexisting augite enstatite assemblages from Lindsley and Andersen (1983). The authors estimate that the positions of these isotherms have an uncertainty of $\pm 20^{\circ}$ – 30° C plus about 5° . Using these to directly estimate temperatures, however, requires recalculation of the analyses based on mineral stoichiometry to exclude nonquadrilateral components. As we have not done this, the pyroxene isotherms are plotted here only to illustrate the behavior of coexisting pyroxenes during crystallization and subsolidus reequilibration. Inset shows the trend for coexisting pyroxenes in the Skaergaard intrusion from Wager and Brown (1967).

may contain extremely Cr-rich spinel (up to a Cr# = 0.85; Moutte, 1979). Many ophiolites, such as Papua (England and Davies, 1973), also contain no reported primary clinopyroxene, and extremely alumina- and calcium-poor enstatite undersaturated with respect to diopside. This is consistent with melting well into the diopside-out three phase field where the residue consists only of olivine, enstatite, and spinel. Up until the point at which diopside disappears from the residue, the calcium content of coexisting enstatite is buffered by the enstatite-diopside solvus and by the mantle temperature to a narrow range near 2 wt% (Fig. 7; Dick et al., 1984; Hess, 1993). The coexistence of diopside and enstatite during melting also apparently buffers the minimum alumina content of enstatite, and therefore the upper limit of Cr# in coexisting spinel as well. Experimental petrology shows that additional melting beyond the diopside-out point requires substantially more heat per unit volume of melt produced, and this phase boundary, accordingly, provides a natural limit for dry mantle melting beneath ocean ridges (Dick and Fisher, 1984; Hess, 1993).

Thus, despite the high degree of depletion in trace elements compared to other abyssal peridotites, melting of the mantle beneath the EPR appears to have been limited to the four phase field, and represents thermal conditions not too different than beneath other ocean ridges. By contrast, many ophiolites must represent substantially different melting environments. Since it seems unlikely that the mantle beneath an island-arc would be hotter than that beneath an ocean ridge, the extremely refractory compositions of pyroxene and spinel most likely reflects hydrous mantle-melting in a supra-subduction zone environment, with the formation of hydrous, and high silica

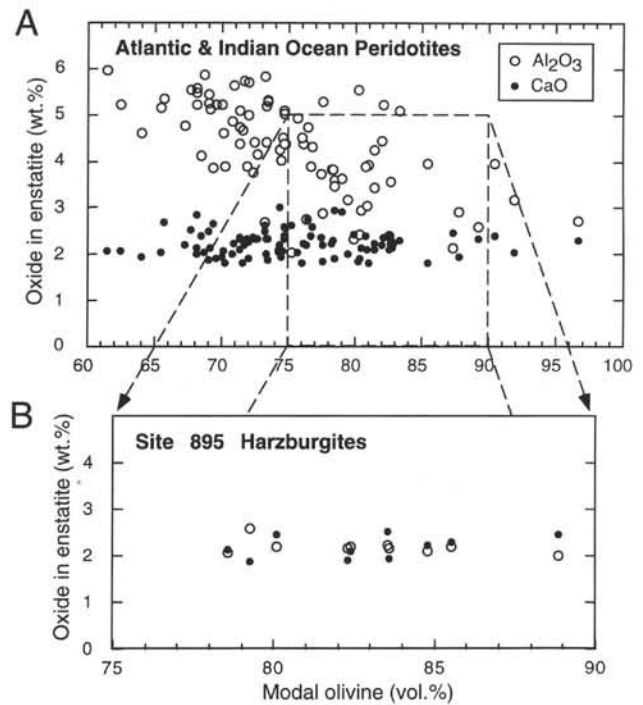


Figure 7. Alumina and calcium contents of enstatite plotted against modal olivine in vol% for Hess Deep Site 895 harzburgites. **A.** Compositions of enstatite in Atlantic and Indian Ocean abyssal peridotites modified from Dick and Fisher (1984). **B.** Composition of enstatite from Site 895 harzburgites as reported in this paper.

magmas (Dick and Bullen, 1984), and more extensive melt-rock reaction in response to a thicker lithosphere than in the oceans.

Geochemistry

Rare earth and trace elements analyses for diopsides from Hess Deep harzburgites are given in Table 8. Hess Deep harzburgites have extreme depletions in incompatible trace elements as demonstrated by the Zr and Ti plot in Figure 9. Shown for comparison are data from Johnson et al. (1990) for the Southwest Indian and American-Antarctic Ridges. A feature of this plot, which may not be real, is the extreme depletion in Ti relative to Zr, which offsets the Hess Deep peridotites from the mantle array of Johnson et al. (1990). To the degree that Zr/Ti ratios define a mantle source region, this would indicate that the EPR mantle is compositionally different from that beneath the Indian and Atlantic Oceans as represented by the array of Johnson et al. (1990). Our analyses for Zr, however, are near the known detection limit of the ion probe, and the abundances measured may be more a function of undetected random electronic spiking in the background than the actual abundance. The latter conclusion is strongly suggested by the fact that all the Site 895 gabbroic segregation, including those known to have undergone extensive melt-rock reaction with the Site 895 harzburgites, as well as the Hole 894G high-level gabbros, lie along the trend of Johnson et al. (1990) in Figure 8 and project down toward the most depleted harzburgites analyzed by Johnson et al. (1990). This suggests that the Zr content of the Site 895 harzburgite diopsides was in fact below our detection limit, and should lie along the extension of the Johnson et al. trend.

Rare earth elements are also extremely depleted relative to other abyssal peridotites (Fig. 10). Of particular interest is the extreme depletion in HREE, which gives the Site 895 patterns a somewhat higher Ce/Yb ratio than some, but not all, of the peridotites dredged near the Marion and Bouvet hot spots on the Southwest Indian Ridge (Fig.

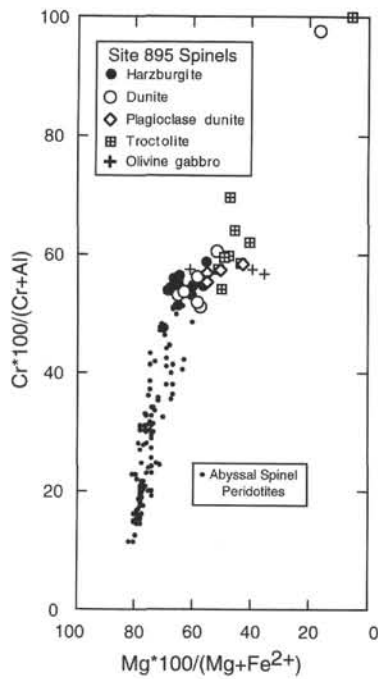


Figure 8. Compositions of Hess Deep Site 895 spinels plotted on the Cr-Al-Mg-Fe²⁺ face of the spinel composition prism (Irvine, 1965, 1967). The Y-axis length is equal to two times the X-axis, reflecting the relative molecular proportions of R²⁺ and R³⁺ cations. Composition of abyssal chromites from Dick and Bullen (1984).

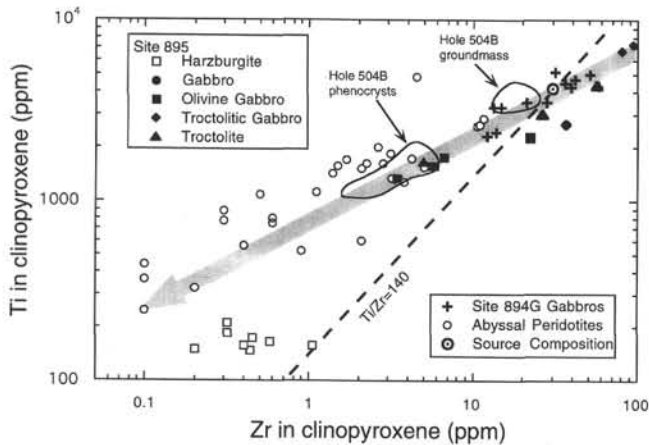


Figure 9. Ti vs. Zr content for diopsides and augite from Hess Deep Site 895 and Hole 894G peridotites and gabbros. Data for Hole 894G gabbros from Natland and Dick (this volume). Representative abyssal peridotite data (open circles) is for Southwest Indian and American-Antarctic Ridge peridotites from Johnson et al. (1990). Arrow shows projection of data for Site 895 gabbroic segregations along the trend for abyssal peridotites to Zr contents appropriate for Hess Deep residual harzburgites, assuming that the measured values represent noise at the detection limit of the ion probe. Dashed line shows a constant Ti/Zr ratio of 140 passing through an assumed source composition used by Johnson et al. (1990).

10A). In addition to the HREE-depletion, the second defining characteristic of the Site 895 harzburgite REE patterns is the strong depletion in middle rare earths, which contrasts sharply to peridotites associated with N-type or "normal" MORB. The latter are characterized by a convex upward pattern with strong enrichment in the middle REE relative to the LREE. A strong depletion in MREEs is also a

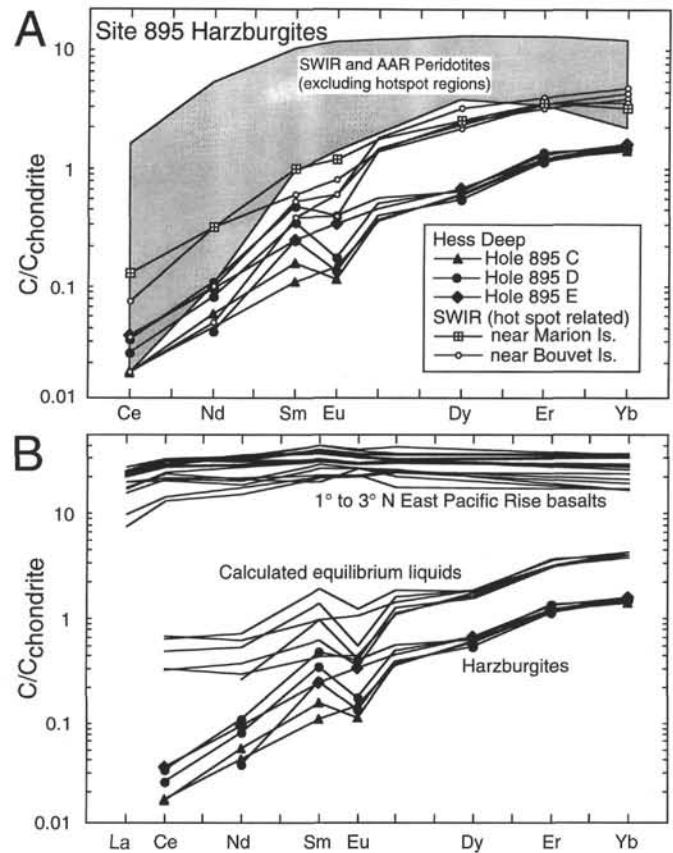


Figure 10. A. REE in diopsides from Site 895 harzburgites normalized to chondrites (solid symbols). Shown for comparison is the field of Southwest Indian and American-Antarctic Ridge harzburgites sampled far from mantle hot spots from Johnson et al. (1990). REE patterns for Bouvet and Discovery Fracture Zone harzburgites (open symbols), from near the Bouvet and Marion hot spots, respectively, are shown from Johnson et al. (1990). B. Calculated equilibrium liquid compositions for Site 895 harzburgites and representative 1°–3° EPR basalts from Lonsdale et al. (1992).

characteristic feature of the Bouvet and Discovery hot spot peridotite diopsides (Fig. 10A), which has been attributed to more extensive melting in the garnet stability field than peridotites far from mantle hot spots (Johnson et al., 1990).

DISCUSSION OF THE SITE 895 HARZBURGITES

Mantle Composition and Melting Anomalies Beneath the EPR

In terms of major elements, the primary mineral phases in the Hess Deep harzburgites were previously recognized as depleted relative to most abyssal peridotites and some ophiolites (Girardeau and Francheteau, 1993; Hekinian et al., 1993). This includes peridotites from the Garret Fracture Zone on the EPR at 13°30'S, as indicated by their significantly more aluminous spinel ($Cr\# = 0.40\text{--}0.45$). The absolute concentration of incompatible elements in Hess Deep peridotites, however, is even lower than that associated with peridotites dredged near the Bouvet and Marion hot spots. Peridotites with strong depletions in the middle rare earths have previously been found only in association with enriched-MORB dredged near mantle hot spots on the Southwest Indian Ridge. This pattern, and the highly depleted major element compositions of these peridotites, then, have been attributed to anomalously high mantle temperatures producing high degrees of mantle in association with mantle plumes on or near

ocean ridges (Dick et al., 1984; Michael and Bonatti, 1985a). EPR basalts from 1° to 3°N to the west of Hess Deep, however, have normal LREE-depleted patterns characteristic of N-MORB (Fig. 10B; Lonsdale et al., 1992), and there is no known bathymetric expression of a mantle hot spot along this region of the EPR. This shows, therefore, that the characteristic shape of the Bouvet and Marion peridotites is not a function of a plume vs. MORB source mantle, but is related to other environmental factors.

Following the rationale of Johnson et al. (1990), then, mantle melting could have begun anomalously deep compared to that in N-MORB regions of the Atlantic and Indian Oceans. If this is the case, it would require a hotter mantle beneath this region of the EPR. We note, however, that the EPR crust near Hess Deep is somewhat thinner than normal (Zonenshain et al., 1980), which indicates that despite the middle REE-depletion, and low HREE compared to the rest of the global data set, that the total amount of melting beneath the EPR was less than that associated with normal sections of slow-spreading ridges. This suggests to us that the mantle beneath the EPR in this region was initially more depleted in both major and trace elements, perhaps due to an earlier mantle melting event. The latter event could have occurred in the garnet peridotite field, whereas the event associated with the EPR may have largely occurred in the spinel field, consistent with a more normal mantle geotherm. This might explain the shape of the REE pattern in the Site 895 harzburgite clinopyroxenes as an inherited feature; the relatively low Ce/Yb ratio and low HREE abundances would then reflect additional melting beneath the EPR in the spinel field. A more critical examination of the melting history for these peridotites, however, must await detailed numerical modeling.

Two-dimensional vs. Three-dimensional Mantle Flow

Another, not necessarily conflicting, hypothesis is that the unusual depletion of the Site 895 harzburgites may be a characteristic of a zone of focused melt flow in the mantle. Certainly the presence of abundant dunite demonstrates the presence of a major flow channel through the Site 895 mantle section. In contrast, dunite is rare in dredge collections from slow-spreading ocean ridges (Dick, 1989) for which most of the existing data for abyssal peridotites to which we are comparing the Hess Deep data comes. Both basalts and gabbros from the Hess Deep area, however, reflect crystallization from refractory primary liquids normally associated with unusually high degrees of melting of spatially associated mantle peridotites, and thus indicate derivation from a highly depleted source. As shown in Figure 11, the gabbros from Hole 894G and from the north wall of Hess Deep together define a rough trend in a plot of plagioclase Ca/(Ca+Na) vs. clinopyroxene Mg/(Mg+Fe) that is significantly offset to more calcic plagioclase at a given Mg/(Mg+Fe) value (Fig. 11A). A similar offset can be seen in a plot of Ca/(Ca+Na) vs. Mg/(Mg+Fe) for EPR basalt glasses dredged from the walls of Hess Deep (Fig. 11B). This upward shift of the crystallization trends in these figures is analogous to very high basalt Na₈ values and is expected for gabbros (Meyer et al., 1989) and basalts crystallized from liquids reflecting very high degrees of melting of the mantle source (Dick et al., 1984; Klein and Langmuir, 1987; Schouten et al., 1987), or alternatively for normal degrees of melting of an initially more refractory source mantle composition (Dick et al., 1984). The unusual depletion of the Hess Deep harzburgites is apparently not a local feature of the mantle section beneath the EPR, but is a regional characteristic reflected in the composition of the overlying basalts and gabbros over a wide area. Thus, if the unusual compositional characteristics of the Site 895 harzburgites compared to most Atlantic and Indian Ocean abyssal peridotites are a reflection of focused melt flow, then it is likely that such flow channels are rather broadly distributed in the mantle section beneath the EPR compared to slow-spreading ridges. A greater dispersal of such flow channels beneath a ridge axis might be expected if mantle flow beneath fast-spreading ridges is more two

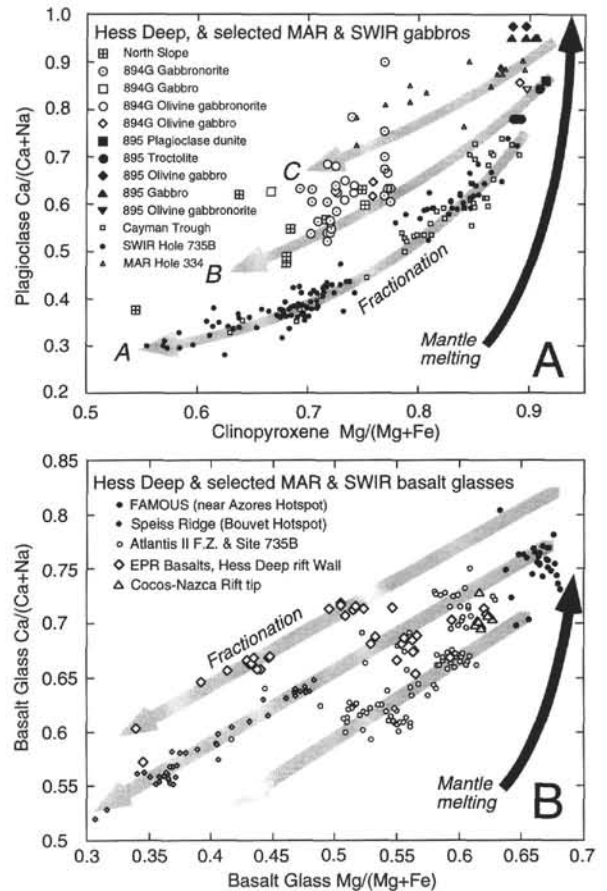


Figure 11. **A.** Plagioclase Ca/(Ca+Na) plotted against Mg/(Mg+Fe) for Hess Deep gabbros from Hole 894G (open large symbols), Site 895 (closed large symbols), and the north wall (slope) of the Cocos-Nazca Rift north of Hess Deep (divided squares). Shown for comparison are the composition of gabbros spatially associated with basalts and peridotites reflecting low degrees of mantle melting (Dick et al., 1984), including: the Cayman Trough (Elthon, 1987) and Hole 735B in the Indian Ocean (Ozawa et al., 1991). For contrast, gabbro suites from Hole 334 near the Azores hot spot (Hodges and Papike, 1976) are shown. The latter are associated with basalts and mantle peridotites reflecting some of the highest degrees of melting anywhere in the Atlantic and Indian Oceans (Dick et al., 1984; Klein and Langmuir, 1987). Lightly shaded arrows indicate the general direction of crystal fractionation trends; the darkly shaded arrow shows the contrasting general effect of progressive mantle melting on primary melt compositions. **B.** Plot of Ca/(Ca+Na) vs. Mg/(Mg+Fe) for basalt glasses from the Hess Deep (data from Nilsson, 1993). Shown for comparison are suites from the Atlantis II Fracture Zone near Hole 735B (Dick et al., 1991b), which are believed to reflect low degrees of melting and mantle depletion (Dick et al., 1984; Dick et al., 1991b), and suites from Speiss Ridge on the Southwest Indian Ridge near the Bouvet hot spot (Dick, unpubl. data) and the FAMOUS region of the MAR near Hole 334 and the Azores hot spot (Bryan and Moore, 1977), which reflect high degrees of melting and mantle depletion. Arrows as in (A).

dimensional than at slow-spreading ridges as suggested by Lin and Phipps Morgan (1992).

Evidence for Fractional Melting and Ultra-depleted Melts

Petrographically, clinopyroxene and spinel morphologies in the Hess Deep harzburgites appear to reflect late-stage percolative melt flow, with much of the clinopyroxene occurring in lineated trains of

intergranular grains believed to have crystallized at the very end of melting in the zone of conductive heat loss beneath the crust at the ridge axis. In Figure 10B we show calculated liquid compositions in equilibrium with the Site 895 harzburgite clinopyroxenes using partition coefficients provided by Sobolev and Shimizu, with values for Cr and V from Hart and Dunn (Hart and Dunn, 1993; Sobolev and Shimizu, 1993). As found for other abyssal peridotites (Johnson et al., 1990), calculated liquid compositions in equilibrium with Hess Deep harzburgites are ultra-depleted compared to MORB and, except for the absence of the characteristically convex upward shape, are similar to the ultra-depleted melt inclusions reported by Sobolev and Shimizu (Sobolev and Shimizu, 1993). These authors suggest that the ultra-depleted inclusions would be in equilibrium with the mantle at low pressures (5–10 kb), and model them as an instantaneous fractional melt produced at 17% melting with a retained melt fraction of 2.2 wt%. The analyzed clinopyroxene compositions we have used for our calculations are those of the host diopside after any subsolidus orthopyroxene exsolution, not actual compositions at magmatic temperatures. Although we have not seen much evidence for extensive exsolution in the diopsides in these peridotites, any exsolution of enstatite with cooling would likely increase the REE abundances in the host diopside. This would make the actual liquids that were last in equilibrium with these harzburgites even more refractory than those we calculate. The depleted composition of the Hess Deep harzburgite tectonites, then, are consistent with other abyssal peridotites in seeming to require near-fractional melting of the mantle beneath both fast- and slow-spreading ridges. Thus, the Hess Deep harzburgites represent the end-point of a near-fractional melting sequence, whereas the spatially associated basalts represent the aggregation of many melt fractions from the sequence—presumably somewhere in the underlying mantle melting column.

It is difficult to assess the proportion of ultra-depleted melts, representing the later stages of sequential fractional fusion of the upwelling mantle, which need to be added into the equation for the bulk composition of the ocean crust. Such melts, generated in the upper levels of the melting column might well escape the principal zone of melt aggregation and percolate directly to the base of the crust. Sobolev and Shimizu (1993) report such refractory melt inclusions in olivine phenocrysts in MORB, demonstrating that such liquids intrude the crust. However, numerical modeling of aggregate melts by Johnson et al. (1990) does show that ordinary MORB may incorporate much of this melt fraction. Petrographically, there is evidence that the residual harzburgites at Hess Deep contain some component of intergranular clinopyroxene precipitated from such melts trapped in the mantle in the zone of conductive cooling beneath the crust. The amount of such pyroxene is small but significant, probably in the range of 0.5%. This would correspond to perhaps as much as 1% trapped ultra-depleted melt, back-reacted with olivine to form clinopyroxene and enstatite (e.g., Kelemen et al., 1992). It is therefore possible that relatively little of the shallowest, most extreme fractional melts escape from the mantle, but remain trapped in the residue by the “lithospheric” or conductive lid at the top of the mantle melting column. Where such melts do escape to the crust, perhaps due to local fracturing in the shallow mantle, they could account for wehrlitic intrusions in the lower crust, because clinopyroxene with olivine is likely to precede plagioclase on their liquidus at low pressure.

A bimodal distribution of ultra-depleted and MORB primary liquids intruded to the crust is consistent with most melting models. The incompatible-element-rich early melt fractions required to make MORB are generated deep within the mantle-melting column, and are most likely to be affected by any mechanism focusing melt flow in the mantle. Later melt fractions, generated at moderate and high levels, would have highly depleted compositions quite distinct from MORB. Such melts would likely only preserve their depleted character, however, where they escaped the principal zone of melt aggregation where incompatible-element-rich melt fractions flowing from greater depth are concentrated.

DUNITES AND GABBROIC SEGREGATIONS

Petrography

The dunite, over large intervals, is composed entirely of serpentinized olivine with varying amounts of Cr-spinel, ranging from none to several percent. Dunite is generally more altered than harzburgite, consistent with the overall increase in serpentinization with original olivine content seen in the harzburgites (Table 2). Frequently olivine is completely replaced, though many samples contain relict olivine and spinel. Textures vary, but most commonly are anhedral granular. Kink bands and evidence of plastic deformation are common. Spinel is typically euhedral or subhedral. Locally, one small centimeter-scale podiform spinel segregation was found. Euhedral, holly-leaf, and vermiform spinel occur, often together, in the dunites. Euhedral spinel is often taken to indicate crystallization at high melt percentages, whereas vermiform and holly-leaf spinel may represent crystallization and overgrowth of spinel during late-stage melt percolation through a nearly solid dunite.

Two kinds of troctolites are present (Fig. 12). The first contains 1% to 18% plagioclase and appears to be an autoclastic igneous breccia consisting of disaggregated polycrystalline dunite clasts impregnated by plagioclase and minor intergranular clinopyroxene (Fig. 12C). The contacts of these troctolites with dunite may be either gradational (Fig. 12A) or sharp (Fig. 12F). Locally the dunite clasts may assume a near idiomorphic texture, evidently reflecting cotectic crystallization of olivine with the plagioclase accompanied by dissolution of the angular dunite fragments at their corners (Fig. 12F). Similar textures have been reported formed in peridotites disaggregated during partial melting experiments (Boudier and Nicolas, 1977).

There is an abrupt transition from troctolites formed by dunite disaggregation and impregnation to the second kind of troctolite—those with gabbroic proportions of plagioclase to olivine (Fig. 12B, E). Gabbroic proportions of plagioclase relative to mafic minerals [$0.55-0.60 \text{ Plag}/(\text{Plag}+\text{Ol})$] are those expected for cotectic crystallization of olivine and plagioclase directly from a basaltic melt based on the position of the natural cotectics defined by MORB glasses. Consistent with this, the proportion of plagioclase to olivine and clinopyroxene are relatively constant in most crustal gabbros (e.g., Bloomer et al., 1991). This nearly constant proportion of plagioclase is due to the lack of curvature of the plagioclase-olivine cotectic in the plagioclase-olivine-clinopyroxene ternary, its fixed position parallel to the diopside-forsterite join, and its relatively constant position with pressure (Presnall et al., 1979; Presnall et al., 1978; Dick and Bryan, 1978). This argues that the proportion of melt locally exceeded the limit for a grain-supported matrix, allowing direct crystallization of “gabbroic” troctolites within dikes and fractures in the dunites. Many of these troctolitic gabbros have extreme inequigranular textures and may contain obvious xenoliths of disaggregated wall-rock dunite (Fig. 12C, D). Locally gabbroic troctolites cut disaggregation troctolites as dikes parallel to their contacts with the adjacent dunite (Fig. 12F). Individual dunite clasts along these contacts are cut by the gabbroic troctolite, though the contact, on a thin section scale, is sutured rather than sharp, suggesting local dissolution and reprecipitation of olivine along it during intrusion (Fig. 12F). These features demonstrate that many of the dunites and their gabbroic segregations represent compound dikes and flow channels in the peridotite, with more than one phase of intrusion and melt flow.

Within the troctolites, clinopyroxene may form selvages or narrow coronas around olivine grains. These may locally coarsen to form isolated, coarse, anhedral, subophitic to ophitic pyroxene grains (Fig. 12B). Locally, such pyroxene may occur within the troctolites in sufficient quantity to constitute pegmatitic patches of olivine-gabbro, olivine gabbronorite, and gabbro (Fig. 12A). Elsewhere, much thicker units of olivine-gabbro and olivine gabbronorite are enclosed within the troctolites, apparently forming true gabbro dikes. All these gabbros have typical anhedral granular and intergranular gabbroic textures. Chromian spinel is a common accessory phase in the troct-

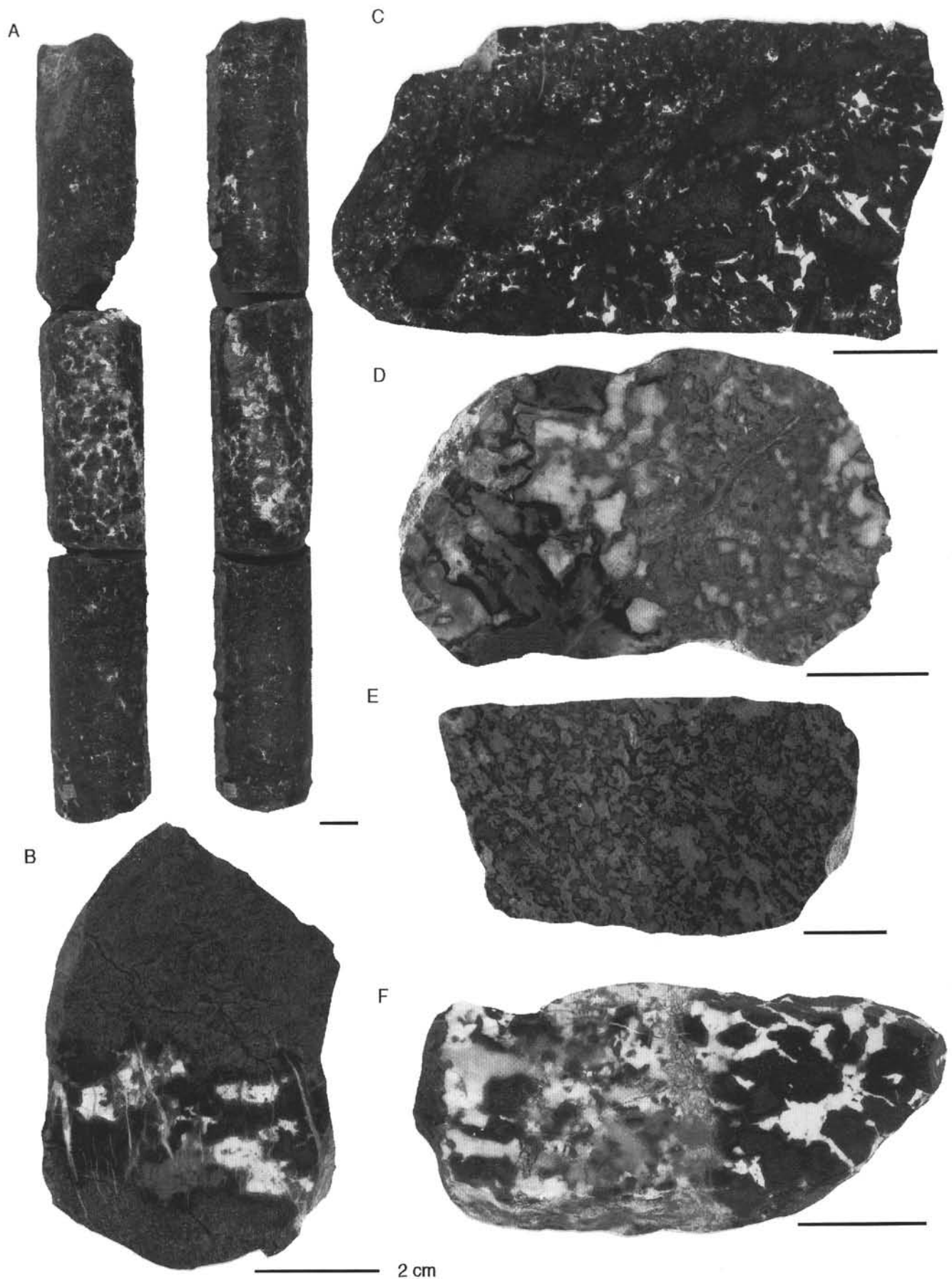


Figure 12. See caption on facing page.

olites and gabbroic segregations, ranging from virtually absent to several volume percent, and is generally euhedral or subhedral. Spinel generally occurs as small euhedra enclosed in either plagioclase or olivine. In Section 2 of Core 147-895C-4R (Fig. 12A), however, the troctolite contains unique coarse skeletal spinel intergrown with plagioclase.

The troctolitic gabbroic segregations in the Site 895 dunites have usually undergone substantial calc-silicate metasomatism (rodingitization), but typically contain cores of fresh plagioclase and relict olivine and pyroxene. Relict plagioclase is often entirely replaced by chlorite, while prehnite and various amphiboles are also found as replacements. Olivine is commonly replaced by talc and talc-amphibole. A characteristic feature of the alteration is that either only plagioclase- or only olivine-relicts occur in most samples, and samples with relicts of both are not common.

The gabbroic segregations may be locally overprinted by high-temperature solid-state deformation textures oriented obliquely to the contacts between the gabbros, dunites, and harzburgites (Gillis, Mével, Allan, et al., 1993). Such deformation is absent, however, in many if not most of the segregations, and it appears that only minor solid-state flow and deformation occurred after formation and emplacement of the gabbroic segregations. Some foliations may also reflect late melt flow and synmagmatic deformation (Fig. 12E), rather than subsolidus deformation. This suggests that the locus of dunite formation was near the end of emplacement of the peridotite at fairly low pressures close to the base of the crust.

Mineralogy

Mineral analyses of a representative suite of dunites, troctolites, and other gabbroic segregations are given in Tables 3 through 7. There is a significant range in olivine composition, with the dunites ranging from Fo_{93} to $Fo_{89.3}$, troctolites from $Fo_{89.6}$ to $Fo_{87.1}$, olivine gabbronorites from $Fo_{88.8}$ to $Fo_{86.7}$, and a single olivine-gabbro with $Fo_{85.9}$. Although there is considerable overlap in composition, a general progression in olivine composition toward more iron-rich compositions is seen with the successive appearance of plagioclase and then clinopyroxene in the gabbroic segregations. This is consistent with an inferred sequence of the successive formation of dunite, followed by troctolite, olivine-gabbro, and then olivine-gabbronorite and gabbro.

The single analysis of olivine in the dunites with a forsterite content (Fo_{93}) higher than that in the wall-rock harzburgite, is believed to be due to local subsolidus reequilibration of spinel and olivine. Subsolidus reequilibration, where the local proportion of spinel to olivine is high, will shift the composition of the olivine to more magnesian compositions (Dick and Bullen, 1984; Irvine, 1965, 1967), and it is likely that we analyzed an olivine grain sufficiently close to a spinel grain that its forsterite content was raised by reequilibration. For the remainder of the analyses, significant reequilibration of spinel did occur with olivine, producing a substantial shift toward more iron-rich spinel compositions (geothermometry for our olivine-spinel pairs should give temperatures of around 800°C based on similar suites). The shift in spinel composition due to reequilibration, however, is a function of relative proportions of spinel and olivine (the lever-rule) and the relevant partition coefficients for the spinel end-members and olivine. Because spinel is an accessory phase, this shift in composition is relatively uniform and a direct function of olivine composition, preserving the original igneous trend. Olivine greatly exceeds spinel in volume (average mode: 83.6% olivine and 0.7% spinel [in the harzburgites]), so the effect of subsolidus spinel-olivine reequilibration on olivine composition is negligible.

The gabbroic segregations locally contain abundant clinopyroxene and more rarely orthopyroxene. Clinopyroxene is also found as an intragranular accessory phase in plagioclase-bearing dunites and troctolites. In the pyroxene quadrilateral (Fig. 6), the pyroxenes in the gabbroic segregations plot immediately to the right of the harzburgite array. Whereas clinopyroxene in the harzburgites has an average $Mg\#$ [$Mg/(Mg+Fe)$] of 92.3 ± 0.5 , it is significantly less magnesian in the dunites and gabbroic segregations, averaging 90.0 ± 1.0 and extending to values as low as $Mg\#$ 88.5 in one gabbro.

Although pyroxenes in the gabbroic segregations lie close to the harzburgite array in the pyroxene quadrilateral, they are compositionally very different with respect to incompatible elements. Notably they contain 1 to 2 orders of magnitude more titanium and sodium. Alumina contents range upward from that of pyroxene in the harzburgites to twice as much (2.16 to 4.26 wt%). It is clear, therefore, that the melts with which these pyroxenes last equilibrated were too evolved to have been in equilibrium with the harzburgite.

Chromian spinel is a ubiquitous accessory in the dunites and gabbroic segregations. It is plotted with the spinels from the harzburgites on the Cr-Al-Mg-Fe⁺² face of the spinel composition prism in Figure

Figure 12 (facing page). Representative troctolitic segregations from Site 895. A 2-cm scale bar is shown at the lower right of each photo. A, C, and F are oriented fragments with top toward the bottom of A, and to the left for C and F. **A.** Sample 147-895C-4R-2, 93–135 cm, back sides of archive and working halves of the core (to the left and right, respectively), showing an irregular subvertical gabbroic intrusion located between 108 and 120 cm. The segregation grades toward the lower left and upper right in the photo into troctolite, then plagioclase dunite, and locally dunite at its margins. Note that the segregation also grades internally from a coarse breccia of troctolite consisting of dunite clasts cemented by plagioclase on the backside of the archive half, to a 13 × 3 cm olivine gabbro lens on the backside of the working half of the core. **B.** Sample 147-895E-3R-1, Piece 16, 105–111 cm, (working half) showing a small coarse-grained granular gabbro vein with irregular sutured margins in serpentinized dunite. The gabbro is heavily altered, with plagioclase completely replaced by secondary hydrothermal minerals. It contains coarse granular clinopyroxene, occasionally enclosing round olivine chadacrysts, intergrown with coarse-grained plagioclase (pseudomorphs) and olivine. Locally plagioclase encloses subhedral chrome spinel. The dunite is 98% serpentine after olivine, contains about 1% holly leaf to subhedral chrome spinel and 1% relict olivine. No clinopyroxene relicts were observed in the dunite. **C.** Sample 147-895D-7R-1, Piece 8, 44–56 cm (working half). Disaggregated dunite with irregular poly-mineralic dunite clasts cemented by plagioclase. Sample grades from lower right from an autoclastic breccia of dunite cemented by plagioclase to the upper left where it is composed largely of medium-grained troctolite with gabbroic proportions of plagioclase that locally encloses several very coarse angular dunite clasts. **D.** Sample 147-895D-8R-2, Piece 4, 32–41 cm (archive half). Heterogeneous troctolite with plagioclase content ranging from gabbroic proportions (approximately 60 vol%) on the right, to areas with disaggregated dunite clasts at lower left where dunite clasts make up close to 85% of the sample. Clinopyroxene is present in several large intergranular grains, but mostly as coronas or selvages between plagioclase and olivine (Gillis, Mével, Allan, et al., 1993). **E.** Sample 147-895E-1R-3, Piece 9, 114–124 cm (archive half). Troctolite with gabbroic proportions of plagioclase and olivine showing a moderate foliation of possible late-magmatic origin (Gillis, Mével, Allan, et al., 1993). **F.** Sample 147-895D-8R-1, Piece 10, 66–75 cm (archive half). Compound dike consisting of a thin selvage of medium-grained granular dunite on the left in sharp contact with coarse-grained troctolite cut in turn by medium-grained troctolite. The coarse-grained troctolite consists of coarse angular clasts of medium-grained granular dunite enclosed in a lesser amount of coarse-grained intergranular plagioclase. The contact between the medium and coarse troctolites, while sutured on a thin section scale, macroscopically cuts across individual dunite clasts and is sharp in hand specimen. The medium-grained troctolite has medium- to coarse-grained poikilitic to subophitic granular plagioclase enclosing numerous medium- to fine-grained round olivine chadacrysts. The olivine is frequently rimmed by a thin selvage or corona of clinopyroxene, suggesting a late reaction-relation between olivine and melt. The coarse troctolite is interpreted as a disaggregated dunite impregnated by cumulus plagioclase, clinopyroxene, and olivine.

8, and presented in an expanded projection in Figure 13. The spinels in the dunites and gabbroic segregations define a trend extending upward from the harzburgite array toward more iron-rich and somewhat more chromian compositions. This trend is expected for fractionation of olivine and plagioclase as crystallization of plagioclase increases melt Cr# even as coprecipitation of olivine rapidly reduces melt Mg/(Mg+Fe) (Dick and Bullen, 1984). By contrast, early precipitation of clinopyroxene, which contains substantial Cr, would cause the trend to drop toward less chromian compositions with increasing iron content.

We note that while subsolidus reequilibration shifts the composition of accessory spinel to more iron-rich compositions, this cannot account for the variations in Cr and Al, which must relate to igneous petrogenesis. Reequilibration with clinopyroxene will affect slightly the partitioning of Cr and Al, shifting the composition of the co-existing spinel to higher chrome contents (Komor et al., 1985a). Where there are large modal variations in the proportion of pyroxene, this can produce a considerable spread in spinel Cr#. In our samples, however, reequilibration with clinopyroxene obviously cannot account for the systematic trend toward higher chrome contents in the dunites and troctolites that contain little or no diopside. Interestingly, the olivine-gabbros, which do contain significant diopside, and therefore potentially could have higher spinel Cr# due to reequilibration, define a separate field shifted toward lower Cr and Mg. This drop in spinel Cr#, then, likely reflects three-phase saturation and precipitation of chromian diopside. Similarly, the large spread in spinel Mg# requires large variations in the relative proportions of silicates and oxides in the various samples to account for by reequilibration (Dick and Bullen, 1984; Irvine, 1965, 1967). Together with the systematically lower forsterite content of the coexisting olivine, however, this variation is easily explained by crystal-fractionation.

Shown in Figure 14 is Cr number (Cr/(Cr+Al)) plotted against the weight percent TiO₂ in spinel. It is once again clear from this plot that the melt from which the spinels precipitated was not in equilibrium with spinel in the harzburgite which consistently has far lower TiO₂. High TiO₂ in spinel is associated with the crystallization of trapped melt in abyssal peridotites, and is a characteristic feature of Cr spinel in dunites and troctolites in both ophiolitic and oceanic peridotites and dunites (Dick, 1977b; Hebert et al., 1983; Dick and Bullen, 1984; Girardeau and Francheteau, 1993; Cannat et al., 1990). The enrichment and extreme variation of TiO₂ in the gabbroic segregations and dunites is quite notable, particularly when it is examined in a plot against olivine composition (Fig. 15), where there is a six-fold increase in spinel TiO₂ over only a 2% to 4% change in olivine forsterite content. This variation cannot be accounted for by reequilibration, as the dunites contain no titaniferous phase other than spinel. It must, therefore, reflect large variations in the composition of the liquids migrating through the dunites.

Plagioclase in the gabbroic segregations has a bimodal composition distribution (Fig. 16) with a peak in abundance, confined to olivine gabbros and gabbros, at around An₉₇, and a second higher peak, represented by all rock types at An₈₆. Individual spot analyses in the first group, which we term ultra-calcic, extends from An_{93.9} up to An_{98.7}, and in the second group, which is merely calcic, from An_{88.5} down to An_{74.6}. Shown in Figure 17 are plagioclase core and rim compositions. Substantial zoning exists, with two of the ultra-calcic anorthites exhibiting slight reverse zoning toward more calcic rims, while three are weakly and two strongly normally zoned with more sodic rims. The more "sodic" calcic population also shows both normal and reverse zoning. Overall, reverse zoning is somewhat more common than normal zoning.

The plagioclase in the Site 895 gabbroic segregations is significantly more calcic overall than the plagioclase found in the Hole 894G gabbros, though there are some very calcic plagioclase xenocrysts in the Hole 894G gabbros. This is clearly illustrated by gabbroic Sample 147-894G-9R-4, 84–88 cm, which contains both a high calcium plagioclase suite, and a more sodic suite lying close to

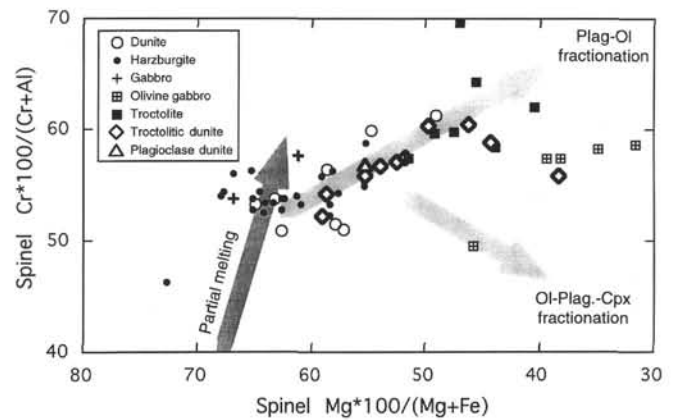


Figure 13. Expanded plot of spinel compositions in the Cr-Al-Mg-Fe face of the spinel composition prism. The Mg-Fe axis is distorted (lengthened) to allow better discrimination of the composition fields for different types of gabbroic segregation. General trends for spinel compositions for progressive partial melting (dark shaded arrow) and for plagioclase-olivine and olivine-plagioclase-clinopyroxene fractionation are shown from Dick and Bullen (1984).

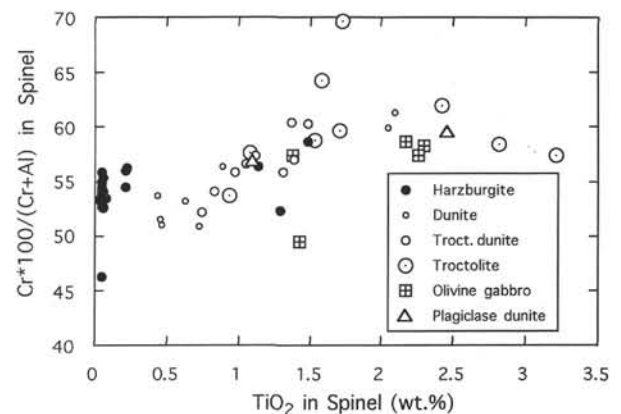


Figure 14. Weight percent TiO₂ plotted against the molecular Cr/(Cr+Al) (Cr#) for spinel in Site 895 harzburgites, dunites, and gabbroic segregations.

the maxima in plagioclase abundance for Hole 894G (Fig. 16). Natland and Dick (this volume) postulate that the high-calcium plagioclase suite from Hole 894G represents xenocrysts crystallized in the shallow mantle or lower crust, arguing that this represents intrusion of relatively unmodified mantle melts to high levels in the plutonic sequence directly beneath the melt lens. The more sodic main plagioclase suite at Hole 894G, they believe, derives by crystallization from liquids representing post-cumulus migration of highly fractionated (ferrobasaltic to ferroandesitic) melts through an open crystal network. The more calcic plagioclase xenocrysts were preserved due to incomplete reequilibration prior to sealing of the cumulate by accumulative crystal growth.

In Figure 11, we show that the anorthite content of the calcic plagioclase suite from Site 895 plots along a reasonable extension of the field for the Hole 894G high-level gabbros. The Site 895 calcic suite also lies within the composition range for depleted MORBs similar to those from Hole 504B (Kempton et al., 1985; Natland et al., 1983). The majority of MORB glasses are characterized by Ca/(Ca+Na) values from 64 to 78 corresponding to equilibrium feldspar compositions ranging from An₆₀ to An₈₅, though MORBs as calcic as Ca/(Ca+Na) = 84 do occur (Panjasawatwong et al., 1995). Since the more calcic Hess Deep basalt glasses plotted in Figure 11 project back to Ca/(Ca+Na) greater than 80 (Fig. 11B), we conclude that the

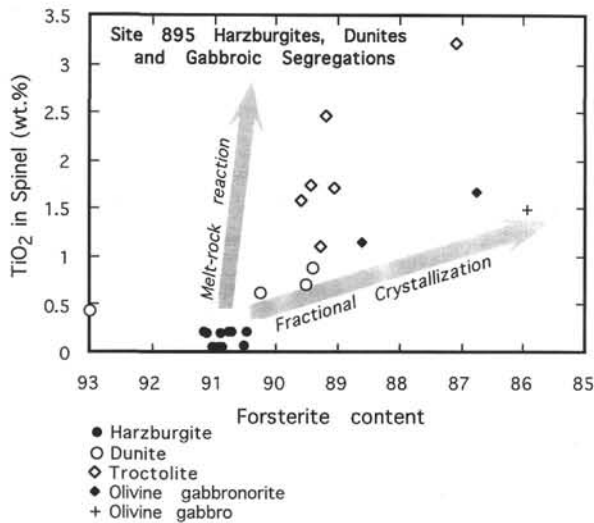


Figure 15. Weight percent TiO_2 plotted against the forsterite content of co-existing olivine. Shown for comparison are the approximate trends for melt-rock reaction where $\text{Mg}/(\text{Mg}+\text{Fe})$ is buffered by the mantle, and for closed-system fractional crystallization without interaction with the mantle.

liquids that crystallized the Site 895 calcic plagioclase suite may also be reasonable parent magmas for the Hole 894G gabbros.

The composition range of the ultra-calcic plagioclase suite, however, lies entirely outside the known range of equilibrium compositions for erupted MORB and would seem too calcic to have crystallized from a reasonable parent magma for most of the Hole 894G gabbros. Based largely on textural evidence, and the presence of ultra-calcic plagioclase xenocrysts in some Hole 894G gabbros (Natland and Dick, this volume), we prefer the hypothesis that the ultra-calcic plagioclase is igneous, not metamorphic. It should be noted, however, that given the extensive alteration it is possible that the ultra-calcic plagioclase could represent cryptic metasomatic effects related to rodingitization of the gabbroic segregations during serpentinization. Igneous plagioclase this calcic has previously been reported only in high-calcium boninite lavas from island arcs (Falloon and Crawford, 1991). The petrogenesis of high-calcium boninite lavas dredged from the north Tonga ridge (Falloon and Crawford, 1991) and from some ophiolitic boninites and associated gabbros from the Troodos ophiolite (Duncan and Green, 1987; Malpas et al., 1989; Thy et al., 1989). The bimodal population, and the presence of both normal and reverse zoning argues for a complex crystallization history involving mixing of a highly refractory calcium- and alumina-rich melt with less calcic and aluminous primitive MORB.

Geochemistry

Clinopyroxenes in the gabbroic segregations from Site 895 have incompatible trace element concentrations that overlap those from the Hole 894G gabbros, despite the more evolved major element composition of the latter, and exhibit both higher and lower concentrations (Fig. 9). Also shown for comparison are the fields for phenocryst and groundmass clinopyroxene in Hole 504B diabase. The groundmass 504B clinopyroxenes provide values appropriate for in situ crystallized melt at low pressures where most of the titanium is contained in ilmenite and other late magmatic phases not found in the Site 895 gabbroic segregations. Notably, several Site 895 troctolites and troctolitic gabbros extend to values eight times that of the 504B groundmass. Such high values indicate that, despite the lack of late magmatic phases, these segregations most likely represent hybrid rocks composed of disaggregated dunite impregnated by crystallized trapped melt.

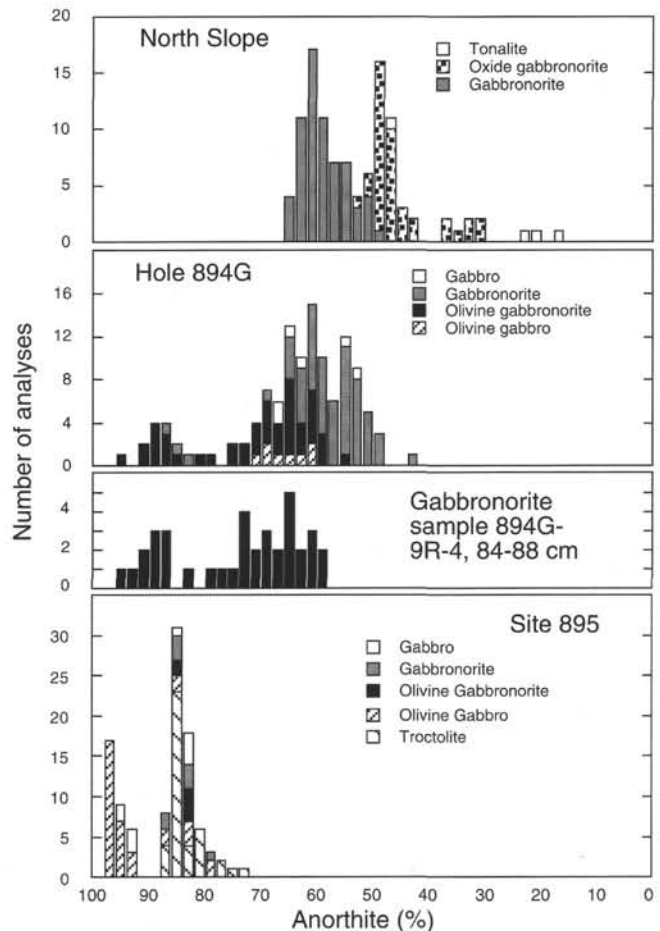


Figure 16. Histogram of plagioclase compositions from the North Wall (slope) of Hess Deep and Site 894 and 895 gabbros and gabbroic segregations. Data for the North Wall (slope) and for Hole 894G are from Natland and Dick (this volume). The plot represents the unaveraged compositions from the data used to compute the average compositions reported here and in Natland and Dick (this volume).

The large range in Zr/Ti ratios drops toward values within the composition field of the abyssal harzburgite array of Johnson et al. (1990). This spread in composition argues for a range in melt compositions. This range could be explained by melts derived by varying degrees of melting in the underlying mantle column and varying degrees of aggregation. More likely, the large variation in Figure 9 represents reaction with mantle peridotite. This is strongly supported by the REE patterns plotted for the same rocks in Figure 18. Progressive fractional melting produces sequential melts with a range of slopes in such REE-plots (Johnson et al., 1990), yet the Site 895 gabbroic segregations have nearly uniform patterns, indicating derivation from a single primary melt.

Based on rare earth element concentrations, there are two populations of gabbroic segregations, labeled C- and L-type in Figure 18. The calculated liquid compositions in equilibrium with the C-type gabbros are similar to normal MORB and overlap the more depleted end of the field for EPR basalts dredged to the west of Hess Deep (Fig. 19A). The second population has higher REE concentrations relative to the first, but with the same slope and shape except for a pronounced Eu-anomaly indicating significant plagioclase fractionation. It is entirely overlapped by the field for the Hole 894G gabbros (Fig. 19B), which is consistent with their derivation from the same magma by similar degrees of crystallization. In the case of the Site

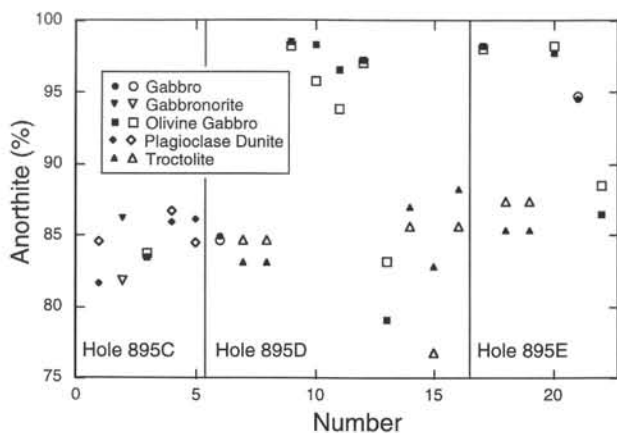


Figure 17. Anorthite contents of rims (open symbols) and cores (solid symbols) of individual plagioclase grains for Site 895 gabbros and troctolites plotted sequentially by analysis number to highlight the zoning patterns in the two populations represented in Figure 16.

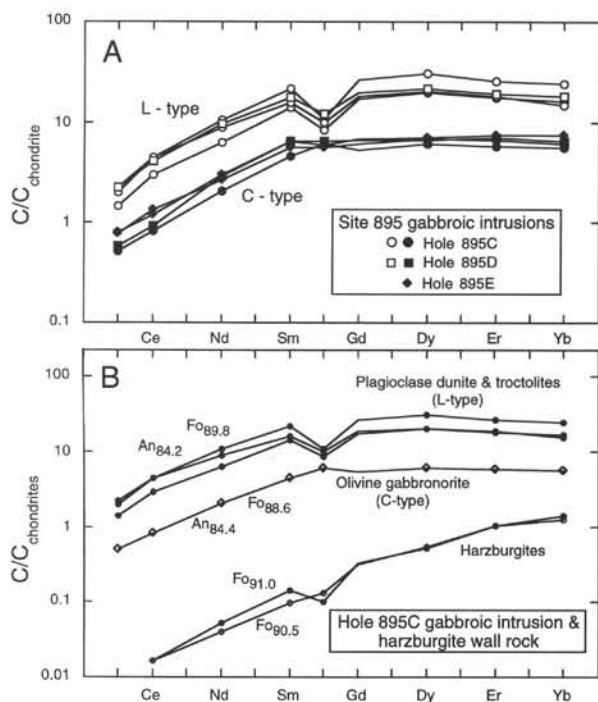


Figure 18. **A.** REE patterns for all Site 895 gabbroic segregations analyzed normalized to chondrites using the values of Anders and Grevesse (1989). **B.** REE patterns for diopsides in the gabbronorite and troctolite segregation and the wall-rock harzburgite from Hole 895C annotated with the composition of coexisting plagioclase and olivine. L-type refers to gabbroic segregations that have REE patterns and mineralogy suggestive of the crystallization of trapped melt. C-type refers to gabbroic segregations believed to reflect some form of cumulus crystallization from a liquid.

895 gabbros, however, the very forsteritic olivine, and very calcic plagioclase indicates that the composition of the melt was buffered during crystallization by melt-rock reaction.

Clinopyroxene in two olivine gabbros and one gabbro containing ultra-calcic plagioclase were analyzed for REE, and all contained C-type REE patterns. In contrast, clinopyroxene in segregations containing more sodic plagioclase included both L- and C-type patterns. Thus, the bimodal distribution of plagioclase compositions appears

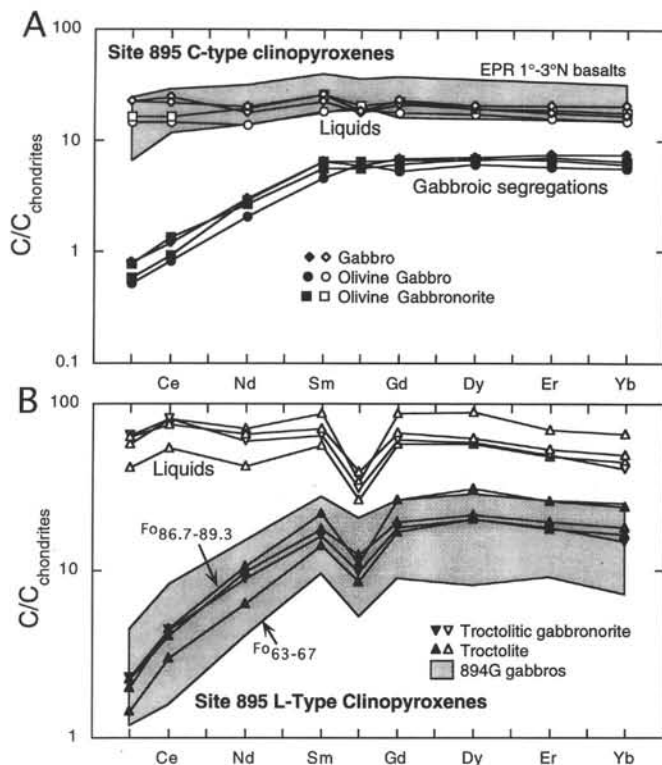


Figure 19. **A.** REE patterns for diopsides in C-type gabbroic segregations (solid symbols) and the composition of calculated co-existing liquids (open symbols). Field for East Pacific Rise basalts is from Lonsdale et al. (1992). **B.** REE patterns of diopsides in L-type gabbroic segregations (solid symbols) with the calculated equilibrium liquid compositions (open symbols). Shown for comparison is the field for Hole 894G gabbros (Dick, unpubl. data).

unrelated to the phenomena giving rise to the L- and C-type REE patterns.

Shown in Figure 12A is a small planar zoned gabbroic intrusive vein in harzburgite tectonite that displays the entire range of REE concentrations seen in the gabbroic segregations at Site 895. It consists of patchy olivine gabbronorite segregations at the center, enclosed in clinopyroxene-bearing troctolite, which in turn grades outward into plagioclase dunite. The feature is oriented near-vertically, is 2 to 4 cm thick, and extends several meters up a near continuous section of core from Hole 895C, though it locally tapers out. This is also the troctolite containing the complex coarse skeletal spinels intergrown with plagioclase. The preservation of such textures argues for relatively rapid formation of this small intrusion. Most of the feature consists of disaggregated dunite impregnated with plagioclase and minor clinopyroxene. The intrusion is reasonably interpreted as being close to the tip of a fracture-controlled intrusive dike in the harzburgite. The perfectly preserved primary igneous textures demonstrate that intrusion followed emplacement of the peridotite to near the base of the crust, as plastic deformation accompanying further mantle flow would have destroyed the delicate spinel textures.

Shown in Figure 18B are the REE patterns of diopside in the olivine gabbronorite at the center of the intrusion, several patterns from the troctolites and plagioclase dunite and an extremely depleted diopside pattern from the overlying wall-rock harzburgite. The olivine gabbronorite has the lowest REE concentrations in the intrusion and no europium anomaly (C-type segregation). The troctolites and one plagioclase dunite show the same pattern, but with a pronounced europium anomaly and a five-fold enrichment in REE (L-type). At the same time the C-type olivine gabbronorite has more iron-rich olivine. The intrusion does not contain any of the ultra-high-calcium plagioclase

clase, though, despite the enrichment in incompatible trace elements, plagioclase is only very slightly less calcic in the plagioclase dunite than that in the gabbronorite.

Ordinarily, a five-fold enrichment in highly incompatible elements is associated with about 80% crystallization of a MORB melt. The behavior of the major elements in the gabbroic vein contrasts sharply to that of the incompatible elements, and is contrary to that expected for normal fractional crystallization where $Mg/(Mg+Fe)$ and $Ca/(Ca+Na)$ should drop significantly. Where a melt crystallizes through reaction with the mantle, however, as its mass shrinks, the melt becomes more magnesian due to both assimilation of enstatite from the harzburgite, and reequilibration with residual olivine and pyroxene in the matrix. At the same time, as it fractionates, only olivine, plagioclase, and minor clinopyroxene, the incompatible elements are strongly enriched in the melt. Calcium addition from assimilated enstatite and diopside, as well as melt reequilibration with the remaining residual mantle mineralogy offsets the effects of plagioclase fractionation on melt Ca/Na , causing it to remain nearly constant in the case of the gabbroic vein.

DISCUSSION OF THE GABBROIC SEGREGATIONS

The Site 895 section bears a close resemblance to the stratigraphy in ophiolite complexes immediately beneath the "petrologic" Moho (e.g., Boudier and Coleman, 1981; Ceuleneer and Nicolas, 1985; Nicolas, 1989; Nicolas et al., 1988; Nicolas and Violette, 1982; Quick, 1981a; Ramp, 1961; Savel'yeva et al., 1980). These latter rocks correspond to zones in the ophiolite mantle sections where harzburgites are crosscut by dunite pods, which often contain melt segregations and impregnations at their cores. Dunite and gabbroic impregnations in dunite occurring with harzburgite tectonites appear to be widely distributed across the intra-rift high based on the dive and dredge results of Francheteau et al. (1990), and have been previously interpreted as representing the mantle transition zone immediately underlying the crust (Hekinian et al., 1993). The lack of in situ stratigraphy, however, has limited detailed interpretation of the dredge and submersible grab samples as the exact relationship of one rock to another can only be done by inference based on the stratigraphy of ophiolites. Hekinian et al. (1993) also report an extensive suite of primitive gabbros in their dredge and dive collections that they interpret as corresponding to the layered gabbros seen in the lower portions of the Oman ophiolite plutonic sequence. Many of these mineralogically fall in a compositional gap between the Site 895 gabbroic segregations and the Hole 894G high-level gabbros. Some of the samples they include in this suite, however, resemble the gabbroic segregations drilled at Site 895, and may have been inadvertently placed in the wrong part of the crust mantle sequence.

Origin of the Dunites

The origin of dunites crosscutting mantle harzburgite tectonites is now fairly well understood. Thermodynamically, a melt formed at high pressure must shift its composition to remain in equilibrium with the mantle as it moves upward (O'Hara, 1968; Kelemen et al., 1990; Kushiro, 1964; Kushiro, 1972). It can do this by fractionating olivine, and by dissolving pyroxene from the mantle as it ascends. If melt flow through the mantle is sufficiently rapid, or sufficiently focused, then the melt may fall out of equilibrium with the four-phase mantle assemblage. In this case it will incongruently dissolve enstatite and diopside, leaving only an olivine residue behind. The "podiform dunites" found in the mantle sections of many ophiolites are widely believed to be the products of such melt-rock reaction between mantle and ascending magmas (Dick, 1977a; Kelemen, 1986; Kelemen et al., 1990; Quick, 1981a). This disequilibrium process is potentially a major modifier of melt chemistry and may contradict many common assumptions about MORB petrogenesis if it is how

the Hess Deep dunites formed. Some of the dunite, however, may represent simple fractional crystallization of olivine from an ascending melt (e.g., O'Hara, 1968) in a permeable flow conduit where the mantle is already stripped of pyroxene.

The inferred lithologic sequence at Site 895, with harzburgite enclosing dunite, which in turn encloses troctolite, which then may enclose olivine gabbro and gabbronorite (Fig. 3) provides direct chemical and textural evidence that the melts from which the gabbros crystallized were not in equilibrium with the wall rock. This supports formation of the dunites by melt-rock reaction during migration of melts from higher pressures through the shallow mantle.

In only one case did we find a gabbroic segregation directly in contact with harzburgite. In all other cases, where the relationships were preserved, gabbro was in contact with dunite. This is also locally the case in the Oman ophiolite where melt extraction and hydrofracture are postulated to have occurred in the shallow mantle section (Ceuleneer and Rabinowicz, 1992; Nicolas, 1990). In such areas, troctolites with virtually identical textures to those shown in Figure 12 are abundant in dunite pods and dikes cutting the harzburgite. Elsewhere in the Oman mantle section, gabbroic dikes are found directly in contact with the harzburgite. These gabbros are believed to represent higher level melt transport through the mantle near the base of the crust when the section was cooler than in the zone of melt aggregation and segregation (Ceuleneer and Rabinowicz, 1992; Nicolas, 1990). This is also the likely origin for the one Hess Deep gabbroic segregation found in contact with harzburgite.

Sequence and Depth of Crystallization of the Gabbroic Segregations

From the textural and chemical progression corresponding to the Site 895 lithostratigraphy we conclude that the sequence of crystallization in these melts is olivine, olivine-spinel, olivine-spinel-plagioclase, olivine-spinel-plagioclase-clinopyroxene, olivine spinel-plagioclase-clinopyroxene-orthopyroxene, and finally in the extreme plagioclase clinopyroxene. A similar sequence, with plagioclase preceding olivine, was previously reported for gabbros dredged with peridotites and dunites at the Garret Fracture Zone (Hebert et al., 1983); a sequence that has lately also been attributed to the crust-mantle transition zone beneath the EPR (Cannat et al., 1990). This is the same sequence as seen in abyssal tholeiites (Bryan and Grove, 1986; Miyashiro et al., 1969; Miyashiro et al., 1970), and would be expected for the crystallization of MORB in the shallow mantle.

At high pressure, however, or for extremely depleted melt compositions, such as high magnesian andesite or boninite, clinopyroxene would be expected to precede plagioclase on the liquidus (Elthon, 1979). Petrogenetically, then, the order of appearance of olivine, plagioclase and clinopyroxene is important to the debate over the depth of segregation of MORB. Thus, particular significance has been attached to the appearance of wehrlites in many ophiolite complexes as an indicator of high pressure crystallization for MORB (Casey et al., 1983; Elthon, 1989; Elthon and Scarfe, 1984). Alternatively, the presence of such primitive olivine and clinopyroxene cumulates has been taken to indicate the melt from which they crystallized was not a MORB, but an arc-related magma. We have found no such wehrlites in any of the gabbroic segregations we have examined: a rock where clinopyroxene is an early crystallizing (cumulus) phase with olivine preceding the appearance of plagioclase.

Hekinian et al. (1993) refer to wehrlitic segregations and impregnations in their Hess Deep dredge and dive samples. The term wehrlite, however, used in the context of the Hess Deep samples is somewhat misleading in light of the preceding debate. None of the Hess Deep rocks appear to equate to the wehrlitic sequences seen in many ophiolites such as Oman and Troodos where clinopyroxene occurs as an early cumulus phase with olivine in massive wehrlite outcrops. Although clinopyroxene occurs locally in the Hess Deep dunites in the absence of plagioclase, it is volumetrically minor, and can be ex-

plained as the result of late-stage crystallization of an intergranular highly reacted MORB magma (Girardeau and Francheteau, 1993; Hekinian et al., 1993). If these clinopyroxene-bearing "wehrlitic" rocks have indeed crystallized at high pressures, it is then hard to explain why they are not extensively recrystallized due to plastic deformation accompanying extensive mantle flow to the base of the crust.

The Origin of the Bimodal REE Patterns: Evidence for Trapped Melt

A striking feature of the REE patterns of the Site 895 gabbroic segregations is their bimodal distribution. We consider two scenarios to explain this feature:

(A) The intrusion represents the following sequence: (1) initial intrusion of a MORB-like liquid near the tip of a fracture system into harzburgite immediately below the Moho at a temperature significantly below the liquidus, but above the solidus of the basalt; (2) reaction with the harzburgite, dissolving enstatite and diopside to form dunite, locally disaggregating the peridotite at the center of the fracture; (3) initial crystallization of olivine and skeletal spinel occurred due to slight undercooling of the melt; (4) a rapid, near simultaneous appearance of plagioclase and clinopyroxene on the liquidus with spinel and olivine as the liquid cooled, producing a C-type olivine gabbro cumulate at the center of the vein; (5) migration of the crystallizing liquid out into the dunite as it fractionated, precipitating clinopyroxene reflecting close to 80% reduction of the liquid mass, and therefore a five-fold enrichment in incompatible elements, but with liquidus compositions of olivine, plagioclase, and pyroxene buffered by melt-mantle reaction to high-Mg and high-Ca compositions.

(B) The above scenario, however, does not explain the striking bimodal composition of the REEs in the gabbroic segregations. As the bimodality is found for all the gabbroic segregations, including segregations from holes 250 m apart, we suggest that the type-L patterns represent in situ crystallization of trapped melt, and the type-C represent cumulus crystallization from primitive MORB passing up through the open fracture. The sequence of events we envision for this scenario is: (1) At the initiation of the fracture, dilation at the fracture tip opens up the harzburgite matrix, allowing melt to invade it and dissolve pyroxene by reaction, producing dunite. (2) As dike propagation proceeds, melt in the matrix is gradually expelled back into the dike, mixing with fresh MORB moving through the dike. Locally, the melt may not be fully expelled from the matrix, and the trapped melt may undergo extensive in situ crystallization to form L-type gabbroic segregations.

Such in situ crystallization of trapped melt produces a gabbroic assemblage of olivine, plagioclase, and clinopyroxene that impregnates the residual dunite. A characteristic feature of this assemblage is that it has the same REE pattern as the Hole 894G high-level gabbros, because both represent extensive in situ cotectic crystallization of MORB. The five-fold enrichment of REE in the clinopyroxene reflects the percentage of clinopyroxene that crystallized from the melt relative to plagioclase and olivine, which much more efficiently exclude these elements (roughly 20% clinopyroxene, 20% olivine, and 60% plagioclase assuming cotectic crystallization). The large Eu anomaly reflects uptake of Eu by the plagioclase in the impregnating assemblage. The Mg-rich olivine and calcic plagioclase, relative to the Hole 894G assemblage, on the other hand, reflects the extensive reaction of the melt with the mantle assemblage and buffering of melt Mg and Ca during crystallization. It could be, as for the Hole 894G gabbros (Natland and Dick, this volume), that the impregnating assemblage may not represent complete liquid crystallization, and that some late liquid may have escaped by infiltration out through the peridotite or to the center of the dike. Determining the latter, however, requires a full mass balance, with complete major and trace element compositions for all the phases, and accurate modal proportions for the troctolite, which may not be possible to obtain given the degree of alteration of the gabbroic segregations. The high Zr and Ti

contents of the L-type clinopyroxenes, on the other hand, do make it reasonable that some of these gabbroic segregations do represent trapped liquid (Fig. 9; Table 8).

The solidification of trapped melts by reaction in the shallow mantle, as proposed for the L-type gabbroic segregations, can simply be thought of as equating to the bulk composition of trapped melt + peridotite lying below the mantle solidus. Thus, by reaction, a liquid initially at 1230°C that is not in equilibrium with the mantle, will react, bringing its composition toward equilibrium with the host peridotite. As this reaction proceeds, if the bulk composition of mantle plus melt is below the solidus, then the liquid will completely crystallize before it reaches equilibrium with the mantle assemblage and becomes a stable phase. An interesting sidelight to this process is that it proceeds essentially isothermally, buffered by the mantle temperature. This likely explains the absence of late-magmatic phases such as apatite, ilmenite, or zircon in the L-type gabbroic segregations, as these generally become stable on the basalt liquidus at relatively low temperatures (<1100°C). Instead, clinopyroxene (and spinel for titanium) proxies as a host for the highly incompatible elements, and has concentrations reaching those found in some primitive MORBs (e.g., Fig. 9; Table 8).

The Bimodal Composition of Plagioclase and the Origin of Ultra-calcic Plagioclase

Another striking feature of the Site 895 gabbroic segregations is the bimodal plagioclase compositions that argue for the presence of at least two different liquids. The ultra-calcic plagioclase found in a number of the olivine gabbros are at present unique from a mid-ocean ridge environment. Similar ultra-calcic plagioclase, though not extending to quite as high anorthite-contents (An_{94}), has been widely reported in MORB (Duncan and Green, 1980; Elthon and Scarfe, 1984; Panjasawatwong et al., 1995; Sinton et al., 1993). The anorthite content of plagioclase has been found to be dependent on three major factors, increasing with melt Ca/(Ca+Na), alumina content Al/(Al+Si) and decreasing pressure over the range 5–10 kb (Panjasawatwong et al., 1995). Several models have been used to explain these xenocrysts. One suggests that they are the products of high-pressure fractionation in association with high-Mg pyroxene of MORB (Elthon, 1984). Another model suggests that they are the product of crystallization from refractory melts formed at the end of the melting process at relatively shallow depths (Duncan and Green, 1980; Panjasawatwong et al., 1995; Sobolev and Shimizu, 1993).

The presence of high-calcium plagioclase in the Hess Deep Site 895 gabbroic segregations associated with high-Mg diopside, however, suggests a third possibility. They may be the products of melt-rock reaction where melts stagnate in melt-transport conduit in the shallow mantle. Wall-rock reaction, with dissolution of enstatite from a highly depleted mantle section and precipitation of olivine, essentially adds only silica, calcium, alumina, and minor titanium to the melt, while at the same time buffering melt Mg/Fe. This reaction will bring plagioclase, and eventually clinopyroxene, onto the liquidus, as observed in the Hess Deep gabbroic segregations. Thus, a monitor of the reaction progress, in addition to spinel TiO_2 , will be melt alumina and CaO/Na₂O, which will change dependent on the relative proportions of assimilated and precipitant during reaction and the composition of the assimilated and precipitate. Melt-rock reaction can increase melt Ca/Na and alumina where only olivine is fractionated whether melt mass increases or decreases.

Simple mass balance (Table 9) shows that melt alumina and Ca/Na ratio increases simply through assimilation of pyroxene and fractionation of olivine and plagioclase where the mass proportion of pyroxene dissolved roughly exceeds the mass fraction of plagioclase precipitated. If the mass fraction of plagioclase precipitated exceeds that of pyroxene assimilated, Ca/Na should drop. By simple dissolution of pyroxene and precipitation of olivine during isobaric crystallization of trapped melt in the Hess Deep section, however, it is very

Table 9. Simple mass balances for melt-mantle reaction.

	Melt		Assimilant		Precipitant		Add 10% Px			Add 10% Px		1270°C
	ALV528, 4-1 FAMOUS		Enstatite	Diopside	Olivine	Plagioclase	Add 10% Px ppt 5% Ol	Add 10% Px ppt 10% Ol	Add 10% Px ppt 20% Ol	ppt 4% Ol ppt 6% Pl	ppt 8% Ol ppt 12% Pl	High alumina melt inclusion
SiO ₂	49.93	55.90	52.90	40.50	47.10	51.19	51.74	53.01	51.31	52.07	48.13	
TiO ₂	0.72	0.02	0.04	0.01	0.01	0.69	0.73	0.81	0.73	0.81	0.67	
Al ₂ O ₃	15.82	2.19	3.22	0.03	33.60	15.36	16.13	17.94	14.10	13.42	18.14	
FeO	8.37	5.60	2.65	8.97	0.05	8.10	8.06	7.96	8.59	9.15	7.13	
MnO	0.15	0.15	0.09	0.16		0.15	0.15	0.15	0.16	0.17	0.15	
MgO	9.78	32.40	18.40	50.50	0.10	9.97	7.93	3.17	10.96	9.92	10.44	
CaO	12.67	2.45	22.10	0.09	16.90	12.47	13.10	14.55	12.08	12.29	12.88	
Na ₂ O	1.96	na	na	na	1.65	1.88	1.97	2.19	1.87	1.97	2.12	
K ₂ O	0.05	na	na	na	0.09	0.05	0.05	0.06	0.04	0.04	0.02	
P ₂ O ₅	na	na	na	na	na	0.00	0.00	0.00	0.00	0.00	0.05	
Cr ₂ O ₃	0.08	0.78	na	na	na	0.15	0.15	0.17	0.15	0.17		
Total	99.53	99.49	99.40	100.26	99.49	100.00	100.00	100.00	100.00	100.00	99.73	
Mg#	0.68	0.91	0.93	0.91	0.78	0.69	0.64	0.42	0.69	0.66	0.72	
CaO/Na ₂ O	6.46				10.24	6.65	6.64	6.64	6.46	6.24	6.08	
Ca/(Ca+Na)	0.78					0.79	0.79	0.79	0.78	0.78	0.77	
Al/(Al+Si)	0.27					0.26	0.27	0.29	0.24	0.23	0.31	

Notes: FAMOUS basalt glass is from Bryan and Moore (1977); all other data come from this paper. The relative proportion of enstatite to diopside in the average Hess Deep harzburgite is 0.94:0.06, which is the ratio used for the assimilant (Px) in the calculations. The proportion of plagioclase to olivine (0.6:0.4) used in some of the calculations is equal to the plagioclase-olivine cotectic proportions found for natural MORB (e.g., Dick and Bryan, 1978). Mg# = Mg/(Mg+Fe) using atomic proportions. Px = pyroxene, Ol = olivine, Pl = plagioclase, na = not analyzed. High alumina melt inclusions in An₉₁ plagioclase quenched at 1270°C from a high alumina tholeiitic basalt from the Galapagos Platform (Sinton et al., 1993).

unlikely that the liquid would reach Ca/Na ratios in equilibrium with the most calcic igneous plagioclase we have found. This reflects the low proportion of clinopyroxene in the Hess Deep harzburgites. The simple mass balance in Table 9, however, does show that melt-rock reaction can account for the near constant anorthite content of plagioclase in the Hole 895C micro-intrusion described earlier (Fig. 18B).

We also note that simple mass balance accounts only for the effects of dissolution and precipitation of phases and excludes reequilibration with the residual matrix mineralogy. About 12% of the total calcium in Site 895 harzburgites is included in olivine, and reequilibration between trapped melt and residual olivine alone may have a dramatic effect on melt Ca/Na. Progressive equilibration of melt with the residual mantle matrix seems likely to be part of the explanation for the highly calcic plagioclase found in many of the gabbroic segregations from Site 895.

Sinton et al. (1993) have suggested a model similar to what we envisage based on high alumina melt inclusions in high calcium plagioclase (An₉₁ to An₉₄) in Galapagos Platform tholeiites. These authors note the pseudoinvariant crystal-liquid reaction presented by Kinzler and Grove (1992), in which spinel + clinopyroxene + orthopyroxene react to liquid + olivine + plagioclase, and that during such a reaction, both crystal and liquid compositions are effectively buffered in terms of major elements by the bulk mineralogy of the mantle while major and trace elements are free to vary. They envisaged, therefore, the magma bodies undergoing such a reaction as occurring as relatively small dikes within a crystal mush region in the lower crust or upper mantle. We believe that we have documented exactly this scenario in the Site 895 gabbroic segregations.

The alternative model that the ultra-calcic plagioclase represents crystallization of ultra-depleted liquids produced at the end of a fractional melting sequence is undoubtedly viable for such plagioclase in some MORBS, given the presence of such liquids in MORB xenocrysts (Sobolev and Shimizu, 1993). In this light it is interesting to note that the ultracalcic plagioclase is limited to C-type olivine gabbros and one gabbro calculated to be in equilibrium with a primitive East Pacific Rise MORB from the region, not an ultra-depleted melt. While an ultra-depleted melt has a great depletion in LREE and a very steep REE pattern, melt-rock reaction in the shallow mantle will have little effect on the trace element composition of MORB as the mantle at this level is essentially stripped of trace elements. In the same light, simple in situ crystallization of trapped melt reacting with a relatively small volume of mantle matrix also does not appear to produce appropriate liquids as evidenced by the Hole 895C micro-intrusion.

We note that the effect of melt-rock reaction in the mantle is very sensitive to the ratio of diopside to enstatite, with melts becoming substantially more calcic by reaction with increasing mantle diopside content. The local harzburgite at Site 895 is extremely depleted in diopside, which may account for why crystallization of the Hole 895C microintrusion did not produce very calcic plagioclase. Aggregate MORB melts reacting at depth with a less depleted mantle, however, are likely to be much more calcic, and this may account for the magmas producing the ultra-calcic plagioclase in the Site 895 gabbroic segregations. It is reasonable that such melts may represent the migration of late stagnating melt up a dying conduit at the end of a cycle of hydrofracture-driven melt extraction from the mantle.

Reintrusion of new batches of melt up through a conduit containing stagnated melt would mix with the remaining basalts. As the volume of stagnated melt is presumably small, it would have little effect on the liquid composition of the erupted basalt, though it may account for much of the vertical scatter of the Hole 894G plagioclase about any likely crystallization trend for a single primary melt in Figure 11.

Fractional Crystallization vs. Melt-rock Reaction

We have found considerable evidence in the Site 895 gabbroic segregations, and in the petrography of the residual mantle harzburgites for the effects of conductive cooling beneath the EPR on the evolution of shallow magmas. This potentially argues for significant chemical fractionation of the magmas by simple crystallization, as opposed to the putative effects of melt-rock assimilation.

Considerable insight into this process can be gained by comparing the titanium content of spinel to the composition of the coexisting olivine. For melt-rock reaction, the Mg# of the melt is effectively buffered by the mantle, while there is a large systematic decrease in liquid Mg# for fractional crystallization. Titanium, on the other hand is present in relatively small quantities in the residual mantle and behaves as an incompatible element with nearly linear enrichment throughout much of the early stages of fractional crystallization. Given the very small proportion of spinel in the gabbros and dunites (typically 1% or less), precipitation of spinel cannot have had a significant effect on titanium in the melt. Moreover, neither olivine or plagioclase takes up titanium. Thus, titanium should behave as a nearly incompatible element in the melt during formation of the dunites and troctolites. The large enrichments in titanium seen in Figure 15, therefore, would require 80%–90% closed system fractional crystallization accompanied by a very large change in Mg/(Mg+Fe) in olivine precipitating with the spinel. Such extensive fractional crystalli-

zation would also normally be accompanied by the appearance of late magmatic phases such as apatite and ilmenite, none of which is present in the Site 895 gabbroic segregations and dunites. Thus, simple closed-system fractional crystallization alone cannot account for the trend in spinel and olivine composition observed in the Site 895 dunites and gabbroic segregations.

Large increases in titanium in spinel with little or no change in the composition of the coexisting olivine, however, have been identified in dunites dredged with abyssal peridotites and in podiform dunite complexes crosscutting mantle harzburgites in ophiolites (Dick and Bullen, 1984). These enrichments are believed to represent melt-rock reaction between migrating melt and the mantle (Dick and Kelemen, 1991). Assimilation of mantle peridotite by decompressing melts migrating through the peridotite is driven by the shift in the liquidus away from olivine, leading to precipitation of olivine and dissolution of pyroxene, while buffering the liquid composition close to equilibrium with mantle olivine. If this takes place at constant melt mass, then there is little or no increase in melt titanium. If, on the other hand, more olivine is precipitated than pyroxene is dissolved, then the concentration of incompatible elements may increase rapidly as shown by the melt-rock reaction trend in Figure 15 with little or no change in the composition of the liquidus olivine.

Thus, the titanium content of spinel precipitated from a migrating melt can be controlled by two different processes: (1) the degree of melt-rock interaction and the extent to which melt mass is increasing or decreasing during melt transport, and (2) the amount of fractional crystallization of olivine and plagioclase due to simple closed-system fractional crystallization where interaction between mantle and melt is negligible. Where melt mass decreases, with limited interaction with the mantle, the composition of spinel and olivine precipitating from the melt will be affected by both processes and will lie between the two trends as shown in Figure 15. This is an assimilation-fractional-crystallization (AFC) composition field for melt-mantle interaction.

It is important to note that the degree of melt-rock interaction will be strongly affected by the velocity and flux of melt through the mantle conduit. Thus, where large volumes of melt pass through, there will be a negligible effect on melt composition. If melts pass slowly up through the conduit or stagnate there for any period, then the effects can be extreme. It is clear that most of the melts from which the spinels in the Site 895 gabbroic segregations precipitated were strongly influenced by interaction with the mantle, but were also affected to a significant degree by fractional crystallization. This would again appear to demonstrate that the gabbroic segregations formed at shallow depths where there was significant conductive heat loss in excess of the mantle adiabat.

Fracture Control of Late-stage Melt Transport

The mantle section at Hess Deep provides direct evidence of melt transport and melt-rock interaction in the shallow mantle. The occurrence of numerous dunite dikes argues for an episodic tapping and transport of melt out of the shallow mantle by repeated fracture events. The existence of brittle fracture in the mantle beneath the EPR suggests that there is an effective "lithosphere" there capable of supporting significant shear stress on the time scale needed for brittle fracture. How this might work is illustrated in Figure 20. As melt rises through the shallow mantle toward the crust, the melt velocity slows and melt fraction increases. The increased melt fraction weakens the mantle immediately beneath the crust, reducing the effective strength and thickness of the "lithospheric" zone. This, in turn, results in local failure and fracture in the zone of "lithospheric" necking beneath the ridge. These fractures then provide a high permeability pathway for melt, causing it to migrate out of the surrounding mantle toward, into, and up along the fractures. As melt drains from the mantle, however, the lithospheric zone strengthens and becomes thicker, and the melt conduits close as smaller and smaller volumes of late,

presumably more reacted, melt migrate up the conduit from depth. C-type gabbroic segregations crystallize at this stage from variably reacted melts ranging from primitive MORB to high-alumina basalt moving up the conduits from depth. At some point pockets of melt may be trapped, either by sealing of the surrounding rock by accumulate growth, or by simple closing of the fissure. This melt then slowly crystallizes in situ by reaction with the mantle to produce L-type gabbroic segregations. The process then repeats itself as melt continues to rise up into the base of the lithosphere from the mantle melting column. We note that our model for melt migration beneath the EPR is similar to those presented by workers studying gabbroic segregations and dunites in mantle ophiolites (Ceuleneer and Rabinowicz, 1992; Ceuleneer et al., 1988; Nicolas et al., 1988; Rabinowicz et al., 1987; Rabinowicz et al., 1984).

An interesting consequence of such a model, however, is that the mantle in the zone of melt aggregation and hydrofracture should be close to equilibrium with the melt. This is clearly not the case for the Hess Deep section, yet it is also clear from the extensive evidence for melt-rock interaction that the gabbroic segregations and the dunites formed at high temperatures near the liquidus of primitive MORB, conditions expected in the mantle immediately beneath the ridge. This observation, however, is consistent with a highly focused flow of melt in the mantle beneath the EPR. In such a situation, where melt may be aggregating and flowing up through the mantle by porous flow in a narrow finger extending up toward the base of the lithosphere perhaps only hundreds of meters wide, fracture and the formation of a melt-transport conduit would be initiated where the conduit extends into and locally weakens the overlying "lithospheric" cap. Once initiated, however, such fractures would likely rapidly propagate laterally for considerable distance into the mantle on either side as well as up toward the crust in a manner analogous to the formation of sheeted dikes. This would bring fully aggregated MORB into contact with the highly depleted mantle outside or above the zone of focused melt-flow, where it would react with and be modified by that mantle.

Thus, the geochemistry of the Site 895 section strongly supports a model of highly focused local melt flow in the mantle beneath the EPR. A simple uniform two-dimensional flow of melt through the mantle geometrically requires the shallowest mantle immediately below the crust to be nearly everywhere in equilibrium with MORB. This is clearly not the case. The focusing might be on quite a different scale than at slow-spreading ridges, however, with many local zones beneath a single ridge segment rather than a single major zone, reflecting a more two-dimensional structure of mantle (as opposed to melt) flow beneath fast-spreading ridges (Lin and Phipps Morgan, 1992).

The gabbroic segregations and the enclosing dunites are best explained as the products of shallow-level melt transport through the mantle accompanied by crystallization of olivine, plagioclase, clinopyroxene, and spinel. The crystallization of the type-C gabbroic assemblage demonstrates that fully aggregated MORB passed through the dunites, as fractional melts would have crystallized melts with REE patterns with varying slopes reflecting melt extraction at different degrees of melting (Johnson et al., 1990). The crystallization of the three-phase silicate assemblage, however, would not be expected if melting of the mantle continued to the base of the crust. Experimental petrology shows that liquids ascending through the mantle with increasing magma mass will precipitate only olivine and spinel, as melt composition shifts to maintain equilibrium with the wall rocks (Kushiro, 1964; Kushiro and Schairer, 1963; O'Hara, 1968). Crystallization of plagioclase and clinopyroxene in addition to olivine requires magma mass to decrease, and therefore to undergo conductive heat loss to the mantle wall rock. The temperature of the mantle at the time of crystallization of the melt segregations can be estimated using the composition of the olivine, plagioclase, and pyroxene. The extent of crystallization of melts passing through the conduit will be limited by the wall-rock temperature, and hence the

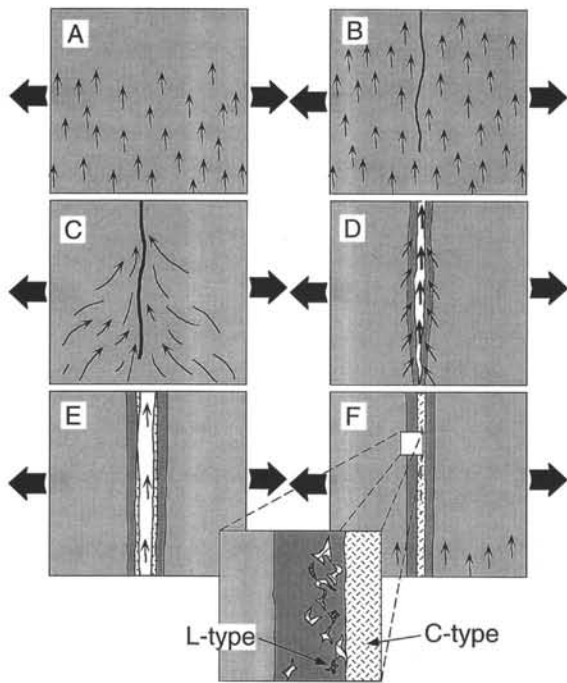


Figure 20. Model for dunite dike formation and melt migration in the shallow mantle beneath the East Pacific Rise. Light stippled pattern is harzburgite; lightweight arrows show direction and locus of percolating porous melt flow. Heavy black line in (B) indicates a downward propagating crack in the mantle beneath the ridge. Heavy stippled pattern indicates dunite formation due to accelerated upward melt flow, which causes the melt to lose saturation in pyroxene. Heavyweight arrow shows flow of segregated melt in open fracture. Hashed pattern at center of dunite in (E) is a C-type gabbroic segregation crystallizing on the walls of the conduit from melt migrating from depth up through the open conduit. Final panel shows the dike after conduit collapse, with a renewed upward percolation of melt through the mantle matrix. Inset shows late intergranular clinopyroxene (heavy diagonal lines) and plagioclase (light diagonal lines) crystallized from trapped melt in the dunite, forming an L-type gabbroic segregation. Scale is intentionally left ambiguous, but the average thickness measured for dunite at Site 895, corrected for the steep inclination of most harzburgite-dunite contacts, is about 0.3 m.

minimum forsterite and anorthite contents of the olivine and clinopyroxene. Allan and Dick (this volume) use this principle to estimate a mantle temperature of roughly 1230°C for the Site 895 mantle section at the time of crystallization of the gabbroic segregations.

CONCLUSIONS

As a result of our investigations and analysis of the Site 895 mantle section, we draw a number of major conclusions relevant to the generation of melts, shallow mantle melt transport and the nature of the mantle beneath the equatorial EPR.

1. The highly depleted composition of the Site 895 harzburgites and their unusual REE patterns, when considered in the light of the composition of the spatially associated basalts and gabbros, show that the Hess Deep section of EPR crust was generated by melting of an initially major- and trace-element-depleted mantle source compared to the mantle source in the Atlantic and Indian Oceans. Given the somewhat thinner than normal EPR crust in the region (5–5.5 km; Zonenshain et al., 1980), no unusual geothermal gradient or initial mantle temperature seems called for. We note that an unusually depleted

mantle source has also been invoked to explain the highly depleted nature of Hole 504B MORB at 84°W–1°N (Autio et al., 1989; Autio and Rhodes, 1983) some 1500 km to the east of Hess Deep south of the Cocos-Nazca Ridge. Collins et al. (1989) reported anomalously thin seismic crust at Site 504B, and a discrepancy with the correlation of Na_8 and crustal thickness postulated by Klein and Langmuir (1987). The nature of the depletion at these locations may be somewhat different in nature and origin; nonetheless, this points up the dangers in assuming that the Pacific mantle can be even roughly equated in composition to that of the Atlantic and Indian Oceans (e.g., Klein and Langmuir, 1987), and certainly challenges simple correlations of the major element depletion of basalts and peridotites to crustal thickness.

2. Like mantle peridotites dredged from the Atlantic and Indian Oceans (Johnson et al., 1990), the Hess Deep mantle harzburgites are in equilibrium with only extremely refractory late near-fractional melts of any reasonable mantle source composition. This demonstrates that East Pacific Rise MORB is also generated by open-system near-fractional melting and not by batch equilibrium melting.
3. The gabbroic segregations from Site 895 show that late-stage mantle-melt transport immediately beneath the Moho is, at least in part, fracture controlled. Parental melts transported through these conduits were fully aggregated MORB, demonstrating that fractional melts are aggregated at some point prior to intrusion to the crust, at least at this location.
4. Melt-rock (mantle) interaction in the shallow mantle has produced a significant volume of dunite in the Site 895 section. The overall effect on MORB melt composition may be small, but this does have significant ramifications for interpreting the genesis of MORB based on experiments on natural basalts: (A) the assimilation of arbitrary amounts of diopside and enstatite from the wall-rock harzburgite implies that the depth of melt segregation cannot be interpreted simply from these experiments; (B) MORB ascending through the shallow mantle is generally in equilibrium with mantle olivine at low pressures, but not much else; (C) high-magnesium pyroxene and high-calcium plagioclase, found as occasional xenocrysts in MORB at many localities in the oceans, may have originated as products of melt-rock reaction in the mantle, and should not, by themselves, be interpreted as evidence for fractional crystallization of these phases from MORB at high pressures. Taken together, these results show that high-magnesian primary MORB magmas segregated at high pressures are not as strong as has been previously suggested.
5. The best estimate of the composition of primary MORBS, and therefore of the overall ocean crust, is probably made by taking the composition of typical mid-ocean-ridge basalts saturated in olivine and plagioclase and extrapolating back along liquid lines of descent to simple equilibrium with olivine in the shallow mantle. Two additional components may be important in accounting for MORB composition and variability: (1) a more aluminous calcic liquid representing reacted melts produced during shallow mantle melt transport, and (2) ultra-depleted partial melts of mantle peridotite generated high in the melting column that did not share the mantle “plumbing system” traversed by more typical basalts.

ACKNOWLEDGMENTS

This research was supported in part by grants from the JOIDES US Science Support Advisory Committee, by funds provided by The Van Allen Clark Chair at Woods Hole Oceanographic Institution, and by funds provided by NSF Grant OCE 94-817404.00. Nilanjan Chatterjee provided technical assistance and conducted most of the

actual electron microprobe analysis. Dr. Nobu Shimizu provided enormous help in running the ion microprobe. This manuscript benefited greatly from reviews by Fred Frey and Jean Louis Bodinier, and from discussions with Peter Kelemen, Stan Hart, Nobu Shimizu, Peter Mayer, and Greg Hirth. We would also like to acknowledge the able crew of the *JOIDES Resolution*, without whom none of this would have been possible.

REFERENCES

- Albee, A.L., and Ray, L., 1970. Correction factors for electron microprobe analysis of silicates, oxides, carbonates, phosphates and sulfates. *Anal. Chem.*, 42:1408–1414.
- Anders, E., and Grevesse, N., 1989. Abundances of the elements: meteoritic and solar. *Geochim. Cosmochim. Acta*, 53:197–214.
- Autio, L.K., and Rhodes, J.M., 1983. Costa Rica Rift Zone basalts: geochemical and experimental data from a possible example of multistage melting. In Cann, J.R., Langseth, M.G., Honnorez, J., Von Herzen, R.P., White, S.M., et al., *Init. Repts. DSDP*, 69: Washington (U.S. Govt. Printing Office), 729–745.
- Autio, L.K., Sparks, J.W., and Rhodes, J.M., 1989. Geochemistry of Leg 111 basalts: intrusive feeders for highly depleted pillows and flows. In Becker, K., Sakai, H., et al., *Proc. ODP, Sci. Results*, 111: College Station, TX (Ocean Drilling Program), 3–16.
- Bence, A.E., and Albee, A.L., 1968. Empirical correction factors for the electron microanalysis of silicates and oxides. *J. Geol.*, 76:382–403.
- Bloomer, S.H., Meyer, P.S., Dick, H.J.B., Ozawa, K., and Natland, J.H., 1991. Textural and mineralogical variations in gabbroic rocks from Hole 735B. In Von Herzen, R.P., Robinson, P.T., et al., *Proc. ODP, Sci. Results*, 118: College Station, TX (Ocean Drilling Program), 21–39.
- Bonatti, E., Peyve, A., Kepezhinskas, P., Kurentsova, N., Seyler, M., Skolotnev, S., and Udintsev, G., 1992. Upper mantle heterogeneity below the Mid-Atlantic Ridge, 0°–15°N. *J. Geophys. Res.*, 97:4461–4476.
- Boudier, F., and Coleman, R.G., 1981. Cross section through the peridotite in the Samail ophiolite, southeastern Oman Mountains. *J. Geophys. Res.*, 86:2573–2592.
- Boudier, F., and Nicolas, A., 1972. Fusion partielle gabbroïque dans la lherzolite de Lanzo. *Bull. Suisse Mineral. Petrogr.*, 52:39–56.
- , 1977. Structural controls on partial melting in the Lanzo peridotites. *Bull.—Oreg. Dep. Geol. Miner. Ind.*, 96:63–78.
- Bryan, W.B., and Grove, T.L., 1986. Contrasting Atlantic and Pacific MORB phenocryst assemblages. *Eos*, 67:1255.
- Bryan, W.B., and Moore, J.G., 1977. Compositional variations of young basalts in the Mid-Atlantic Ridge rift valley near lat 36°49'N. *Geol. Soc. Am. Bull.*, 88:556–570.
- Cannat, M., 1993. Emplacement of mantle rocks in the seafloor at mid-ocean ridges. *J. Geophys. Res.*, 98:4163–4172.
- Cannat, M., Bideau, D., and Hebert, R., 1990. Plastic deformation and magmatic impregnation in serpentinized ultramafic rocks from the Garrett transform fault (East Pacific Rise). *Earth Planet. Sci. Lett.*, 101:216–232.
- Casey, J.F., Karson, J.A., Elthon, D., Rosencrantz, E., and Titus, M., 1983. Reconstruction of the geometry of accretion during formation of the Bay of Islands Ophiolite Complex. *Tectonics*, 2:509–528.
- Cassard, D., Nicolas, A., Rabinovitch, M., Moutte, J., Leblanc, M., and Prinzhofer, A., 1981. Structural classification of chromite pods in Southern New Caledonia. *Econ. Geol.*, 76:805–831.
- Ceuleneer, G., and Nicolas, A., 1985. Structures in podiform chromite from the Maqsd district (Sumail ophiolite, Oman). *Miner. Deposita*, 20:177–185.
- Ceuleneer, G., Nicolas, A., and Boudier, F., 1988. Mantle flow patterns at an oceanic spreading centre: the Oman peridotite record. *Tectonophysics*, 151:1–26.
- Ceuleneer, G., and Rabinowicz, M., 1992. Mantle flow and melt migration beneath ocean ridges: models derived from observations in ophiolites. In Phipps Morgan, J.B., Blackman, D.K., and Sinton, J.M. (Eds.), *Mantle Flow and Melt Generation at Mid-Ocean Ridges*. Geophys. Monogr., Am. Geophys. Union, 71:123–154.
- Chayes, F., 1956. *Petrographic modal analysis: an elementary statistical approach*: London (John Wiley & Sons).
- Collins, J.A., Purdy, M.G., and Brocher, T.M., 1989. Seismic velocity structure at Deep Sea Drilling Project Site 504B, Panama Basin: evidence for thin oceanic crust. *J. Geophys. Res.*, 94:9283–9302.
- Dick, H.J.B., 1977a. Evidence of partial melting in the Josephine Peridotite. *Bull.—Oreg. Dep. Geol. Miner. Ind.*, 96:59–62.
- , 1977b. Partial melting in the Josephine peridotite. I. The effect of mineral composition and its consequence for geobarometry and geothermometry. *Am. J. Sci.*, 277:801–832.
- , 1989. Abyssal peridotites, very slow spreading ridges and ocean ridge magmatism. In Saunders, A.D., and Norry, M.J. (Eds.), *Magmatism in the Ocean Basins*. Geol. Soc. Spec. Publ. London, 42:71–105.
- Dick, H.J.B., and Bryan, W.B., 1978. Variation of basalt phenocryst mineralogy and rock compositions in DSDP Hole 396B. In Dmitriev, L., Heirtzler, J., et al., *Init. Repts. DSDP*, 46: Washington (U.S. Govt. Printing Office), 215–225.
- Dick, H.J.B., and Bullen, T., 1984. Chromian spinel as a petrogenetic indicator in abyssal and alpine-type peridotites and spatially associated lavas. *Contrib. Mineral. Petrol.*, 86:54–76.
- Dick, H.J.B., and Fisher, R.L., 1984. Mineralogical studies of the residues of mantle melting: abyssal and alpine-type peridotites. In Kornprobst, J. (Ed.), *Kimberlites II: The Mantle and Crust-Mantle Relationships*: Amsterdam (Elsevier), 295–308.
- Dick, H.J.B., Fisher, R.L., and Bryan, W.B., 1984. Mineralogical variability of the uppermost mantle along mid-ocean ridges. *Earth Planet. Sci. Lett.*, 69:88–106.
- Dick, H.J.B., and Kelemen, P.B., 1991. Chromian spinel as a petrogenetic indicator of magmagenesis in shallow mantle rocks. *Eos*, 72:142.
- Dick, H.J.B., Meyer, P.S., Bloomer, S., Kirby, S., Stakes, D., and Mawer, C., 1991a. Lithostratigraphic evolution of an in-situ section of oceanic Layer 3. In Von Herzen, R.P., Robinson, P.T., et al., *Proc. ODP, Sci. Results*, 118: College Station, TX (Ocean Drilling Program), 439–538.
- Dick, H.J.B., Robinson, P.T., and Meyer, P.S., 1992. The plutonic foundation of a slow-spreading ridge. In Duncan, R.A., Rea, D.K., Weissel, J.K., von Rad, U., and Kidd, R.B. (Eds.), *The Indian Ocean: A Synthesis of Results from the Ocean Drilling Program*. Geophys. Monogr., Am. Geophys. Union, 70:1–39.
- Dick, H.J.B., Schouten, H., Meyer, P.S., Gallo, D.G., Bergh, H., Tyce, R., Patriat, P., Johnson, K.T.M., Snow, J., and Fisher, A., 1991b. Tectonic evolution of the Atlantis II Fracture Zone. In Von Herzen, R.P., Robinson, P.T., et al., *Proc. ODP, Sci. Results*, 118: College Station, TX (Ocean Drilling Program), 359–398.
- Dick, H.J.B., and Sinton, J., 1979. Compositional layering in alpine peridotites: evidence for pressure solution creep in the mantle. *J. Geol.*, 87:403–416.
- Dickey, J.S., Jr., Yoder, H.S., Jr., and Schairer, J.F., 1971. Incongruent melting of chromian diopside and the origin of podiform chromite deposits. *Geol. Soc. Am., Abstr.*, 3:543–544.
- Duncan, R.A., and Green, D.H., 1980. Role of multistage melting in the formation of oceanic crust. *Geology*, 8:22–26.
- , 1987. The genesis of refractory melts in the formation of oceanic crust. *Contrib. Mineral. Petrol.*, 96:326–342.
- Elthon, D., 1979. High magnesia liquids as the parental magma for ocean floor basalts. *Nature*, 278:514–518.
- , 1987. Petrology of gabbroic rocks from the Mid-Cayman Rise spreading center. *J. Geophys. Res.*, 92:658–682.
- , 1989. Pressure of origin of primary mid-oceanic ridge basalts. In Saunders, A.D., and Norry, M.J. (Eds.), *Magmatism in the Ocean Basins*. Geol. Soc. Spec. Publ. London, 42:125–136.
- Elthon, D., and Scarfe, C.M., 1984. High-pressure phase equilibria of a high-magnesia basalt and the genesis of primary oceanic basalts. *Am. Mineral.*, 69:1–15.
- England, R.N., and Davies, H.L., 1973. Mineralogy of ultramafic cumulates and tectonites from eastern Papua. *Earth Planet. Sci. Lett.*, 17:416–425.
- Falloon, T.J., and Crawford, A.J., 1991. The petrogenesis of high-calcium boninite lavas dredged from the northern Tonga Ridge. *Earth Planet. Sci. Lett.*, 102:375–394.
- Francheteau, J., Armijo, R., Cheminée, J.L., Hekinian, R., Lonsdale, P.F., and Blum, N., 1990. 1 Ma East Pacific Rise oceanic crust and uppermost mantle exposed by rifting in Hess Deep (equatorial Pacific Ocean). *Earth Planet. Sci. Lett.*, 101:281–295.
- Gillis, K., Mével, C., Allan, J., et al., 1993. *Proc. ODP, Init. Repts.*, 147: College Station, TX (Ocean Drilling Program).
- Girardeau, J., and Francheteau, J., 1993. Plagioclase-wehrlites and peridotites on the East Pacific Rise (Hess Deep) and the Mid-Atlantic Ridge (DSDP Site 339) evidence for magma percolation in the oceanic upper mantle. *Earth Planet. Sci. Lett.*, 115:137–149.

- Hart, S.R., and Dunn, T., 1993. Experimental CPX/melt partitioning of 24 trace elements. *Contrib. Mineral. Petrol.*, 113:1–8.
- Hebert, R., Bideau, D., and Hekinian, R., 1983. Ultramafic and mafic rocks from the Garret transform fault near 13°30'S. on the East Pacific Rise: igneous petrology. *Earth Planet. Sci. Lett.*, 65:107–125.
- Hekinian, R., Bideau, D., Francheteau, J., Cheminée, J.L., Armijo, R., Lonsdale, P., and Blum, N., 1993. Petrology of the East Pacific Rise crust and upper mantle exposed in the Hess Deep (eastern equatorial Pacific). *J. Geophys. Res.*, 98:8069–8094.
- Hess, P.C., 1993. Phase equilibria constraints on the origin of ocean floor basalts. In Phipps Morgan, J., Blackman, D.K., and Sinton, J.M. (Eds.), *Mantle Flow and Melt Generation at Mid-Ocean Ridges*. Geophys. Monogr., Am. Geophys. Union, 71:67–102.
- Hodges, F.N., and Papike, J.J., 1976. DSDP Site 334: magmatic cumulates from oceanic layer 3. *J. Geophys. Res.*, 81:4135–4151.
- Irvine, T.N., 1965. Chromium spinel as a petrogenetic indicator, Part 1: theory. *Can. J. Earth Sci.*, 2:648–672.
- , 1967. Chromium spinel as a petrogenetic indicator, Part 2: petrological applications. *Can. J. Earth Sci.*, 4:71–103.
- Jacques, A.L., and Green, D.H., 1980. Anhydrous melting of peridotite at 0–15 kb pressure and the genesis of the tholeiitic basalts. *Contrib. Mineral. Petrol.*, 73:287–310.
- Johnson, K.T.M., and Dick, H.J.B., 1992. Open system melting and temporal and spatial variation of peridotite and basalt at the Atlantis II fracture zone. *J. Geophys. Res.*, 97:9219–9241.
- Johnson, K.T.M., Dick, H.J.B., and Shimizu, N., 1990. Melting in the oceanic upper mantle: an ion microprobe study of diopsides in abyssal peridotites. *J. Geophys. Res.*, 95:2661–2678.
- Karson, J.A., Hurst, S.D., and Lonsdale, P.F., 1992. Tectonic rotations of dikes in fast-spread oceanic crust exposed near Hess Deep. *Geology*, 20:685–688.
- Kelemen, P.B., 1986. Assimilation of ultramafic rocks in subduction-related magmatic arcs. *J. Geol.*, 94:829–843.
- Kelemen, P.B., Dick, H.J.B., and Quick, J.E., 1992. Formation of harzburgite by pervasive melt/rock reaction in the upper mantle. *Nature*, 358:635–641.
- Kelemen, P.B., Joyce, D.B., Webster, J.D., and Holloway, J.R., 1990. Reaction between ultramafic rock and fractionating basaltic magma II. Experimental investigation of reaction between olivine tholeiite and harzburgite at 11–15 kbar and 5 kb. *J. Petrol.*, 31:99–134.
- Kempton, P.D., Autio, L.K., Rhodes, J.M., Holdaway, M.J., Dungan, M.A., and Johnson, P., 1985. Petrology of basalts from Hole 504B, Deep Sea Drilling Project, Leg 83. In Anderson, R.N., Honnorez, J., Becker, K., et al., *Init. Repts. DSDP*, 83: Washington (U.S. Govt. Printing Office), 129–164.
- Kinzler, R.J., and Grove, T.L., 1992. Primary magmas of mid-ocean ridge basalts, I. Experiments and methods. *J. Geophys. Res.*, 97:6885–6906.
- Klein, E.M., and Langmuir, C.H., 1987. Global correlations of ocean ridge basalt chemistry with axial depth and crustal thickness. *J. Geophys. Res.*, 92:8089–8115.
- Komor, S.C., Elthon, D., and Casey, J.F., 1985a. Mineralogic variation in a layered ultramafic cumulate sequence at the North Arm Mountain Massif, Bay of Islands Ophiolite, Newfoundland. *J. Geophys. Res.*, 90:7705–7736.
- , 1985b. Serpentinization of cumulate ultramafic rocks from the North Arm Mountain massif of the Bay of Islands ophiolite. *Geochim. Cosmochim. Acta*, 49:2331–2338.
- Kushiro, I., 1964. The system diopside-forsterite-enstatite at 20 kilobars. *Yearbook—Carnegie Inst. Washington*, 63:101–108.
- , 1972. The effect of water on the composition of magmas formed at high pressures. *J. Petrol.*, 13:311–334.
- Kushiro, I., and Schairer, J.F., 1963. New data on the system diopside-forsterite-silica. *Yearbook—Carnegie Inst. Washington*, 62:95–103.
- Lin, J., and Phipps Morgan, J., 1992. The spreading rate dependence of three-dimensional midocean ridge gravity structure. *Geophys. Res. Lett.*, 19:13–16.
- Lindsley, D.H., and Andersen, D.J., 1983. A two-pyroxene thermometer. *J. Geophys. Res.*, 88:A887–A906.
- Lonsdale, P., 1988. Structural pattern of the Galapagos microplate and evolution of the Galapagos triple junctions. *J. Geophys. Res.*, 93:13551–13574.
- Lonsdale, P., Blum, N., and Puchelt, H., 1992. The RRR triple junction at the southern end of the Pacific-Cocos East Pacific Rise. *Earth Planet. Sci. Lett.*, 109:73–95.
- Malpas, J., Brace, T., and Dunsworth, S.M., 1989. Structural and petrologic relationships of the CY-4 drill hole of the Cyprus Crustal Study Project. *Pap.—Geol. Surv. Can.*, 88-9:39–68.
- Medaris, L.G., Jr., 1972. High-pressure peridotites in southwestern Oregon. *Geol. Soc. Am. Bull.*, 83:41–58.
- Medaris, L.G., Jr., and Dott, R.H., Jr., 1970. Mantle-derived peridotites in southwestern Oregon: relation to plate tectonics. *Science*, 169:971–974.
- Meyer, P.S., Dick, H.J.B., and Thompson, G., 1989. Cumulate gabbros from the Southwest Indian Ridge, 54°S–7°16'E: implications for magmatic processes at a slow spreading ridge. *Contrib. Mineral. Petrol.*, 103:44–63.
- Michael, P.J., and Bonatti, E., 1985a. Peridotite composition from the North Atlantic: regional and tectonic variations and implications for partial melting. *Earth Planet. Sci. Lett.*, 73:91–104.
- , 1985b. Petrology of ultramafic rocks from Sites 556, 558, and 560 in the North Atlantic. In Bougault, H., Cande, S.C., et al., *Init. Repts. DSDP*, 82: Washington (U.S. Govt. Printing Office), 523–528.
- Miyashiro, A., Shido, F., and Ewing, M., 1969. Diversity and origin of abyssal tholeiite from the Mid-Atlantic ridge, 24° and 30°N latitude. *Contrib. Mineral. Petrol.*, 23:38–52.
- , 1970. Crystallization and differentiation in abyssal tholeiites and gabbros from mid-oceanic ridges. *Earth Planet. Sci. Lett.*, 7:361–365.
- Moutte, J., 1979. Le Massif de Tiebaghi, Nouvelle Calédonie et ses gites de chromite [Ph.D. thesis]. L'École Nationale Supérieure des Mines de Paris.
- Mysen, B.O., and Boettcher, A.L., 1975. Melting of a hydrous mantle, I. Phase relations of natural peridotite at high pressures and temperatures with controlled activities of water, carbon dioxide, and hydrogen. *J. Petrol.*, 16:520–548.
- Natland, J.H., Adamson, A.C., Laverne, C., Melson, W.G., and O'Hearn, T., 1983. A compositionally nearly steady-state magma chamber at the Costa Rica Rift: evidence from basalt glass and mineral data, Deep Sea Drilling Project Sites 501, 504, and 505. In Cann, J.R., Langseth, M.G., Honnorez, J., Von Herzen, R.P., White, S.M., et al., *Init. Repts. DSDP*, 69: Washington (U.S. Govt. Printing Office), 811–858.
- Nicolas, A., 1989. *Structure of Ophiolites and Dynamics of the Oceanic Lithosphere*. Dordrecht (Kluwer).
- , 1990. Melt extraction from mantle peridotites: hydrofracturing and porous flow, with consequences for oceanic ridge activity. In Ryan, M.P. (Ed.), *Magma Transport and Storage*: Chichester (Wiley), 159–173.
- Nicolas, A., Boudier, F., and Boullier, A.M., 1973. Mechanisms of flow in naturally and experimentally deformed peridotites. *Am. J. Sci.*, 273:853–876.
- Nicolas, A., Boudier, F., and Ceuleneer, G., 1988. Mantle flow patterns and magma chambers at ocean ridges: evidence from the Oman Ophiolite. *Mar. Geophys. Res.*, 9:293–310.
- Nicolas, A., and Violette, J.F., 1982. Mantle flow at oceanic spreading centers: models derived from ophiolites. *Tectonophysics*, 81:319–339.
- Nilsson, K., 1993. Oxidation state, sulfur speciation, and sulfur concentration in basaltic magmas: examples from Hess Deep and the Lau Basin [Ph.D. dissert.]. Univ. California—San Diego.
- O'Hanley, D.S., 1992. Solution to the volume problem in serpentinization. *Geology*, 20:705–708.
- O'Hara, M.J., 1968. Are ocean floor basalts primary magma? *Nature*, 220:683–686.
- Ozawa, K., Meyer, P.S., and Bloomer, S.H., 1991. Mineralogy and textures of iron-titanium oxide gabbros and associated olivine gabbros from Hole 735B. In Von Herzen, R.P., Robinson, P.T., et al., *Proc. ODP, Sci. Results*, 118: College Station, TX (Ocean Drilling Program), 41–73.
- Panjasawatwong, Y., Danyushevsky, L.V., Crawford, A.J., and Harris, K.L., 1995. An experimental study of the effects of melt composition on plagioclase-melt equilibria at 5 and 10 kb: implications for the origin of magmatic high-An plagioclase. *Contrib. Mineral. Petrol.*, 118:420–432.
- Presnall, D.C., Dixon, J.R., O'Donnell, T.H., and Dixon, S.A., 1979. Generation of mid-ocean tholeiites. *J. Petrol.*, 20:3–35.
- Presnall, D.C., Dixon, S.A., Dixon, J.R., O'Donnell, T.H., Brenner, N.L., Schrock, R.L., and Dycus, D.W., 1978. Liquidus phase relations on the join diopside-forsterite-anorthite from 1 atm to 20 kbar: their bearing on the generation and crystallization of basaltic magma. *Contrib. Mineral. Petrol.*, 66:203–220.
- Quick, J.E., 1981a. The origin and significance of large, tabular dunite bodies in the Trinity peridotite, northern California. *Contrib. Mineral. Petrol.*, 78:413–422.

- , 1981b. Petrology and petrogenesis of the Trinity Peridotite, an upper diapir in the Eastern Klamath Mountains, Northern California. *J. Geophys. Res.*, 86:11837–11863.
- Rabinowicz, M., Ceuleneer, M., and Nicolas, A., 1987. Melt segregation and flow in mantle diapirs below spreading centers: evidence from the Oman ophiolites. *J. Geophys. Res.*, 92:3475–3486.
- Rabinowicz, M., Nicolas, A., and Vigneresse, J.L., 1984. A rolling mill effect in asthenosphere beneath oceanic spreading centers. *Earth Planet. Sci. Lett.*, 67:97–108.
- Ramp, L., 1961. Chromite in southwestern Oregon. *Bull.—Oreg. Dep. Geol. Miner. Ind.*, 52:1–169.
- Savel'yeva, G.N., Shcherbakov, S.A., and Denisova, Y.A., 1980. The role of high temperature in the development of dunite bodies in harzburgites. *Geotectonics*, 11:175–182.
- Schouten, H., Dick, H.J.B., and Kiltgord, K.D., 1987. Migration of mid-ocean-ridge volcanic segments. *Nature*, 326:835–839.
- Sinton, C.W., Christie, D.M., Coombs, V.L., Nielsen, R.L., and Fisk, M.R., 1993. Near-primary melt inclusions in anorthite phenocrysts from the Galapagos Platform. *Earth Planet. Sci. Lett.*, 119:527–537.
- Sinton, J.M., and Detrick, R.S., 1992. Mid-ocean ridge magma chambers. *J. Geophys. Res.*, 97:197–216.
- Sobolev, A.V., and Shimizu, N., 1993. Ultra-depleted primary melt included in an olivine from the Mid-Atlantic Ridge. *Nature*, 363:151–154.
- Stakes, D., Mével, C., Cannat, M., and Chaput, T., 1991. Metamorphic stratigraphy of Hole 735B. In Von Herzen, R.P., Robinson, P.T., et al., *Proc. ODP, Sci. Results*, 118: College Station, TX (Ocean Drilling Program), 153–180.
- Swift, S.A., and Stephen, R.A., 1992. How much gabbro is in ocean seismic layer 3? *Geophys. Res. Lett.*, 19:1871–1874.
- Thy, P., Schiffman, P., and Moores, E.M., 1989. Igneous mineral stratigraphy and chemistry of the Cyprus Crustal Study Project drill core in the plutonic sequences of the Troodos Ophiolite. *Pap.—Geol. Surv. Can.*, 88-9:147–185.
- Wager, L.R., and Brown, G. M., 1967. *Layered Igneous Rocks*: San Francisco (W.H. Freeman).
- Zonenshain, L.P., Kogan, L.I., Savostin, L.A., Golmstock, A.J., and Gorodnitskii, A.M., 1980. Tectonics, crustal structure and evolution of the Galapagos Triple Junction. *Mar. Geol.*, 37:209–230.

Date of initial receipt: 3 August 1994

Date of acceptance: 1 July 1995

Ms 147SR-007